

Structural Investigations of Hepatitis B virus X protein

Dissertation

zur Erlangung des Doktorgrades der Naturwissenschaften
an der Fakultät für Mathematik, Informatik und
Naturwissenschaften
der Universität Hamburg

vorgelegt von

Rana Abdullah Hussein (M.Sc)

aus Bagdad, Irak

Hamburg 2016

Die vorliegende Arbeit wurde im Zeitraum von Oktober 2011 bis Januar 2016 in der Arbeitsgruppe von Prof. Ch. Betzel im Laboratorium für Strukturbiologie von Infektion und Entzündung am Institut für Biochemie und Molekularbiologie des Fachbereichs Chemie

Gutachter:

Herr Prof. **Christian Betzel**

Herr Prof. **Reinhard Bredehorst**

Tag der Disputation: **22.01.2016**

**Gedruckt mit Unterstützung des Deutschen Akademischen Austauschdienstes
(DAAD)**

Printed with the support of the German Academic exchange Service (DAAD)

TO MY HUSBAND, MY SON AND MY NEW BORN DAUGHTER

Table of contents

Table of contents.....	I
List of figures.....	IV
List of tables.....	VI I
List of abbreviations.....	VI II
1. Introduction.....	1
1.1. Hepatitis B virus.....	1
1.2. Hepatitis B virus genome.....	2
1.3. HBV lifecycle.....	7
1.4. Infection with HBV and pathogenesis.....	9
1.5. HBV treatment.....	10
1.6. Hepatitis B virus X genome, protein.....	11
1.7. HBx protein as a transcriptional activator.....	15
1.8. HBx DNA and protein methylation.....	16
1.9. HBx binding activities.....	17
2. Aims of this project.....	20
3. Materials and Methods.....	22
3.1. Material.....	22
3.1.1. Devices.....	22
3.1.2. Plasmids.....	22
3.1.3. Oligonucleotides for cloning.....	25
3.1.4. Buffers and solutions.....	25
3.2. Methods.....	28
3.2.1. Molecular biology methods.....	28
3.2.1.1. PCR.....	28
3.2.1.2. DNA purification.....	29
3.2.1.3. Restriction digestion of DNA fragments.....	29
3.2.1.4. Agarose gel electrophoresis.....	30
3.2.1.5. Ligation.....	30
3.2.1.6. Preparation of chemically competent cells with CaCl ₂	31
3.2.1.7. Isolation and purification of plasmids.....	31
3.2.1.8. DNA-Sequencing.....	32
3.2.1.9. Transformation of <i>E.coli</i> cells.....	32

Table of Contents

3.3.	Biochemical methods.....	32
3.3.1.	Recombinant expression of the HBx genes.....	32
3.3.2.	Recombinant expression of the p53 genes.....	33
3.3.3.	Tobacco etches virus (TEV) protease expression.....	34
3.3.4.	Preparation of TEV protease glycerol stocks.....	34
3.3.5.	Cell disruption for protein purification.....	34
3.3.6.	Purification of the HBx fusion proteins.....	34
3.3.7.	Purification of the p53 proteins.....	35
3.3.8.	Purification of the TEV protease.....	35
3.3.9.	Regeneration of the amylose matrix.....	36
3.3.10.	Regeneration of the GST matrix.....	36
3.3.11.	Regeneration of the Ni-NTA matrix.....	36
3.3.12.	Size-exclusion chromatography (SEC).....	37
3.3.13.	Protein quantification by absorption measurements	37
3.3.14.	SDS-polyacrylamide gel electrophoresis (PAGE).....	37
3.3.15.	Dynamic Light Scattering (DLS).....	38
3.3.16.	Circular dichroism (CD) spectroscopy.....	39
3.3.17.	Mass spectrometry (MS)-based protein identification.....	40
3.3.18.	TEV protease digestion and separation of TEV cleaved proteins.....	41
3.4.	Methods to analyze the 3D structure of proteins.....	41
3.4.1.	Sample preparation for protein crystallization.....	41
3.4.2.	Optimization of initial crystallization conditions.....	44
3.4.3.	Evaluation of the protein crystals.....	45
3.4.4.	Negative staining electron microscopy (EM).....	45
3.4.5.	Small-angle X-ray scattering (SAXS).....	47
3.4.6.	Determination of protein-protein interaction.....	50
4.	Results and Discussion.....	53
4.1.	Amplification of the HBx genes by PCR.....	53
4.2.	Cloning of the HBx genes into the expression pMAL vectors.....	53
4.3.	Expression of the HBx fusion proteins in different <i>E. coli</i> strains.....	55
4.4.	Expression of TEV protease.....	58
4.5.	Solubility of HBx fusion proteins.....	59
4.6.	Purification of the HBx fusion proteins.....	61

Table of Contents

4.7.	Dynamic light scattering (DLS) of the HBx fusion proteins.....	63
4.8.	Secondary structure determination for the HBx fusion proteins.....	65
4.9.	Identification of HBx fusion proteins by MADI TOF/TOF mass Spectrometry.....	66
4.10.	Cleavage of the HBx fusion proteins by TEV protease.....	68
4.11	Crystallization experiments for the HBx fusion proteins.....	71
4.12.	Negative staining electron microscopy (EM) of DHBx fusion protein.....	74
4.13.	DHBx and full HBx fusion proteins SEC-SAXS structure	78
4.14.	Expression of p53 proteins.....	84
4.15.	Solubility of p53 proteins.....	85
4.16.	Purification of full-length and C-terminal p53 proteins.....	86
4.17.	Dynamic light scattering (DLS) for the p53 proteins.....	87
4.18.	Secondary structure determination for the p53 proteins.....	88
4.19.	Interaction of full and mini HBx fusion proteins with p53 protein.....	90
5.	Summary.....	96
6.	Zusammenfassung	99
7.	References.....	103
8.	Appendix	122
9.	Risk and safety statements.....	128
9.1.	Chemicals (GHS classification).....	128
9.2.	Commercial crystallization solutions	132
9.3.	GHS and risk symbols and information about hazard-, risk-, safety- and precaution-statements.....	133
10.	Acknowledgement.....	138
11.	Curriculum Vitae.....	140

List of figures

Figure 1: Global distribution of HBV infection.....	1
Figure 2: Schematic representation of the hepatitis B virus coding organization.....	4
Figure 3: Hepatitis B virions and subviral particles.....	5
Figure 4: Hepatitis B virus genome and cellular micro-RNA target sites.....	6
Figure 5: Illustration of the lifecycle of HBV Infection.....	8
Figure 6: Schematic representation of the HBx characteristic domains	12
Figure 7: Phylogeny of hepadnaviral protein X	15
Figure 8: Vector map for pMAL-c2x	23
Figure 9: Vector map for pMAL-p5x.....	24
Figure 10: Schematic diagram of a dynamic light scattering instrument.....	39
Figure 11: Standard curves for CD measurements of proteins.....	40
Figure 12: Zinsser Pipetting Robot.....	42
Figure 13: Schematic diagram of the loading procedure for sample preparation.....	43
Figure 14: Pipetting robot Oryx 4.....	44
Figure 15: Preparation of carbon coated grids for negative stain EM.....	46
Figure 16: Equipment used for negative stain EM.....	47
Figure 17: Schematic diagram of a SAXS experiment.....	48
Figure 18: SEC-SAXS/TDA set-up.....	49
Figure 19: Octet HTX system.....	51
Figure 20: Agarose gelelectrophoretic analysis of the amplification of the HBx genes.....	54
Figure 21: SDS-PAGE analysis of the DHBx fusion protein expression.....	56
Figure 22: SDS-PAGE analysis of the expression of human mini- and -hHBx fusion proteins	57
Figure 23: SDS-PAGE analysis of the expression of HBx fusion proteins using BL21 DE3 and shuffle cells.....	58
Figure 24: SDS-PAGE analysis of the expression of TEV protease.....	59
Figure 25: SDS-PAGE analysis of the solubility test for HBx fusion proteins.....	60
Figure 26: SDS-PAGE analysis of the solubility test when using BL21 DE3 and shuffle cells.....	60
Figure 27: SDS-PAGE and gel filtration analysis of the HBx fusion proteins purification cloned in pMAL-c2x vector.....	62
Figure 28: SDS-PAGE and gel filtration analysis of the HBx fusion proteins purification cloned in pMAL-p5X vector.....	63
Figure 29: DLS histograms for the HBx fusion proteins.....	65
Figure 30: Secondary structure estimation for the purified HBx fusion proteins.....	66

Figure 31: Tryptic peptide identification.....	68
Figure 32: SDS-PAGE analysis of the mini HBx fusion protein cleavage by TEV protease.....	69
Figure 33: SDS-PAGE analysis of the DHBx fusion protein cleavage by TEV protease.....	70
Figure 34: SDS-PAGE analysis of the full HBx fusion protein cleavage by TEV protease...	70
Figure 35: Observed crystals of the MBP-DHBx fusion protein from the screening plates...	72
Figure 36: Observed crystals of the mini HBx fusion protein from the screening plates.....	72
Figure 37: Observed crystals for MBP-DHBx and mini fusion proteins after optimization....	73
Figure 38: Observed crystals for MBP-DHBx and mini HBx fusion proteins from LCP plates.....	74
Figure 39: Negative staining images of DHBx fusion protein.....	75
Figure 40: Negative staining images of DHBx fusion protein oligomerized molecules.....	76
Figure 41: Native gel analysis of the HBx fusion proteins using a native gel	77
Figure 42: Schematic diagrams of the collected fractions for both DHBx and full HBx fusion proteins when using SEC-SAXS.....	80
Figure 43: Processed solution SEC-SAXS scattering data for DHBx fusion protein used for <i>ab initio</i> modeling	82
Figure 44: Processed solution SEC-SAXS scattering data for full HBx fusion protein used for <i>ab initio</i> modeling.....	83
Figure 45: SDS-PAGE analysis of the expression of full-length p53, as well as truncated N-terminal p53 fusion proteins	85
Figure 46: SDS-PAGE analysis of the solubility test of GST-p53 fusion proteins.....	85
Figure 47: SDS-PAGE analysis of the purification of full-length and C-terminal p53 fusion proteins	86
Figure 48: SDS-PAGE analysis of the separation of both full-length and C-terminal P53 fusion proteins after cleavage.....	87
Figure 49: DLS histograms for p53 fusion proteins.....	88
Figure 50: CD spectra of the purified full p53 fusion protein and free tagged full p53 protein.....	89
Figure 51: CD spectra of the purified C-terminal fusion protein and free tagged C-terminal p53 protein.....	89
Figure 52: Interaction test of HBx and p53 fusion proteins.....	91
Figure 53: Interaction test of HBx fusion proteins and free tagged p53 proteins.....	92
Figure 54: Conformation analysis of the interaction using the Octet device.....	94
Figure 55: Peptide identification of MS results for DHBx after incomplete cleavage.....	122
Figure 56: Observation of positive DHBx fusion protein crystals after screening.....	123

List of Figures

Figure 57: Negative binding of both full and C-terminal p53 fusion proteins on amylase matrix.....	123
Figure 58: The fit graphs of the collected fractions for the DHBx fusion protein after SEC-SAXS preparation.....	123
Figure 59: The fit graphs of the collected fractions for the full HBx fusion protein after SEC-SAXS preparation.....	124
Figure 60: Secondary structure for the HBx fusion proteins using PSIPRED program.....	125
Figure 61: DLS histograms of the mean autocorrelation functions of the HBx fusion Proteins.....	126
Figure 62: DLS histograms of the mean autocorrelation functions of the free p53 and the p53 fusion proteins.....	126
Figure 63: Processed solution SEC-SAXS scattering data for the DHBx fusion protein for the first peak.....	127
Figure 64: Processed solution SEC-SAXS scattering data for the full HBx fusion protein for the first peak.....	127
Figure 65: Hazard symbols.....	133
Figure 66: GHS pictograms.....	133

List of tables

Table 1: Characteristics of endemic patterns of hepatitis B virus infection.....	9
Table 2: Distinct phases of chronic infection	10
Table 3: Selected devices.....	22
Table 4: Amino acid sequences of the HBx proteins.....	25
Table 5: General buffers.....	25
Table 6: Bacteria cell culture.....	26
Table 7: Bacterial strains.....	26
Table 8: Competent cells.....	26
Table 9: Agarose gel electrophoresis.....	26
Table 10: Molecular weight markers.....	26
Table 11: Native gel preparation.....	27
Table 12: SDS-PAGE preparation.....	27
Table 13: GST agarose regeneration.....	27
Table 14: Ni-NTA agarose regeneration.....	27
Table 15: Staining solution for negative staining.....	27
Table 16: Protein purification.....	28
Table 17: Chemicals (GHS classification).....	128
Table 18: Commercial crystallization solutions and kits.....	132
Table 19: GHS hazard statements.....	134
Table 20: GHS precautionary statements.....	135
Table 21: Risk statements.....	136
Table 22: Safety statements.....	137

List of abbreviations

2D	two dimensional
3D	three dimensional
Å	Angstrom (unit, 10 ⁻¹⁰ m)
χ^2	chi ² value
aa	amino acid(s)
Amp	ampicillin
approx.	Approximately
APS	ammonium per-sulfate
bp	base pair
<i>c</i>	concentration
°C	degree Celsius
CD	circular dichroism
cDNA	complementary DNA
DESY	Deutsches Elektronen Synchrotron (German electron synchrotron)
DLS	dynamic light scattering
DNA	deoxyribonucleic acid
dNTPs	2'-deoxynucleoside-5'-triphosphate
DTT	dithiothreitol
<i>E.coli</i>	<i>Escherichia. coli</i>
EDTA	ethylene diamine tetraacetic acid
EM	electron microscopy
EMBL	European Molecular Biology Laboratory
Enh	enhancer
ER	endoplasmic reticulum
<i>et al.</i>	<i>et alii</i>
g	gram (unit)
GST	glutathione S-transferase
hr	hour
HBcAg	Hepatitis B core antigen
HBeAg	Hepatitis B envelope antigen
HBsAg	Hepatitis B surface antigen
HBV	Hepatitis B virus
HBx	Hepatitis B virus x protein
HCC	Hepatocellular carcinoma
I	intensity
IPTG	isopropyl- β -D-thiogalactopyranoside
Kd	dissociation constant

List of Abbreviations

kDa	kilo Dalton
l	litre (unit)
LB	Luria Bertani
M	molar
m	milli- (multiplied by 10^{-3})
mM	milli Molar
MBP	Maltose binding protein
mg	milli gram
min	minutes
MS	mass spectrometry
MW	molecular weight (g/mol or Da)
Ni-NTA	nickel-nitrilotriacetic acid
Nm	nanometer
NPC	Neural Progenitor Cell
NSD	normalized spatial discrepancy
OD	optical Density
ORFs	open reading frames
PAGE	polyacrylamide gel electrophoresis
PBS	phosphate buffered saline
PCR	polymerase chain reaction
PCT	pre-crystallization test
PEG	polyethylene glycol
pgRNA	pre-genomic mRNA
RALS	right angle light scattering
RI	refractive index
Rg	radius of gyration
R _H	hydrodynamic radius
rcDNA	relaxed circular DNA
rpm	revolutions per minute
s	scattering vector (SAXS; depending on angle and wavelength of scattered waves)
s	second(s)
SAXS	small angle X-ray scattering
SDS	sodium dodecyl sulfate
SEC	size-exclusion chromatography
sec.	secondary
ss	single strand (DNA/RNA)
T	temperature [K]
t	time [s]
TAE	Tris-acetate-EDTA
Taq	<i>Thermus aquaticus</i>

List of Abbreviations

TDA	triple detector array
TEMED	<i>N,N,N',N'</i> -tetramethylethylenediamine
TEV	tobacco etch virus
TOF	time of flight
Tris	Tris(hydroxymethyl)aminomethane
UV	ultra violet
UV-vis	ultraviolet-visible light
v/v	volume per volume
w/v	weight per volume
WHO	World Health Organization
WHV	woodchuck hepatitis virus
GSHV	ground squirrel hepatitis virus
wt	wild type
μ	micro- (multiplied by 10 ⁻⁶)

1. Introduction

1.1. Hepatitis B virus

Hepatitis B virus (HBV) is a noncytopathic hepadnavirus that causes one of the world's most common viral infection diseases, which is associated with significant morbidity and mortality and is considered to be a worldwide health problem. Chronic infection with HBV is a major predisposing factor for hepatocarcinogenesis [Beasley, *et al.*, 1981; Chen, *et al.*, 2006] and it has been demonstrated that HBV infections might be involved in the development of hepatocellular carcinoma (HCC) [Tan, *et al.*, 2008; Benhenda, *et al.*, 2009; Kusunoki, *et al.*, 2014]. HBV is considered one of the most common malignancy diseases [Kim & Seung, 2003]. According to the World Health Organization (WHO), 2 billion people are infected with HBV and more than 400 million are chronic carriers of HBV. The risk of infection with HCC is a 100-fold in patients with chronic HBV infection [de Moura, *et al.*, 2005]. In countries with the highest living standards, such as Europe and the USA, prevalence of the HBV-antigen is the lowest (0.1-1%). Very high rates (5-20%) have been reported from China, Africa, the Middle East and South Africa, including some parts of Brazil [Rui, *et al.*, 2001; Rui, *et al.*, 2006]. HCC constitutes 90% of the primary malignant tumors of the liver and it is estimated that each year, more than 500,000 people die from liver cancer worldwide [Hollinger, 1996; Knoll, *et al.*, 2011].

Geographic Distribution of Chronic HBV Infection

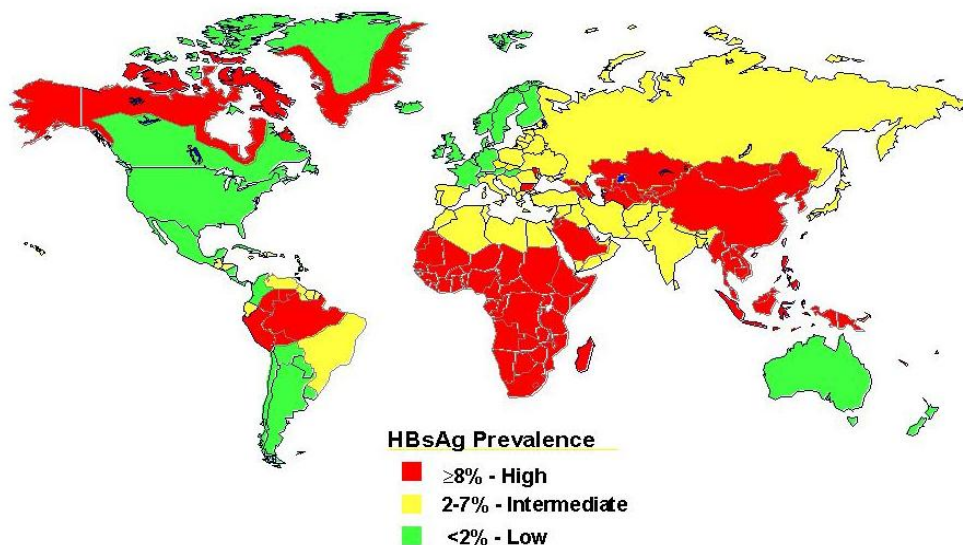


Figure 1: Global distribution of HBV infection. Taken from (Virology-online.com).

The clinical consequences of infection with hepatitis B virus, is very diversified and unexpected. The virus causes a severe disease in variable durations, starting from subclinical to acute, followed by chronic liver damage. Approximately 90% of infected adults recover and develop lifelong immunity to the virus. In other cases, 0.1-0.5%, result in extensive damage to the liver, 5-10% of adults infected with HBV, are incapable of eliminating the virus and therefore develop chronic infection. The nature of chronic infections ranges from continuous necrosis and inflammation of the liver (chronic active hepatitis) to the case of transmission of the disease. Also 90% of children from infected parents become chronically infected [Lee, 1997]. The mechanism of the HBV infection has not been fully clarified. Despite high levels of viral activity within liver cells, HBV carriers can maintain a normal liver function. Other observations conclude that the liver injury is caused by virus infection-immune response [Alberti, *et al.*, 1984; Elizabeth *et al.*, 2011]. The cellular immune response is directed to the envelope and the nucleated capsid. The antibody response to the surface antigen of hepatitis B antigen (HBsAg) contributes to the removal of the virus after acute infection [Chisari, 1995; Elizabeth, *et al.*, 2011]. The HBsAg- vaccination against HBV disease practiced and HBsAg antibodies have been proven to be effective. The mechanisms responsible for the HBsAg-non responsiveness in vaccines, is unknown so far. However, the clinical symptoms caused by hepatitis B virus infection and the variability of the humeral immune response of HBsAg after vaccination, suggests a list of genetic immune response to HBsAg [Milich, 1984; Ott, *et al.*, 2012]. Clarification of the mechanism (s) responsible for the lack of an immune response to HBsAg and HBsAg development immunity to the vaccine, are indispensable against hepatitis B virus. They are considered long-term objectives of the study.

1.2. Hepatitis B virus genome

The HBV genome is unique in the viral world due to its consolidated nature, the use of overlapping reading frames and its dependence on a reverse-transcriptional step, although the virion contains primarily DNA. The human hepatitis B virus is the archetype of a virus family called *Hepadnaviridae* (for hepatotropic DNA viruses). [Rui, *et al.*, 2005; Seeger, *et al.*, 2007; Hodgson, *et al.*, 2012]. HBV is a partially duplexed, relaxed circular DNA molecule (rcDNA) of 3.2kb and it is converted into a covalently closed circular DNA upon entry into the cell. It is phylogenetically related

Introduction

to the retroviruses as it uses its own reverse transcriptase for DNA replication [Rui, *et al.*, 2001; van Hemert, *et al.*, 2011; Hodgson, *et al.*, 2012]. After the identification of HBV in humans, several viruses have been subsequently isolated from mammalian (orthohepadnaviridae). Similarities could be identified due to DNA sequencing and by investigating the genome organization. They could also be identified in avian (avihepadnaviridae) species such as woodchucks, ducks, and herons, even ground squirrels, all were classified as hepadnaviruses. They display high liver tropism, have a narrow host range and cause acute and chronic hepatitis [Chans, *et al.*, 1999; Warren, *et al.*, 1999; Liu, *et al.*, 2009]. The viruses which are related to HBV have been found in woodchucks (WHV) and ground squirrels (GSHV). They possess approximately 70% sequence homology to HBV but are not known to infect human or other primates. In contrast HBV is known to be infectious for the great apes, although the two genera differ in genetic organization, structure and biological properties, for example the avihepadnaviridae lacks a separate gene encoding the HBV-X protein. All the hepadnaviruses are able to induce persistent infections in their natural hosts [Howard, 1994; Scaglioni, *et al.*, 1996]. Hepatitis B virus can be classified into eight genotypes (A to H) based on sequence (nt) diversity of $\geq 8\%$. These genotypes have distinct geographical distributions and varied disease progressions.

HBV encodes four overlapping open reading frames (ORFs), termed **S**, **C**, **P**, and **X**, which encode for seven viral proteins (Fig. 2). The **S** ORF codes for the main hepatitis B surface antigen (HBsAg) protein. This protein and its glycosylated partner are trans-membrane proteins in the envelope of the virus. The S ORF encodes three envelope proteins (S, M, and L) from three alternate in-frame initiation codons, corresponding to the ORF's pre-S1, pre-S2, and S (Fig. 3). While all three envelope proteins share an identical 226 amino acid C-terminus region, called the surface domain [Barrera, *et al.*, 2005], the M and L proteins have additional sequences, which correspond to pre-S2, or pre-S1 and preS2 at their N-terminus. The M protein contains an additional 55 amino acid N-terminal domain called the pre-S2 domain, whereas the L protein is further extended in the N-terminal direction by the 108 amino acid pre-S1 domain [Chouteau, *et al.*, 2001]. All three surface glycoprotein contain the 'a' determinant epitope, located at codon positions 124 to 147 of the **S** gene. The 'a' determinant is one of the major initial immune response targets of anti-HBs antibodies during acute hepatitis B.

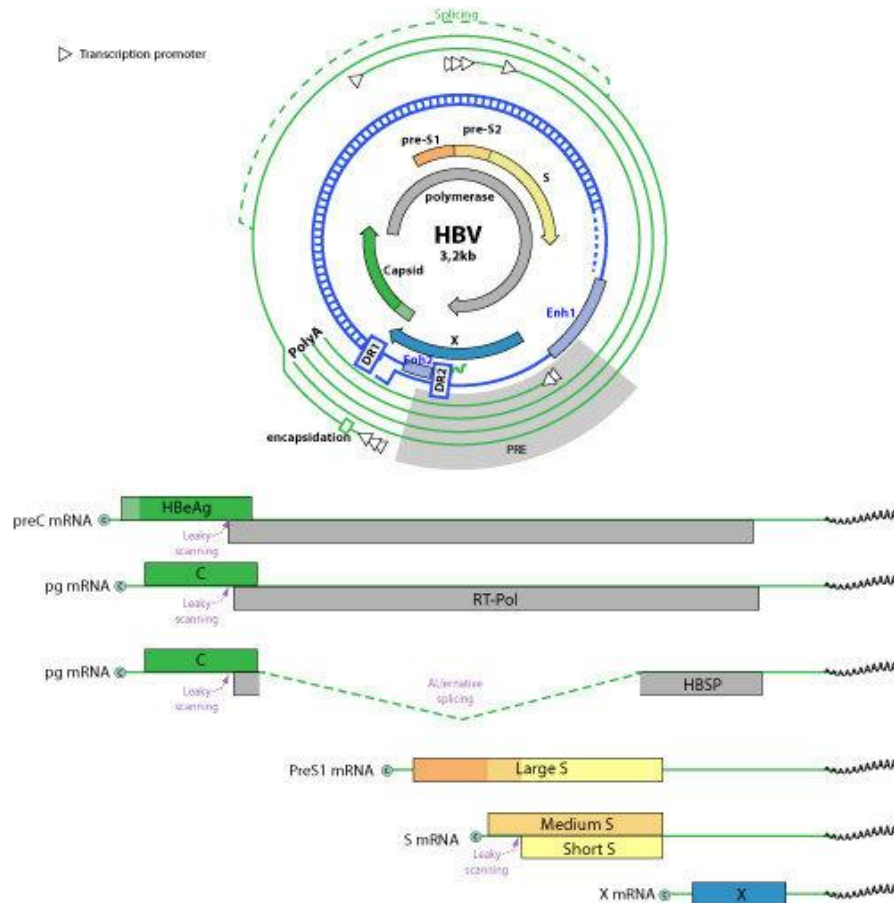


Figure 2: Schematic representation of the hepatitis B virus coding organization. The 3.2 kb HBV has four overlapping open reading frames encoding seven different transcripts. Taken from (ViralZone, 2009 / Swiss Institute of Bioinformatics).

. This determinant can undergo conformational changes, which affect the binding of neutralizing antibodies [Courouce-Pauty, *et al.*, 1978; Kann, 2002; Chongsrisawat, *et al.*, 2006; Lada, *et al.*, 2006; Yokosuka & Arai, 2006] (Fig. 3). The gene C codes for the hepatitis B core antigen (HBcAg) and forms the nucleocapsid of the virus. The C ORF encodes two proteins; core (C) and e-antigen (HBeAg). The core protein self assembles into a capsid-like structure in the cytoplasm of the cells during expression.

The HBeAg contains a signal peptide directing its translation to the endoplasmic reticulum (ER), where it is post-transcriptionally modified and secreted from the cell. The function of HBeAg in HBV is suggested to interfere with the immune responses to prolong infection [Milich & Liang, 2003; Walker, *et al.*, 2008; Liang, 2009; Liaw, *et al.*, 2010]. The core protein is a structural protein with 183–185 amino acids, depending on the genotype of the virus and known to be relatively well conserved [Jazayeri, *et al.*, 2004; Yokosuka & Arai, 2006]. This protein forms dimers in the cytoplasm of the hepatocyte [Kann, 2002; Yokosuka & Arai, 2006].

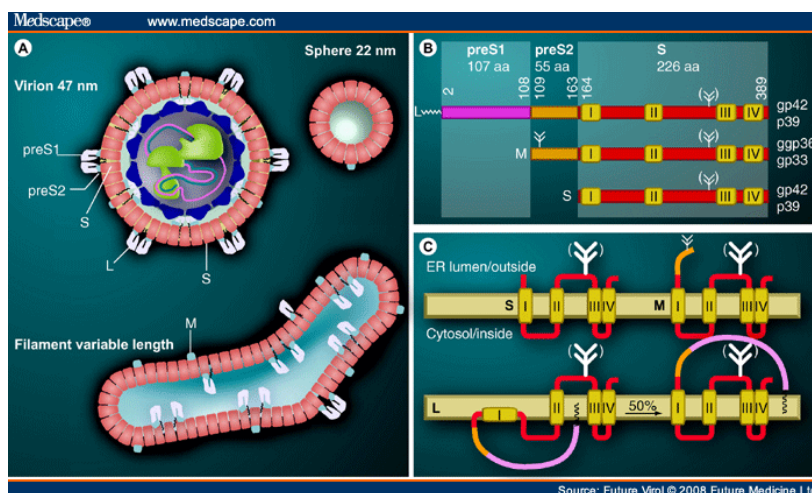


Figure 3: Hepatitis B virions and subviral particles, the three HBV surface proteins large, middle and small and their membrane topologies. (A) The partially dsDNA is covalently associated with the viral polymerase, consisting of the terminal protein, the reverse transcriptase and the RNaseH. The DNA genome is encapsulated by a capsid. The three HBV surface proteins (L, M and S) are embedded in an ER-derived lipid bilayer. **(B)** Domain structures of the three HBV surface proteins L, M and S. The L- and M-proteins contain the S-domain (red). S-protein comprises four transmembrane spanning regions (yellow) that provide membrane anchors. The L-protein (top) is myristoylated at Gly-2 of the preS1 domain (pink). PreS1 is C-terminally connected to the 55 amino acid preS2 domain (orange). The M-protein (middle) consists of preS2 (orange) and the S-domain. **(C)** Depicted at the top are the membrane topologies of the S- and the M-protein with their glycosylation site facing into the ER lumen. Below, the proposed two topologies of the HBV L-protein are shown. The two preS domains of L are initially oriented toward the cytosol, allowing the cytoplasmatic myristoylation of the preS1 domain. Taken from (Future virol, 2008/www.medscape.com).

The **P** region comprises the virus reverse transcriptase which also possesses DNA dependent DNA polymerase activity. The **P** ORF encodes for HBV's only enzyme, the hepatitis B polymerase (pol) is responsible for transcription of pre-genomic mRNA (pgRNA) into the rcDNA viral genome. The polymerase protein is translated from the pregenomic RNA and consists between 834 and 845 amino acids. It has at least four domains, the N-terminal, spacer, polymerase and C-terminal domains [Kann, 2002; Yokosuka & Arai, 2006; Abbas, *et al.*, 2007]. The HBV polymerase protein (pol) is both structurally and functionally similar to the HIV reverse transcriptase, both of which contain a classical tyrosine-methionine-aspartic acid-aspartic acid (YMDD) motif in their catalytic centers [Yokosuka & Arai, 2006]. Finally, the **X** gene codes for the small regulatory protein of the virus, the hepatitis B **X** (HBx) antigen. HBx is a multifunctional non-structural trans-activating, viral oncoprotein that stimulates virus gene expression and replication, protects virus-infected cells against immune-mediated destruction and contributes to the development of hepatocellular carcinoma (HCC) [Liu, *et al.*, 2009, Lizzano, *et al.*, 2011].

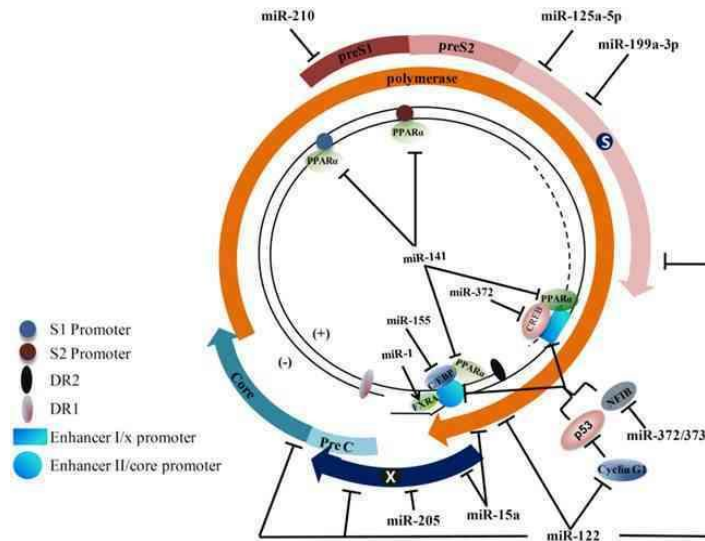


Figure 4: Hepatitis B virus (HBV) genome and cellular microRNA (miRNA) target sites. The partially double-stranded genome is presented with transcription regulatory elements. The viral open reading frames are shown as arrows immediately surrounding the genome. Viral enhancer I and II, promoters, DR1, and DR2 are indicated. The binding positions of transcription factors and nuclear receptors on the HBV genome are shown (C/EBP: CAAT enhancer-binding protein; CREB: C-AMP-response element binding protein; FXRA: Farnesoid X receptor alpha; PPAR α : Peroxisome proliferator-activated receptor alpha; NFIB: Nuclear factor I/B). Cellular factors known for regulating hepatitis B virus (HBV) transcription and the positions of the binding sequences in HBV transcripts targeted by miRNAs are shown. Arrows indicate activation, while the bars indicate an inhibitory effect of miRNAs on HBV transcription. Taken from [Xie, *et al.*, 2014].

HBx also appears to have an enhancing effect on the metabolism of intrahepatic purines and pyrimidines needed for the efficient replication of HBV [Yokosuka & Arai, 2006]. The HBV genome contains a number of both ubiquitous and hepatocyte specific transcription factor binding sites, parts of which cluster in the enhancer 1 (EnhI) and 2 (EnhII) regions (position- and orientation-independent stimulation of transcription). EnhI is located upstream of the X promoter and is targeted by multiple activators, it extends approximately 200 nucleotides between the S and X genes and is considered the major enhancer, [Kann, 2002]. Whereas Enh II promotes liver-specific transcription of the pre-genomic C promoter, and possibly also the preS2/S promoter. Deletion of either enhancer regions result in a strong reduction of viral transcripts [Doitsh & Shaul, 2004]. EnhII is located immediately upstream of the core ORF and confers hepatocyte specificity on the virus as it binds only to specific liver transcription factors, such as C/EBP and HNF-4 [Kann, 2002; Chang, *et al.*, 2004]. Two direct repeat sequences (DR1 and DR2) are located on either side of the gap in the negative DNA strand. DR1 is located at nucleotides 1826–1836 and DR2 at nucleotides 1592–1602 (Fig.4) [Jilbert, *et al.*, 2002]. Both these direct repeat sequences are necessary for the replication of HBV.

1.3. HBV lifecycle

The initial step in the HBV lifecycle is its attachment to a cell, is its capability of supporting replication. The primary cellular host of HBV is the hepatocyte [Seeger, *et al.*, 2007]. The HBV life-cycle begins with the interaction of HBsAg with cellular receptor/s at the surface of hepatocytes (Fig. 5). The Attachment to the host cell is mediate by virion protein(s) binding to specific host surface molecule(s) [Grove & Marsh, 2011]. Binding to the target host molecule(s) leads to entry of a viral genome into the host cell, triggering signaling pathways, or allowing the virion to be carried to a specific organ by host cells. A number of potential cellular receptors that interact with HBsAg during HBV infection have been identified previously, but the mechanisms of their action still remains controversial as none of them have been proven to be functional with HBV. These receptors include the retinoid X receptor (RXR), the peroxisome proliferator-activated receptor (PPAR) and the farnesoid X receptor (FXR). Cell receptors can be classified in two classes: Adhesion receptors, which attach the virus in a reversible manner to target cells or organs. These receptors trigger the entry of the virus by endocytosis/pinocytosis or by inducing fusion/penetration; the consequences of this binding are irreversible. They have often been named "co-receptors". The relaxed circular DNA (RC-DNA) and capsid are transported to the nucleus *via* microtubules, where the DNA is released through the nuclear pore and repaired to form covalently closed circular DNA (cccDNA). The cccDNA molecules play a role in the HBV life cycle analogous to that of integrated pro-viral DNA of retroviruses. The resulting RNAs are transported to the cytoplasm where they are translated into the viral envelope, core, X and polymerase proteins. Nucleocapsids are assembled in the cytosol, during this process; a single molecule of pregenomic RNA is incorporated into the assembling viral core together with the polymerase. The viral DNA synthesis is sequentially initiated: after negative-stranded synthesis and concomitant degradation of the RNA template, positive-stranded DNA synthesis occurs [Leopold & Pfister, 2006]. Crossing of the nuclear membrane occurs in several ways [Kobiler, *et al.*, 2012] e.g. RNA virus and dsDNA virus enter *via* the nuclear pore complex through the cellular importing transport. Also the ssDNA virus capsid observes to be small enough to cross the neural progenitor cell (NPC) and enters the nucleus as an intact capsid. The Hepadnaviridae capsid enters the NPC pore; remains attached to it and release the viral genomic DNA into the

Introduction

nucleoplasm. The retroviridae except lentivirus enters the nucleus during mitosis, when the nuclear membrane is temporarily disintegrated. Integration in the host genome may eventually be followed by transcription of the viral mRNAs and the pregenomic RNA (pgRNA) by RNA polymerase II [Whittaker, *et al.*, 2000].

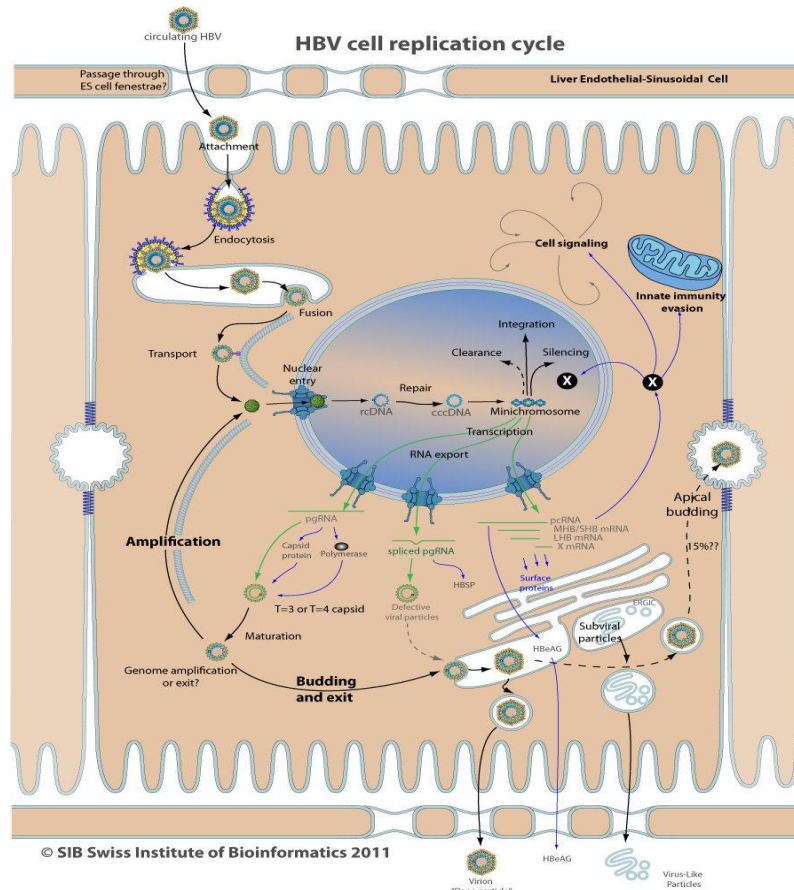


Figure 5: Illustration of the lifecycle of HBV Infection. Taken from (Swiss Institute of Bioinformatics, 2011).

The unspliced pregenomic RNA then leaves the nucleus by nuclear pore export. In the cytoplasm pgRNA is encapsidated, together with the P protein, and reverse-transcribed into new RC-DNA inside the nucleocapsid. The unspliced RNA genome is encapsulated and transcribed reversely before virion budding. The encapsulated pre-genomic RNA (pgRNA) is the template for viral replication. RNase H activity of the RT protein degrades pgRNA hybridized to DNA, except for the DR cap-primer. The DR cap-primer is translocated to the upstream DR motif and plus-strand DNA synthesis takes place from the DR2 to the DR1 motif. The new DNA strand translocates to the DR1 sequence and plus-strand DNA is elongated to form the relaxed-circular DNA (rcDNA). After infection, the rcDNA is transported into the nucleus and converted to closed-circular cDNA (cccDNA) by the host DNA repair

Introduction

machinery [Kobiler, *et al.*, 2012]. All these strategies which are used to cross the nuclear envelope barrier are associated with different levels of capsid disassembly, [Whittaker, *et al.*, 2000]. Budding enables viruses to exit the host cell and is used by the enveloped viruses, which must acquire a host-derived membrane enriched with viral proteins to form their external envelope [Chen & Lamb, 2008].

1.4. Infection with HBV and pathogenesis

Hepatitis B virus (HBV) infection is a serious worldwide health problem and a major cause of chronic hepatitis, cirrhosis and hepatocellular carcinoma (HCC) [Hou, *et al.*, 2005]. The infection of chronic HBV varies in different parts of the world. This infection could be categorized as high (>8%), intermediate (2-7%) and low (<2%) endemicity (Tab.1), (Fig.1). The age of a person at the time of infection is associated with the development of HBV infection. HBV can spread when contacting with blood which is considered the most important part for transmission, but other body fluids have also been implicated, including semen, vaginal fluids, saliva, tears, sweat, urine and breast milk in which HBV is found in low concentrations. The HBV virus is 100 times more infectious than HIV and can survive outside the body for seven days. [Bancroft, *et al.*, 1977; Scott, *et al.*, 1980]. Three ways of HBV transmission have been recognized: Perinatal, sexual and parenteral/percutaneous transmissions. Till now, no reliable evidence regarding airborne infections have occurred, also feces are not considered a source of infection.

Table 1: Characteristics of endemic patterns of hepatitis B virus infection: Adapted from [Alter, 2003].

Characteristic	Endemicity of infection		
	Low (%)	Intermediate (%)	High (%)
Chronic infection prevalence	0.5-2	2-7	≥8
Past infection prevalence	5-7	10-60	70-95
Perinatal infection	Rare (<10)	Uncommon (10-60)	Common (>20)
Early childhood infection	Rare	Common	Very common
Adolescent/adult infection	(<10)	(10-60)	(>60)
	Very common (70-90)	Common (20-50)	Uncommon (10-20)

On the other hand, HBV is not transmitted by contaminated food or water, insects or other vectors. Chronic hepatitis B virus (HBV) infection can be classified into three immune responds: Immune tolerant, immune active and inactive chronic carrier state (Table. 2) [McMahon, *et al.*, 2001; Hoofnagle, *et al.*, 2007; Lok & McMahon,

Introduction

2007; Keefe, *et al.*, 2008; Lok & McMahon, 2009; McMahon, 2010]. These desecrated phases of the chronic infection correspond to the serological patterns and correlate with the patient's immune response to HBV. Generally, the initial immune response of chronic infections depend on the age of the patient obtaining the HBV; also the initial immune response and the phase of the infection may depend on the HBV genotype. Although most adults with acute HBV infection will generate an effective immune response and can be cured from the HBV infection, some people will develop chronic infection and enter the immune active phase of infection.

Table 2: Distinct phases of chronic infection correspond with characteristic serologic patterns and correlate with the patient's immune response to HBV, ALT= Alanine aminotransferase, Adapted from (Natural History of Chronic Hepatitis B Infection, 2013).

Phase	HBeAg	HBV DNA	ALT	Liver Histology	Treatment
Immune Tolerant	Positive	Very high >200,000IU/ml	Normal	Normal or mild inflammation & scant fibrosis	not indicated
Immune Active	Positive or Negative	>200,000IU/ml Usually >200,000 IU/ml	Elevated	Inflammation and fibrosis; Degree Varies	Treatment Candidate
Inactive	Negative	>200,000 IU/ml	Normal	Normal or mild inflammation	not Indicated

Patients who developed to the immune tolerant phase, will advance to the immune active phase state and then enter into the inactive chronic carrier state [Rehermann & Nascimbeni, 2005; Lok & McMahon, 2007]. In addition to the three stages of chronic HBV infection, some patients will resolve their HBV infection, either naturally or occasionally following interferon-based therapy or with oral nucleoside/nucleotide therapy; these patients show clearance of HBsAg, will develop anti-HBs. Reactivation of HBV infection may develop when becoming severely immuno-suppressed. This can occur after receiving chemotherapy, by using potent chemotherapy regimens or immuno-suppressive biologic agents [Perrillo, 2001; Mastroianni, *et al.*, 2011].

1.5. HBV treatment

The treatment of HBV has poor efficacy regarding the medication of patients who obtain immune-tolerant chronic infections [McMahon, 2001; Lok & McMahon, 2007]. Even by using antiviral agents, it is difficult to repress high levels of HBV found in infected patients. However, treatment for patients, which are in the immune tolerant phase state, may bear a risk in developing resistance over time. Patients with

chronic HBV infections, respond better to therapy when obtaining an active immune response to the HBV infection. The American Association for the Study of Liver Disease (AASLD) practice guidelines recommend, that patients with immune tolerant chronic HBV should follow-up ALT testing every 3 to 6 months [Lok & McMahon, 2001], then prepare for a liver biopsy for liver disease evaluation [Lok & McMahon, 2007], also test every 6 to 12 months, since these people are in risk of developing HCC [Lok & McMahon, 2007; Bruix, 2011]. The testing varies depends on whether ALT levels remain normal. Patients with continues chronic HBV infection should start HBV therapy immediately to prevent liver fibrosis progress. If a mild or acute hepatitis is present, antiviral treatments should be initiated. Currently, there are two options for treating chronic HBV infections: Pegylated interferon α (IFN α), which has direct antiviral effects, stimulates T-cell immunity and nucleoside analogs, such as Ribavirin and Lamivudine which interfere with viral DNA replication [Niederau, *et al.*, 1996; de Franchis, *et al.*, 2003; Lim, *et al.*, 2009]. Despite these treatment options, many patients will experience different symptoms e.g. nausea, fever, muscle pain, headache, and fatigue, also depression and suicidal attempts [Negro, 2010; Zoulim, 2011]. Therefore, the development of more effective treatment options with fewer side effects remains a research priority.

1.6. Hepatitis B virus X genome, protein

Hepatitis B virus X protein (HBx) is a non-structural HBV protein that is localized in the nucleus, in the cytoplasm and in mitochondria of HBx-expressing cells [McClain, *et al.*, 2007]. It is a multifunctional regulator, which is supposed to modulate transcription, signal transduction, cell cycle progress, protein degradation, apoptosis and genetic host factors [Bouchard, *et al.*, 2004; Tang, *et al.*, 2008; Liu, *et al.* 2009; Sudhi, *et al.*, 2014]. It also possesses nuclear transcription-activation functions that may interfere with other proteins or possibly show co-activator activity [Doria, *et al.*, 1995; Sudhi, *et al.*, 2014]. The half-life of cytosolic and soluble HBx comprises approximately 15 minutes, whereas the half-life of cytoskeletal-associated HBx is around 3 hours [Schek, *et al.*, 1991]. The encoded X protein (HBx) with a molecular weight of 17 kDa consists of 154 amino acids, with two distinct regions between amino acids 50 to 84 and 105 to 142 being crucial for its activities and interactions with cellular proteins. The N-terminal part of HBx is a negative

Introduction

regulatory domain (1-50 amino acids), which is involved in dimerization and in the negative regulation of transcriptional activation [Lin, *et al.*, 1989; Gottlob, *et al.*, 1998]. The C-terminal trans-activation or co-activation domain (51-154 amino acids) is essential for the productive infection by mammalian HBV, which is associated with the development of HCC and has inhibitory effects on cell proliferation (Fig. 6) [Lin, *et al.*, 1997; Wentz, *et al.*, 2000; Tang, *et al.*, 2005]. However it is very difficult to detect HBx protein in the HBV infected liver in mammalian, due to the very low amount of protein in the hepatocytes. It is known that only mammalian hepadnaviruses encode the X protein, while avian hepadnaviruses either do not encode an X protein or encode a highly manifold one [Mandart, *et al.*, 1984; Sprengel, *et al.*, 1985; Tang, *et al.*, 2005]. Mammalians and particularly primate retroviruses are encrypted for supplemental proteins, as compared to the avian retroviruses. Most of them neutralize host defenses, which are stronger in mammals [Li, *et al.*, 2008].

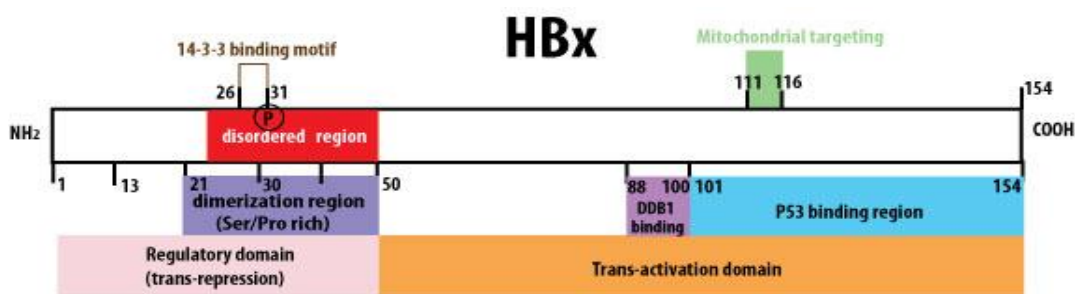


Figure 6: Schematic representation of the HBx characteristic domains. Taken from [Li, *et al.*, 2008].

Although the HBx protein is shown to stimulate cell cycle progression of cells, it is mainly a pleiotropical trans-activator due to its ability to stimulate not only the HBV promoter and enhancer, but also a wide range of other viral promoters [Spandau & Lee, 1988; Koika, *et al.*, 1994]. Since the DNA in the HBV virion is partially double-stranded, HBx might also bind *in vivo* to the viral ssDNA (single-stranded DNA) and may perform a function in the replication process of the virus DNA [Hang, *et al.*, 1995]. Despite the mechanism that has not been definitely clarified, HBx transactivation is important for its oncogenic role, as HBx transactivates not only HBV genes but also various host genes that engage in cell proliferation and acute inflammatory responses [Yen, *et al.*, 1996].

The Full length HBx contains 10 cysteine (Cys) residues; eight of them are claimed to be involved in disulphide bond formation that results in aggregation of various HBx molecules [Urban, *et al.*, 1997]. Protein aggregation will lead to cell cycle arrest

and will initiate cell death [Song, *et al.*, 2003; Kim, *et al.*, 2008]. The absence of structural information of HBx relates to the fact that it has been impossible or difficult so far to produce full length HBx with intact disulfide bonds in a soluble form, or to produce certain districts of HBx that maintain the activity of the full length HBx [Rui, *et al.*, 2001]. Recently, a shorter recombinant construct of the HBx including a diverse called 'truncated mini HBx (Tr-mini HBx), that comprises the amino acids 18-142 have successfully been produced and analyzed [Rui, *et al.*, 2005; Lee, *et al.*, 2012]. The Tr-mini HBx maintains at least some of the known activities, although all cysteine residues have been replaced by serine residues, which prevent the formation of intermolecular disulphide bonds that were associated with HBx aggregation [de Moura, *et al.*, 2005, Rui, *et al.*, 2005]. It has also been shown that the Tr-mini HBx possesses improved solubility compared to the native HBx, since it lacks the highly hydrophobic amino acid residues at the N- and C- termini [Lee, *et al.*, 2012]. Another member of the hepadnaviridae family is the avihepadnavirus that infects avian hosts. The duck hepatitis B virus (DHBV) is assumed to lack the X gene that encodes the HBx protein, which encodes transcription-regulatory proteins and is believed to contribute in the development of hepatocellular carcinoma. This is supported by the missing association of chronic DHBV infection with HCC development. However, the DHBV genome contains a hidden open reading frame from which a transcription-regulatory protein, designated as DHBx, is expressed both *in vitro* and *in vivo*. [Chang, *et al.*, 2001]. DHBx neither enhances expression of viral protein, intracellular DNA synthesis, nor production of virion when assayed in the full-length genome context in LMH (chicken leghorn male heaptoma) cells. However, similar to mammalian hepadnavirus X proteins, DHBx activates cellular and viral promoters *via* the Raf–mitogen-activated protein kinase signaling pathway which is localized primarily in the cytoplasm. The functional similarities as well as the low sequence homologies between both DHBx and the X proteins from the mammalian hepadnaviruses strongly suggest a common originate of ortho- and avihepadnavirus X genes [Chang, *et al.*, 2001]. The major genomic structural differences between members of the hepadnavirus family exist between mammalian and avian hepadnaviruses (Fig.7). It can be observed that the DHBV DNA is almost fully double stranded, whereas the mammalian hepadnaviruses possess only partially double-stranded DNA. The mammalian HBV have two pre-surface regions, preS1 and

Introduction

preS2, whereas the avian viruses only have one preS region [Chang, *et al.*, 2001]. Despite many studies regarding the functions of mammalian X proteins, no data so far excites concerning the precise structure of X-specific mRNA in infected cells from which this protein is translated [Yen, 1996]. Pekin ducks infected with duck hepatitis B virus (DHBV) is the most suitable and useful animal model for studying the life cycle of the hepadnaviruses. It is less convenient for studies of hepadnavirus-mediated hepatocarcinogenesis because DHBV chronic infection with ducks is not shown to be connected to the development of liver cancer [Duflot, *et al.*, 1995]. This is assumed due to the absence believe of the X gene in all known DHBV isolates [Feitelson & Miller, 1988]. Moreover, the existence of an open reading frame (ORF) in the hepadnavirus genomes isolated from grey herons [Netter, *et al.*, 1997] snow geese [Chang, *et al.*, 1999] a Ross goose [Netter, *et al.*, 1997] and white storks [Netter, *et al.*, 1997] in a position similar to that of the X gene of orthohepadnaviruses, disputes that an X-like protein may be expressed from avian hepadnavirus genomes. Many studies which investigate the activities of the highly divergent duck hepatitis B virus (DHBV) X protein have shown that this protein is not required for replication of DHBV [Chang, *et al.*, 2001; Lizzano, *et al.*, 2011]. In cell culture, HBx is localized in both cytoplasm and nucleus [Nomura, *et al.*, 1999; Chang, *et al.*, 2001; Henkler, *et al.*, 2001; Bontron, *et al.*, 2002]. Most studies show that HBx does not act by direct binding to DNA. The nuclear function of this protein in transcription is probably due to the reported ability to interact with several transcription factors and components of the basal transcription machinery. The association of HBx with mitochondria induces mitochondrial dysfunction [Shirakata & Koike, 2003; Lee, *et al.*, 2004], which could be involved in the apoptotic effects modulated by HBx, as mitochondria plays a major role in regulating cell death. Another mechanism which HBx affects apoptosis is by modulating the cellular Ca²⁺ signaling [Chami, *et al.*, 2003]. It is important to note that some of the HBx established activities are conserved among the X proteins, which are encoded by the other mammalian members of the viral family [Schuster, *et al.*, 2002] and are observed upon HBx expression in the context of the entire HBV genome [Schuster, *et al.*, 2000].

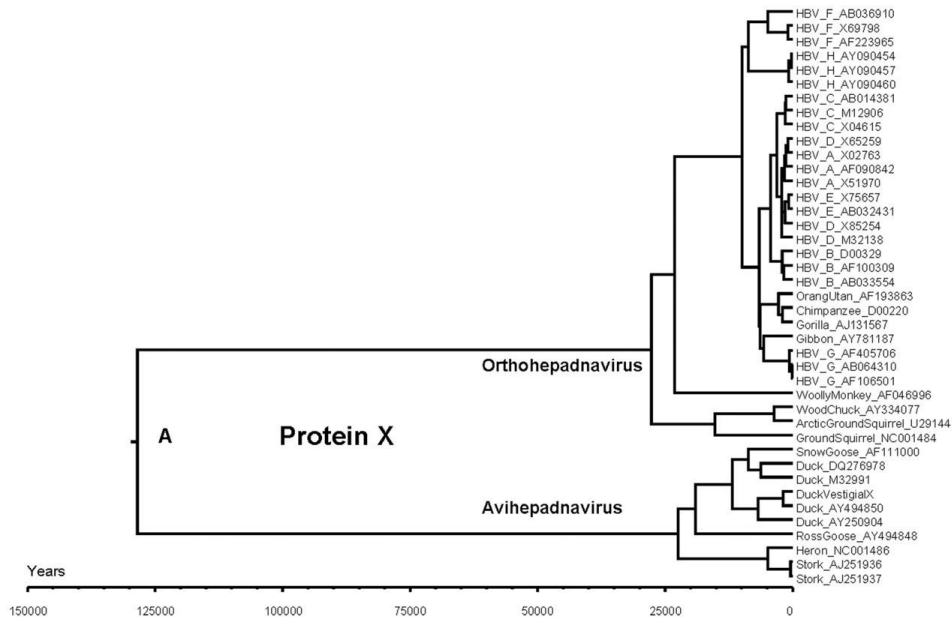


Figure 7: Phylogeny of hepadnaviral protein X. Virus strains are indicated by the common name of their hosts and the GenBank accession identifier. The evolutionary sequence of events is displayed in tree format. In the sequence marked ‘DuckVestigialX’, stop codons were replaced by coding triplets. In the other avian sequences, gaps were introduced at stop codon sites in the vestigial X reading frame prior to translation into protein. Taken from [van Hemert, *et al.*, 2011].

1.7. HBx protein as a transcriptional activator

The HBx protein is an activator of transcription with dual-specificity, when expressed in cell lines in culture; it stimulates signal transduction pathways in the cytoplasm and transcription factors in the nucleus, [Benn, *et al.*, 1996]. The mechanisms for transcriptional activation by HBx were investigated and several studies have suggested that HBx might stimulate transcription at the promoter by enhancing the binding or activity of the transcription factors and components of the transcription apparatus [Benn, *et al.*, 1996]. The transcriptional trans-activation role of HBx protein on the transforming growth factor beta 1 (TGF- β 1) protein may play an important role in liver inflammation and fibrosis [Murata, *et al.*, 2012]. TGF- β 1, encoded by *TGF- β 1* gene, is a cytokine that is produced in response to liver injury by activated hepatocytes, platelets and Kupffer cells [Gressner & Weiskirchen, 2006]. It triggers apoptosis, cell growth and differentiation in human hepatocytes, hepatoma cell lines and transgenic mice [Gressner, *et al.*, 1997; Gressner & Weiskirchen, 2006]. It also promotes the development of fibrosis and cirrhosis in chronic HBV infection and in other liver-related diseases [Sanderson, *et al.*, 1995]. HBx protein induces the expression of TGF- β 1 through transactivation of the *TGF- β 1* gene [Lee, *et al.*, 2001; Song, *et al.*, 2001; Pan, *et al.*, 2004; Murata, *et al.*, 2009]. Studies show that in HBx

transgenic mice and in hepatoma cell lines, HBx protein can transactivate the NF- κ B, MAPK/ERK, STAT3 and PI3K/ Akt cellular signaling pathways by inducing the production of the reactive oxygen species (ROS) [Murata, *et al.*, 2012]. Accumulation of ROS in human cancers is associated with anti-apoptotic activity, DNA damage and mutations that promote malignant transformation [Halliwell, 1999; Evans, *et al.*, 2004; Murata, *et al.*, 2012]. HBx also activates the transcription factor NF-kappa B during transient expression and induces prolonged formation, in a Ras-dependent manner, of transcriptional active NF-kappa B DNA-binding complexes [Wiseman & Halliwell, 1996; Su & Schneider, 1996; Murata, *et al.*, 2012]. Several Investigations showed that the HBx has an effect on HBV transcription and replication as an HBV mutant genome with a defective X gene. This leads to decreased levels of 3.5-kb HBV RNA and HBV replication intermediates. The C-terminal (amino acids [aa] 51 to 154), which contains the trans-activation domain, is required for the function of HBx, whereas the N-terminal (aa 1 to 50) is not required [Tang, *et al.*, 2005]. The alanine scanning mutagenesis strategy was used for demonstration, to observe that the regions from the amino acid 52 to 65 and 88 to 154 are important for the function of the HBx in HBV replication. These results suggest that HBx plays an important role in stimulating HBV transcription and replication, also the transcriptional trans-activation function of the HBx may be critical for its effect on the replication of HBV [Tang, *et al.*, 2005].

1.8. HBx DNA and protein methylation

HBx protein is known as an epigenetic de-regulating agent. It uses its oncogenic ability to induce promoter hypermethylation of certain cellular tumor suppressor genes that contribute to the development of liver cancer HCC [Zheng, *et al.*, 2009]. By modulating the transcriptional activation of DNMTs, HBx protein induces the hypermethylation of tumor suppressor gene promoters and stops their expression [Liu, *et al.*, 2006; Jung, *et al.*, 2007; Zhu, *et al.*, 2010]. HBx protein induces the hypermethylation of the *RAR β 2* gene by up-regulating DNMT1 and 3A activities and by simultaneously down-regulating the expression of the RAR β 2 protein [Arauz, *et al.*, 2002; Jung, *et al.*, 2007; Zheng, *et al.*, 2009; Jung, *et al.*, 2010]. Insulin-like growth factor binding 3 (*IGFBP-3*) is another potential tumor suppressor gene [Park, *et al.*, 2007]. Hypermethylation of the *IGFBP-3* gene is mediated by DNMT 1 and 3A, which is up-regulated *via* the transcriptional activities of HBx protein and this, is

associated with loss of *IGJBP-3* gene expression. *DLEC1* is a functional tumor suppressor gene silenced by promoter methylation in lung, gastric, colon and nasopharyngeal cancers [Kwong, *et al* 2007; Ayadi, *et al.*, 2008; Qiu, *et al.*, 2008; Seng, *et al.*, 2008; Niu, *et al.*, 2010]. HBx protein encoded by HBV genotype A enhances the transcription of the *DLEC 1* gene by increasing the level of histone acetylation through activation of HATs, leading to suppression of tumor progression [Niu, *et al.*, 2010].

Caveolin-1, encoded by the *caveolin-1* gene, is an integral membrane protein, expressed in adipose, fibrous and endothelial tissue [Tse, *et al.*, 2012]. HBx-induced methylation of the *Caveolin-1* gene promoter region suppresses its transcriptional activities and correlates with reduced tumor aggressiveness and metastasis, indicating a role of DNA methylation in HBV related HCC [Tse, *et al.*, 2012]. Hypermethylation of the *p16^{ink4a}* gene is a frequent event in several malignancies, including HBV [Takai, *et al.*, 2000; Jung, *et al.*, 2007; Ayadi, *et al.*, 2008; Kim, *et al.*, 2010]. HBx protein consents the expression of the *p16^{ink4a}* gene through the activation of DNA methyltransferase 1 and the cyclin D1-CDK 4/6-pRb-E2F1 pathway [Kim, *et al.*, 2010]. HBx protein induced DNA hypermethylation and has also been connected with the function loss of the *LINE-1*, *pRB*, *ASPP*, *E-cadherin*, *GSTP1* and *hTERT* tumor suppressor genes [Takai, *et al.*, 2000; Ferber, *et al.*, 2003; Lee, *et al.*, 2005; Ayadi, *et al.*, 2008; Niu, *et al.*, 2010; Zhao, *et al.*, 2010]. Aberrant methylation of these genes is supposed to induce perturbed cellular signaling pathways such as ubiquitination, DNA repair, transcription, proliferation and apoptosis, which may lead to the development of HBV related HCC [Park, *et al.*, 2007; Qiu, *et al.*, 2008; Niu, *et al.*, 2010].

1.9. HBx binding activities

Among viral gene products, the HBx protein has been described as “viral oncoprotein”. HBx is known to be involved in liver cell transformation because of its DNA repair, signaling pathways and its pleiotropic activities on cell cycle regulation [Thiagalingam, *et al.*, 2006; Benhenda, *et al.*, 2009]. HBx is thought to moderate various activities through its interactions with cellular factors. A number of cytoplasmic and nuclear targets have been reported to bind to HBx [Bontron, *et al.*, 2002]. HBx has been observed in viral replication that was detectable in dividing, but

not in quiescent hepatoma cells [Holiday, 2006; Thiagalingam, *et al.*, 2006; Martin-Lluesma, *et al.*, 2008]. Different mechanisms have been involved in the interaction of HBx with UV-damaged DNA binding protein 1 (DDB1), a protein which is involved in DNA repair and cell cycle regulation [Leupin, *et al.*, 2005; Martin-Lluesma, *et al.*, 2008]. The binding of HBx to DDB1 is essential for HBx in transcription activation and cell death induction in culture [Bontron, *et al.*, 2002]. Also, this binding is a conservation feature among the X proteins in mammals. Evidence has observed that this interaction is critical for the hepatitis B virus infection in woodchuck [Bontron, *et al.*, 2002]. DDB1 is a highly conserved functional protein expressed in both nucleus and cytoplasm [Hodgson, *et al.*, 2012]. DDB1 is considered a subunit of the E3 ubiquitin ligase Cul4 complex that functions as an adaptor for the ubiquitin-dependent degradation of target proteins [Bontron, *et al.*, 2002; Hu, *et al.*, 2004; O'Connell, *et al.*, 2007; van Hemert, *et al.*, 2012]. Mechanism deregulations that control the stability of the protein by the viral protein might contribute to eccentric cellular growth and tumor genesis.

Studies have reported the interaction of HBx with HBXIP, which is a major regulator of centrosome duplication and is required for bipolar spindle formation and cytokinesis. It is identified by its interaction with the C-terminus of HBx and is located at the human chromosome 1p13.3 [Wang, *et al.*, 2007]. This interaction observes to be responsible for the formation of a defective spindle and abnormal chromosome segregation [Forgues, *et al.*, 2003; Kim, *et al.*, 2008; Rakotomalala, *et al.*, 2008; Wen, *et al.*, 2008]. On the other hand, HBx has shown to interact with RNA and has the ability to compete with the cellular mRNA binding factor AUF1 [Rui, *et al.*, 2001; de Moura, *et al.*, 2005; Studach, *et al.*, 2009]. The interacting proteins include different functional moieties such as p53 [Edamoto, *et al.*, 2003; Moura, *et al.*, 2005; Dewantoro, *et al.*, 2006]. The p53 tumor suppressor is a protein involved in wide range of cellular processes that are known to be critical in maintaining the genomic integrity of the cells [Qadri, *et al.*, 1996; Thiagalingam, *et al.*, 2006; Zhao, *et al.*, 2010]. It is functionally inactivated by structural mutations [Smith, *et al.*, 1995], by viral proteins such as HBx and by endogenous cellular mechanisms in the human cancers. [Elmore, *et al.*, 1997]. HBx has been shown to form a complex with p53 in the cytoplasm, sequestering the protein and preventing its entry into the nucleus [Wang, *et al.*, 1994; Elmore, *et al.*, 1997]. P53 is an important regulatory protein

Introduction

involved in safeguarding the genomic integrity [Lane, 1992; Hsieh, *et al.*, 2004], sensing of DNA damage [Lee, *et al.*, 1995], monitoring G1 checkpoint of the cell cycle [Kasten, *et al.*, 1992; Clippinger, *et al.*, 2009] and activation of the cellular apoptosis program to kill cells with damaged genomes [Shaw, *et al.*, 1992; Ng, *et al.*, 2007]. The inactivation of p53 function through mutations or by interactions with viral proteins is a common event in human carcinogenesis and the majority of human cancers show mutations in the p53 gene [Hollstein, *et al.*, 1991; Lee, *et al.*, 1999; Russo, *et al.*, 2005]. Due to its both nuclear and cytoplasmatic localization, HBx interacts with bZIP family proteins such as ATF [Barnbas, *et al.*, 1997] and transcription factors such as NF-KB [Assogba, *et al.*, 2002; Payer & Lee, 2008], ATF2 and the JAK/STAT signal transduction pathways [Maguire, *et al.*, 1991; Kim, *et al.*, 2003], the protease tryptase TL2 [Takada, *et al.*, 1994], cellular proteins such as TBP (TATA-binding protein), CREB (cAMP-responsive element binding protein) and TFIIB [Qadri, *et al.*, 1995; Haviv, *et al.*, 1998; Wang, *et al.*, 1998]. It also interacts with proteasome subunits such as XAPC7 [Fischer, *et al.*, 1995] XAP2 [Kuzhanaivelu, *et al.*, 1996] and finally XIP [Melegari, *et al.*, 1998]. HBx activates host genes such as the proto-oncogenes *c-myc* [Balsano, *et al.*, 1991], *c-fos* [Avantaggiati, *et al.*, 1993] and *c-jun* [Twu, *et al.*, 1993; Rui, *et al.*, 2005]. Recently, it has been speculated that HBx can directly interact with the anti-apoptotic proteins Bcl-2 and Bcl_{xL} through its BH3-like motif, which results in elevated cytosolic calcium, efficient viral DNA replication and the induction of programmed cell death [Geng, *et al.*, 2012; Kusunoki, *et al.*, 2014]. Although some HBx activities that interfere with the divisive cell cycle remain to be unclear, these data provide insights into possible mechanisms which might lead to a deregulation of the cellular mitotic machinery by a viral protein [Benhenda, *et al.*, 2009]. These observations also provide a strong link between the expression of the HBx and chromosomal instability in HBV-related carcinogenesis [Benhenda, *et al.*, 2009].

2. Aims of this project

Hepatitis B is a potentially life-threatening liver infection caused by the hepatitis B virus. It is a major global health problem. HBV causes acute and chronic liver diseases of variable severity by mechanisms that are thought to be largely immune mediated. Prevention of HBV-infection through vaccination has been routinely practiced and antibodies against the HBsAg have been shown to be effective in preventing infection after exposure to this agent. However, approximately 5 to 10% of healthy vaccine recipients fail to produce protective levels of antibodies to the hepatitis B vaccine after standard immunization; this is caused by a failure to mount an appropriate immune response to HBV. This phenomenon has been observed in all vaccine evaluation studies, irrespective of the HBsAg vaccine used. The hepatitis B virus (HBV) HBx protein is a small transcriptional activator that is essential for virus infection. The activity of the HBx has been linked to liver carcinoma caused by HBV on the basis of its ability to induce liver tumors in transgenic mice in certain genetic contexts. Research concerning the functions of HBx proteins has been mired in an ever-expanding list of interacting host cell proteins. As such there is no consensus on the exact function of this protein in the HBV lifecycle, and importantly, which role this protein plays in the development of HBV-related HCC.

In this study, HBx proteins (Full HBx, mini HBx, DHBx) were selected for functional and structural investigations. The examinations of these proteins in terms of specificity, oligomerization of the intermediate products and interaction of these proteins with partly and fully processed binding partners resulted in new insights concerning the proteins maturation. Previous attempts in producing HBx from *E. coli* cells suggested that the expression and purification of HBx using these cells would be technically very challenging due to the biochemical nature of HBx. However, progress could only be made regarding the expression, purification, function and structure of HBx by the use of different technical methodologies. This work significantly aims to obtain structural insights and to improve the understanding of the nature of HBx protein by providing new avenues for the production and purification of prokaryotic HBx. Although the structural aspects and potential functions of the HBx proteins are till now only poorly understood, it is necessary to gain information and to obtain insights regarding the structure-function-relationship of HBx proteins by

Aim of the Project

using X-ray crystallographic, solution studies such as SEC-SAXS and electron microscopy.

3. Materials and Methods

3.1. Materials

3.1.1. Devices

Table 3. Selected devices:

Incubator	37-30 °C Incubator Kelvitron® T (Thermo scientific, USA), 4 °C Incubator (Rubarth, Germany), 20 °C Incubator (Rubarth, Germany)
PCR machines	UNO II (Biometra, Germany)
Sonifier	Branson Sonifier 250/450 (Emerson Electric Co, USA)
Centrifuge	Centrifuge 5804R/5810R/5415R/5424 (Eppendorf, Germany), Centrifuge Minispin® Plus (Eppendorf, Germany), Optima TL ultracentrifuge (Beckman Coulter, USA)
Micropipette	Micropipette Research (Eppendorf, Germany)
Spectrophotometer	GeneQuant 1300 (GE Healthcare, UK), Nanodrop 2000c (Thermo Scientific, Peqlab, Germany), GENios microplate reader (Tecan, Schweiz)
Balance	TE3102S (Sartorius AG, Germany), LP224S-OCE (Sartorius AG, Germany)
Thermomixer	Thermomixer comfort (Eppendorf, Germany)
Microwave	Microwave MR-6450 (Hitachi, Japan)
Thermocycler	Mastercycler® gradient, Mastercycler® personal (Eppendorf, Germany)
Electrophoresis power supply	EV 231 (Peqlab, Germany), Power PAC 200 (Bio-Rad, Germany)
SDS-PAGE	EV734 Power Supply (Consort, Belgium)
Microbalance	Sartorius CP224S-OCE (Sartorius, Germany)
pH meter	SevenEASY (Mettler Toledo, USA)
Hot-plate magnetic stirrer	VMS-A (VWR, USA), MR 3001 (Heidolph, Germany)
shaker	IRC-1-U (Adolf Kühner AG, Switzerland), Innova® 43/43R (New Brunswick Scientific, USA), Innova® 4330 (New Brunswick Scientific, USA), GFL 3017 (GFL, Germany)
CD spectrometer	J-815 (Jasco, UK)
Freezer (-20 °C)	Liebherr premium (Liebherr, Germany)
DLS instrument	SpectroSIZE 300 (Xtal-Concepts)
Acryl amide gel chamber	SE275 (Hofer)
Agarose gel chamber	SE260 Mighty Small II Deluxe Mini electrophoresis unit (Hofer)
Pipetting robot	Honeybee 961 (Zinsser Analytic GmbH, Germany), Oryx 4 (Douglas, UK)
UV-light source	CrystalLIGHT 100 (Nabitec, Germany)
SONICC	(Benchtop, Formulatrix.Inc, USA)
Crystal plate incubator	RUMED 3001 (Rubarth, Germany) incubators
Crystal imaging system/device	CrystalScore (Diversified Scientific Inc., USA), microscope SZX12 with camera DP10 (both Olympus, Japan)
Octet HTX system	Forte` Bio, (Pall Corp, Germany)

3.1.2 Plasmids

The pMAL vector enables an easy expressing and purifying strategy of a produced protein from a cloned gene, due to the encoded MBP. The cloned gene is inserted downstream from the malE gene of *E. coli*, which encodes the maltose binding

protein C. The use of MBP results in the expression of an MBP fusion protein [Guan, 1987; Maina, 1988]. The method uses the strong ‘tac’ promoter and the malE translation initiation signals to give high-level expression of the cloned gene [Duplay, 1984; Amann, 1985]. Also, it enables a one-step purification of the fusion protein using MBP’s affinity for maltose [Kellerman, 1982]. The pMAL-c2x vector (Addgene, Germany) (Fig. 8) is designed so that insertion inactivates the β -galactosidase α -fragment activity of the malE-lacZ α fusion, which results in a blue to white color change on X-gal plates when the construct is transformed into an α -complementing host such as TB1 [Johnston, 1986] or JM107 [Yanisch, *et al.*, 1985]. The pMAL-c2x has a spacer between malE and the Factor Xa site, which allows some fusion proteins to bind more tightly to the amylose resin. Additionally, it possesses an M13 origin for making single stranded DNA, resulting in cytoplasmic expression of the fusion protein. The vector also includes a sequence coding for the recognition site of a specific protease. This allows the protein of interest to be cleaved from MBP after purification, without adding any vector-derived residues to the protein.

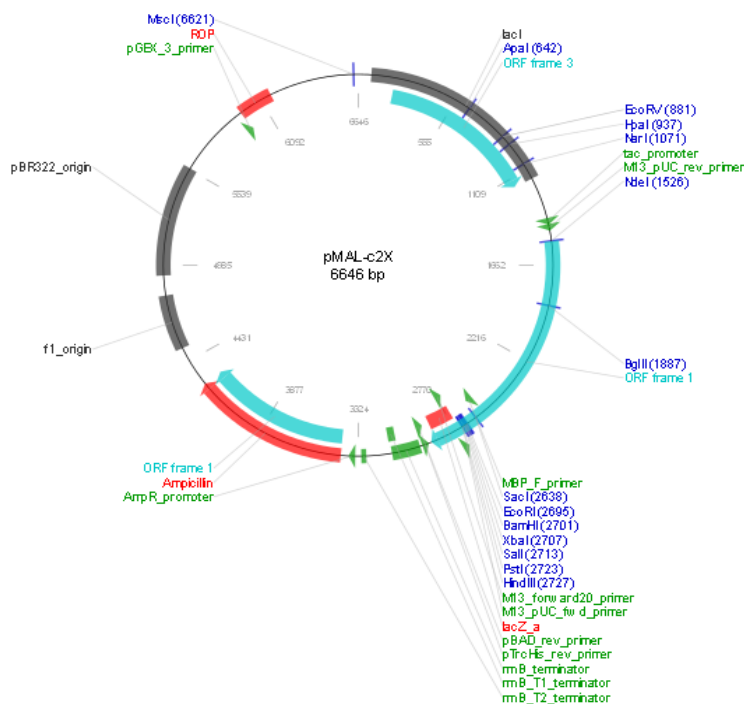


Figure 8: Vector map for pMAL-c2x. Taken from Addgene, Germany

The pMAL-p5x (NEB, UK) (Fig.9) is also a plasmid cloning vector designed for recombinant protein expression and purification, which uses the pMAL protein fusion and purification system [Takagi, 1988; Lauritzen, 1991]. It contains the pMB1 origin

of replication from pBR322 and is maintained at a similar copy number as compared to pBR322. The pMAL-p5x possesses a universal multiple cloning site (MCS) that is followed by stop codons in all three reading frames. The multiple cloning site (MCS) is positioned in a way to allow translational fusion of the *E. coli* maltose binding protein (MBP, encoded by the *malE* gene) to the N-terminus of the cloned target protein. In the pMAL-p5x vector, the signal peptide on pre-MBP, directs fusion proteins to the periplasm, for fusion proteins that can be successfully exported. This allows protein folding and disulfide bond formation to take place in the periplasm of *E. coli* and enables purification of the protein from the periplasm. In addition, *lacZα* and the M13 origin have been removed. In this vector, MBP has been engineered for tighter binding to amylose. This allows easy purification of the fusion protein, and the MBP domain can be subsequently removed using Factor Xa protease [Takagi, 1988]. Transcription of the gene fusion is controlled by the inducible ‘*tac*’ promoter (Ptac). Basal expression from Ptac is minimized by the binding of the Lac repressor, encoded by the *lacI q* gene, to the *lac* operator immediately downstream of Ptac. A portion of the *rrnB* operon, containing two terminators derived from the vector pKK233-2, prevents transcription originating from Ptac from interfering with plasmid functions.

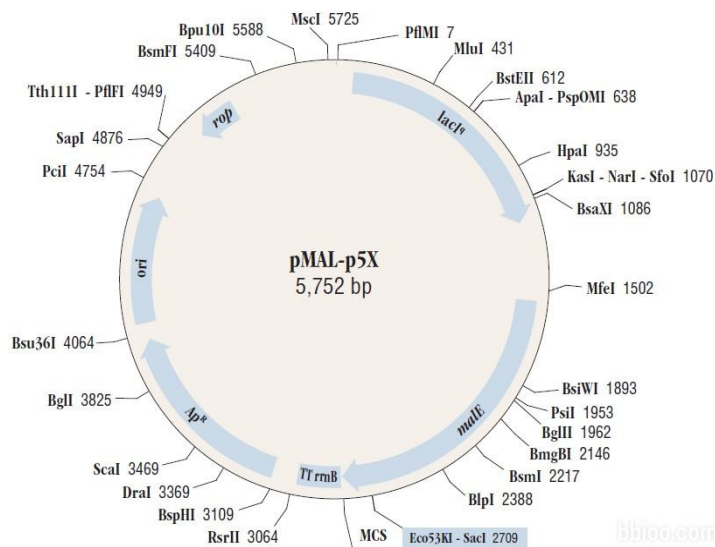


Figure 9: Vector map for pMAL-p5x. Taken from NEB, UK

Table 4: Amino acid sequences of the HBx proteins

DNA sequence	
DHBx	NLYFQGLNLDASYLTQPLFATNVIRRYHGILLCWPN CSNLYNCTLSRANIILLTAHPGTDRLIGRLFHTPLSRK QYIFHIGYVELKNYTPLLRSCLPRYLYVYIAVVVDCD TFGMVHCL
Full HBx	AARLCCQLDPARDVLCLRPVGAESCGRPFSGSLGTL SPSPSAVPTDHGAHLSLRGLPVCASFSSAGPCALRFTS ARRMETTVNAHRMLPKVLHKRTLGLSAMSTTDLEAY FKDCLFKDWEELGEEIRLKVFVVLGGCRHKLYCAPAP CNFFTSA
mini HBx	RPVGAESSGRPFSGSLGTLSSPSPSAVPTDHGAHLSL RGLPVSAFSSAGPSALRFTSARRMETTVNAHRMLPK VLHKRTLGLSAMSTTDLEAYFKDSLFKDWEELGEEI RLKVFVVLGGSRHKLY

3.1.3. Oligonucleotides for cloning

oligonucleotides for cloning		
pMAL-c2x with the forward and reverse primers		
DHBx	Forward	GGGGATCCTCTTCTGGTGGTGGTGGTTCTTCTGAAAACCTGTATTTCCAGGGC
	Reverse	CGAAGCTTTAGTCATAAACAATGGTACATACCAAA
mini HBx	Forward	GGGGATCCTCTTCTGGTGGTGGTGGTTCTTCTGAAAATCTGTATTTCCAGGGT
	Reverse	CGAAGCTTCTATCATCACACCAGTTTATGACGAGAACC
Full HBx	Forward	GGGGATCCTCTTCTGGTGGTGGTGGTTCTTCTGAAAATCTGTATTTCCAGGGT
	Reverse	CGAAGCTTCTATCATTAGGCGGAGGTGAAAAAGTTACA
pMAL-p5x with only reverse primers-with the same forward primers shown above		
DHBx	Reverse	CGGAATTCCTATCATATAACAATGGTACATACCAAAGG
mini HBx	Reverse	CGGAATTCCTATCATCACACCAGTTTATGACGAGAACC
Full HBx	Reverse	CGGAATTCCTATCATTAGGCGGAGGTGAAAAAGTTACA

3.1.4. Buffers and solutions

For all buffer preparations double distilled water was used and the pH was adjusted with HCl or NaOH.

Table 5: General buffers

Solution	Composition
(1×TAE)-Tris-acetate-EDTA (Agarose gel electrode buffer)	80 mM Tris, 40 mM Acetic Acid, 2 mM EDTA
DNA loading buffer	30% glycerol, 0.25% Bromophenol Blue, 0.25% Xylene Cyanol
2x protein loading buffer	500 mM Tris-HCl, pH 6.8, 5mM DTT, 10% SDS, 0.5% Bromophenol Blue, 50% Glycerol

Table 6: Bacteria cell culture

Solution	Composition
LB-medium/ agar	1.0 % Bacto-Trypton, 0.5 % Bacto-Yeast-Extract, 1.0 % NaCl in dH ₂ O, autoclaved. For LB-agar: 1.5 % agar in LB-medium
Selective antibiotic	100 mg/ml ampicillin in 10 ml water; stock solution 34 mg/ml chloramphenicol in 100% ethanol (abs.); stock solution
IPTG	1 M in dH ₂ O, autoclaved; stock solution

Table 7: Bacterial strains

Strain	Resistance/ selection marker	Supplier
BL21 Star™ (DE3)	/	Invitrogen
BL21 DE3	/	Invitrogen
BL21 AI	/	Invitrogen
DH5α™	Nalidixic acid	Invitrogen
XL10-Gold	Nalidixic acid, tetracycline, chloramphenicol	Stratagene
Shuffle T7	/	NEB

Table 8: Competent cells

Solution	Composition
CaCl ₂	100 mM CaCl ₂ , autoclaved
CaCl ₂ buffer	100 mM CaCl ₂ , 10 % glycerol, (glycerol addition after autoclaving)

Table 9: Agarose gel electrophoresis

Solution	Composition
1% Agarose	1g in 100ml in dH ₂ O
Loading dye	0.05 % Bromophenol Blue, 0.25 % Xylene Cyanol, 1 mM EDTA, 50 % glycerol
Ethidium bromide	10 mg/ml in dH ₂ O

Table 10: Molecular weight markers

Solution	Composition
Protein marker (SDS-PSGE)	Bench Mark prestained protein ladder (Invitrogen, Karlsruhe, Germany)
Protein marker (native gel)	SERVA Native Marker Liquid Mix for BN/CN (SERVA, Germany)
DNA marker	1kb DNA ladder, (Invitrogen, Karlsruhe, Germany)

Table 11: Native gel preparation

Solution	Composition
Native gel	SERVAGel™N 3-12, Vertical Native Gel 3-12%

Table 12: SDS-PAGE preparation

Solution	Composition
2 x sample buffer	2.0ml (10 %) SDS (w/v), 1.25ml (0.5M) Tris, pH 6.8, 2.5ml (100%) glycerol, 0.2ml (0.5 %) Bromophenol Blue (w/v), 0.05 % β-mercaptoethanol (v/v) or DTT in 3.55 ml dH ₂ O
APS	10 % in dH ₂ O
Electrode buffer 10×	30.0g Tris, 1440g Glycine, 10.0g SDS, in 1L dH ₂ O
Separating gel buffer	1.5 M Tris/HCl, pH 8.8 in 100ml dH ₂ O
Stacking gel buffer	0.5 M Tris/HCl, pH 6.8 in 100ml dH ₂ O
SDS buffer	10 % (w/v) in dH ₂ O
Staining solution	0.25% (w/v) Coomassie Brilliant Blue G-250, 25% (v/v) 2-propanol 10% (v/v) acetic acid
Distaining solution	20% (v/v) acetic acid

Table 13: GST agarose regeneration

Solution	Composition
Regeneration solution 1	100mM Tris-HCl, 0.5M NaCl, pH 8.5
Regeneration solution 2	100mM sodium acetate, 0.5M NaCl, pH 4.5

Table 14: Ni-NTA agarose regeneration

Solution	Composition
SDS buffer	2 % (w/v) in dH ₂ O
EDTA buffer	100 mM, pH 8.0 in dH ₂ O
NiSO ₄ buffer	100 mM in dH ₂ O
Regeneration buffer	6 M guanidine chloride, 0.1 M acetic acid
Ethanol buffers	25, 50, 75 % ethanol in dH ₂ O

Table 15: Staining solution for negative staining

Solution	Composition
Staining solution	0.2 g of uranylacetate in 10ml dH ₂ O (kept in the dark)

Table 16: Protein purification

For the target HBx proteins	
Solution	Composition
Lysis, column, washing buffer	20mM Tris, pH 7.4, 200 mM NaCl, 1mM EDTA, 1mM DTT
Elution buffer	20mM Tris, pH 7.4, 200 mM NaCl, 1mM EDTA, 1mM DTT, 10mM Maltose
Gel Filtration buffer	20mM Tris, pH 7.4, 200 mM NaCl, 1mM EDTA, 1mM DTT
CD (Circular Dichroism)	20mM Tris, pH 7.4, 50 mM NaCl, 1mM EDTA, 1mM DTT
SEC-SAXS	20mM Tris, pH 7.4, 200 mM NaCl, 1mM EDTA, 4mM DTT, 4% (v/v) glycerol
Lysis, column, washing buffer (for EM)	20mM Tris, pH 7.4, 200 mM NaCl, 1mM EDTA, 1mM DTT, protease inhibitor cocktail (Roche)
when using shuffle cells	
Solution	Composition
Lysis buffer	50mM Tris, pH 7.5, 150mM NaCl, 1mM EDTA, 1mM DTT, 1mM PMSF, protease inhibitor cocktail (Roche), 20mg/ml Lysozyme
Binding washing buffer	50mM Tris, pH 7.5, 150mM NaCl, 1mM EDTA
Elution buffer	50mM Tris, pH 7.5, 150mM NaCl, 1mM EDTA, 1mM DTT, 10mM Maltose
Gel Filtration buffer	50mM Tris, pH 7.5, 150mM NaCl, 1mM EDTA, 1mM DTT
For P53 proteins	
Solution	Composition
PBS(Lysis, equilibrium, washing buffer)	137mM NaCl, 2.7mM KCl, 10mM Na ₂ HPO ₄ , 2mM KH ₂ PO ₄ , pH 8.0
Elution buffer	50mM Tris, pH 8.0, 25mM reduced glutathione
CD (Circular Dichroism)	50mM Tris, pH 8.0, 50mM NaCl
Gel Filtration buffer	50mM Tris, pH 8.0, 150mM NaCl
Dialysis buffer	50mM Tris, pH 8.0
For TEV protease	
Solution	Composition
Lysis, column, washing buffer	50mM NaH ₂ PO ₄ , pH 8.0, 100mM NaCl, 25mM imadizol, 10% (v/v) glycerol
Elution buffer	50mM NaH ₂ PO ₄ , pH 8.0, 100mM NaCl, 250mM imadizol, 10% (v/v) glycerol
Dialysis (storage) buffer	50mM Tris, pH 8.0, 150mM NaCl, 1mM EDTA, 1mM DTT
Dialysis buffer after protein cleavage (stabilizing buffer)	20mM Tris, pH 8.0, 25mM NaCl, 500mM urea, 0.05% SDS

3.2. Methods

3.2.1. Molecular biology methods

3.2.1.1. PCR

PCR was performed for DNA fragment amplification by using the *pfu/taq*-polymerase (Invitrogen, USA). The reaction was carried out with a thermocycler (Eppendorf, Germany) and the samples were applied according to the standard protocol. For the reaction, primers (Metabion, Germany) were diluted to a final

concentration of 20pM and 1 μ l of each forward and reverse primer was used, in addition to 1 μ l (approx. 100 ng) template. The first step in the amplification reaction was denaturation for 2 min at 96°C followed by denaturation for 30sec at 96°C. The second step, annealing, was performed for 1 min at 54°C (based on the oligonucleotide annealing temperature, determined by the supplier) and was followed by the third step, elongation, for 1 min at 72°C. The elongation step could be modified based on the number of base pairs to be amplified, as *Taq*-polymerase is able to amplify 1,000 base pairs per minute. 30cycles were used when performing this procedure. When the reaction was carried out overnight, samples were stored at 4°C within the PCR device. The final PCR product was analyzed by gel electrophoresis using 1 % agarose gels. For a single PCR reaction, the components listed below were typically mixed in a 0.5ml reaction tube and placed in a thermocycler.

components	amount
DNA template up to 100 ng	1 μ l
Polymerase buffer (10 \times) (Thermo Scientific)	5 μ l
dNTPs, (2 mM)	5 μ l
Forward primer	1 μ l
Reveres primer	1 μ l
<i>Pfu/taq</i> polymerase (2.5 U μ l ⁻¹ / 1 U μ l ⁻¹) (Thermo Scientific)	1 μ l
MgCl ₂ (25 mM; for Mg ²⁺ -free <i>taq</i> polymerase buffer)	3 μ l
DMSO	2 μ l
dH ₂ O	ad 50 μ l

3.2.1.2. DNA purification

To separate the PCR products from salts and DNA-fragments, purification was performed by using the PCR clean-up kit (NucleoSpin Extract II Kit, Macherey-Nagel). All steps were carried out according to the manufacturer's specifications. Instead of elution buffer, 50 μ l dH₂O was used to extract the DNA.

3.2.1.3. Restriction digestion of DNA fragments

Restriction enzyme digestion was used to either prepare DNA fragments for ligation preparation into a plasmid or to examine the success of ligation. In the cloning procedure, all fragments were ligated into pMAL-c2x and pMAL-p5x vectors (addgene, Germany). PCR products and vectors were digested for 2h at 37°C using conditions according to the manufacturer's protocol. After digestion, the vectors were dephosphorylated by addition of 1 μ l calf intestinal alkaline phosphatase (CIAP)

followed by incubation at 37°C for 1h, while the digested DNA fragments were stored on ice.

The PCR products and vectors were purified separately (Section 3.2.1.2); the PCR products were eluted in 50µl dH₂O, whereas the vectors were eluted in 30µl dH₂O. To verify the success of cloning, 0.5µg of DNA preparation was digested with relevant restriction endonucleases after transformation in *E. coli*, typically using *BamHI* and *HindIII* (NEB, USA) for the pMAL-c2x vector and *EcoRI* and *HindIII* (NEB, USA) for the pMAL-p5x vector and were then visualized by agarose gels.

3.2.1.4. Agarose gel electrophoresis

Agarose electrophoresis is a technique that is used to separate DNA fragments based on their size. Negatively charged DNA is attracted by the anode and moves through an agarose gel with a rate depending on agarose concentration, size and conformation of the fragment and the power used during electrophoresis. DNA samples were applied to a 1% agarose gel and further analyzed. The gel was prepared by dissolving 1% (w/v) agarose in 1×TAE buffer supplemented with 5µl ethidium bromide solution (Sigma, USA) to visualize the DNA fragments with UV-light. The DNA sample was mixed with 6×DNA loading dye and applied to the gel. A suitable size marker was used to estimate the length of the DNA fragments. The electrophoresis run was performed at a constant voltage of 100V. The DNA fragments from the PCR and restriction digestion were exposed to UV light for detection, were then cut out from the gel with a scalpel and were further purified using the peqGOLD gel extraction kit (PEQLAB Biotechnology GmbH).

3.2.1.5. Ligation

Plasmid vectors and DNA fragments were ligated using a molecular ratio of 1:5 with the addition of 1 µl of T4 ligase and 2µl of 10x ligation buffer in a total volume of 20 µl. The reaction mixtures were incubated overnight at 18°C. Afterwards the ligation mixtures were directly incubated at 65°C for 15 min to stop the reaction of the T4 ligase. The reaction mixtures were transformed into XL10-Gold or DH5α *E.coli* cells. The cells were plated out onto agar plates containing 100 mg/ml ampicillin and were further incubated overnight at 37°C.

$$\frac{m_{\text{vector}}[\text{ng}] \times l_{\text{insert}}[\text{kb}]}{l_{\text{vector}}[\text{kb}]} \times \frac{m_{\text{insert}}}{\text{vector}} = m_{\text{insert}}[\text{ng}]$$

$\mathbf{l}_{\text{insert}}$ = Length of the insert DNA

$\mathbf{l}_{\text{vector}}$ = Length of the vector DNA

$\mathbf{M}_{\text{insert}}$ = Mass of insert DNA

$\mathbf{m}_{\text{vector}}$ = Mass of vector DNA

$\mathbf{mr}_{\text{insert} / \text{vector}}$ = Molar ratio insert: vector

3.2.1.6. Preparation of chemically competent cells with CaCl_2

A single *E.coli* colony or a 100 μl *E.coli* glycerol stock was used to inoculate 100 ml Luria Bertani (LB)-medium and was incubated overnight at 37°C. The overnight culture was diluted to 1:50 in LB-medium (10 ml of overnight culture was added to 500 ml LB-medium) and incubated at 37°C until reaching an optical density of 0.6-0.8 at 600 nm wave length.

After reaching the required OD600, the solution was cooled immediately on ice for 10 min and then centrifuged at 4°C for 10min at 4000rpm. The supernatant was discarded and the cells were resuspended with 10ml of a sterilized solution containing 0.1M CaCl_2 /10% (w/v) glycerol and incubated for 15min on ice. The suspension was again centrifuged for 10min at 4000rpm at 4°C and the supernatant was discarded. The cells were resuspended in 1 ml of 0.1M CaCl_2 /10% (w/v) glycerol solution. Aliquots of 100 μl were prepared, shock frozen in liquid nitrogen and stored at -80°C.

3.2.1.7. Isolation and purification of plasmids

The XL10-Gold and *E. coli* DH5 α strains were used for the preparation of DNA plasmids. DNA plasmid amplification was performed on a preparative scale by incubating a 5ml *E. coli* culture at 37°C overnight. The amplified DNA was isolated from cells using the peqGOLD mini-prep kit1 (PEQLAB Biotechnology GmbH), according to the manufacturer's instructions. After preparation of the samples, the nucleic acid concentrations were determined using a Nanodrop spectrophotometer at a wavelength of 260nm. Purity of the isolated DNA was determined by calculation of the ration between absorption at 260nm and 280nm.

3.2.1.8. DNA-Sequencing

To investigate the success of cloning or mutation insertion, plasmid DNA was sequenced by SeqLab with extended hotshot sequencing. Samples were prepared by mixing 5µl of DNA with 5µl of forward or reverse primer.

3.2.1.9. Transformation of *E.coli* cells

An aliquot of chemically competent cells was incubated with 1 µl (100 ng) of the plasmid DNA for 30min on ice. A thermomixer (Eppendorf, Germany) was preheated to 42°C and the cell-DNA mixture was incubated for 45sec at 42°C. Subsequently the sample was cooled on ice for 1min and 500µl sterile LB-medium was added. The suspension was then incubated for 1h at 37°C under continuous shaking at 300rpm. Cells were resuspended with residual LB-medium and plated in a sterile environment, with plates containing 1.5 % agar-agar supplemented with a selective antibiotic. After incubation at 37°C overnight, colonies were picked and further analyzed. For subsequent DNA isolation, competent *E. coli* XL10-Gold or DH5α cells were used. For expression, several cells such as BL21 DE3, BL21 Star (DE3), BL21 AI, and shuffle cells were used for transformation.

3.3. Biochemical methods

3.3.1. Recombinant expression of the HBx genes

A pre-culture of 250ml LB-medium containing 100µg/ml ampicillin (Amp) (Roth, Germany) was inoculated in a 1L flask with one single colony from the transformed *E. coli* cells and incubated over night at 37°C under continuous shaking at 180rpm. The main culture was prepared by a 1:50 dilution of the overnight pre-culture into 1L LB medium containing the same antibiotic in a 5L flask followed by incubation at 37°C until the OD600 value reached approximately a value of 0.5-0.6. 1ml of the growth culture was collected for electrophoresis analysis. Subsequently, protein expression was induced by adding IPTG to a final concentration of 0.03mM, followed by cultivation at 30°C for 5 hours. When using the Shuffle cells, protein expression was induced by adding IPTG to a final concentration of 0.5mM, followed by an overnight cultivation at 37°C [Sidhu, *et al.*, 2014]. 1ml of the cell suspension was collected for analysis of the protein expression level. The collected samples were analyzed by SDS-PAGE after centrifugation at 4°C for 10min at 12.000rpm and discarding the supernatant. The cell pellet was resuspended in 50µl of 2×sample

buffer and boiled at 96°C for 10min. The denatured samples were loaded onto a 10% SDS-PAGE gel for further examination. The suspended volume of the sample that was analyzed by SDS-PAGE was calculated using the following formula:

$$V_{Sample}(t_n) = \frac{OD_{600}(t_0) \times 1000 \mu l}{OD_{600}(t_n)}$$

$V_{sample}(t_n)$ = The extracted volume for SDS-PAGE in μl of the cell suspension at time $t_n = 1, 2, 3$ or 4 h after induction.

$OD_{600}(t_0)$ = Optical density at a wavelength of 600 nm immediately prior to the induction.

$OD_{600}(t_n)$ = Optical density at a wavelength of 600 nm at the time $t_n = 1, 2, 3$ or 4 h after induction.

The cells of the large-scale expression culture were harvested after 5hrs of incubation by centrifugation at 4°C for 30min at 12.000rpm. The supernatant was discarded and the pellet was stored at -20°C.

3.3.2. Recombinant expression of the p53 genes

A pre-culture of 250ml LB-medium containing 100 μ g/ml ampicillin (Amp) (Roth, Germany) was inoculated in a 1L flask with one single colony from the transformed *E. coli* BL21 DE3 cells and incubated over night at 37°C under continuous shaking at 160rpm. The main culture was prepared by diluting the overnight pre-culture by 1:50 and addition of 50 ml into 1L LB medium containing the appropriate antibiotic within a 5L flask. This culture was incubated at 37°C until the OD600 value reached approximately 0.6-0.7. 1ml of the growth culture was collected for electrophoretic analysis. Subsequently, the p53 proteins expression were induced by addition of IPTG to a final concentration of 1mM, followed by cultivation at 30 °C for 5hours. For analysis of the protein expression level, 1ml of the cell suspension was collected. The samples were analyzed by SDS-PAGE after centrifugation at 4°C for 10min at 12.000rpm and discarding the supernatant. The cell pellet was resuspended in 50 μ l of 2 \times sample buffer and boiled at 96°C for 10min. The denatured samples were loaded on a 15% SDS-PAGE gel for following examination. The cells of the large-scale expression culture were harvested after 4hrs of incubation by centrifugation at 4°C for 45min and 4.000rpm. The supernatant was discarded and the pellet was stored at -20°C for further studies.

3.3.3. Tobacco etches virus (TEV) protease expression

Glycerol stocks of TEV-protease mutant S219V overproducing BL21 (DE3)-RIL cells were obtained from Dr. Nasser Yousef. TEV protease was encoded on the pRK793 plasmid under *lac*-operon control. An overnight culture was grown at 37 °C in LB medium with addition of 34µg/ml chloramphenicol (Cam) (Sigma, USA) and 100µg/ml ampicillin (Amp) (Roth, Germany).

The overnight culture was diluted 1:50 in the same medium as used for the overnight culture and grown until the OD600 reached a value of 0.6-0.7. The expression was induced by adding Isopropyl β-D-1-thiogalactopyranoside (IPTG) (Roth, Germany) to a final concentration of 1mM, followed by cultivation at 30 °C for 4hours. After 4hrs of incubation the cells were harvested by centrifugation at 4°C for 30min and 12.000rpm. The supernatant was discarded and the pellet was stored at -20°C.

3.3.4. Preparation of TEV protease glycerol stocks

For glycerol stock preparation, respective plasmids were transformed into *E. coli* BLR (DE3) expression cells and plated on LB-Amp agar. An overnight culture was inoculated with a single colony and incubated at 37 °C. 800µl of overnight culture was mixed thoroughly with 200 µl of glycerol, frozen in liquid nitrogen and stored at -80°C.

3.3.5. Cell disruption for protein purification

To determine whether the target protein is expressed in a soluble form or in inclusion bodies, which is an insoluble form, the stored cell pellets were resuspended in 30ml of lysis buffer. To guarantee a complete solubilization of the proteins, sonification was carried out with the resuspended pellets using a Branson sonifier 250 (Emerson Electric Co, USA). Sonification was applied 5 times for 30sec at 250W followed by 10sec incubation on ice, respectively. The lysate was centrifuged at 12.000rpm for 30min at 4°C and the supernatant, which contains the soluble form of the target protein, was transferred into a fresh tube. Both the supernatant and the pellet were analyzed on a 10% SDS-PAGE gel and stored at 4°C.

3.3.6. Purification of the HBx fusion proteins

The purification of the HBx fusion proteins was carried out by affinity column chromatography using an amylose matrix (NEB, Germany). After equilibration of the

column resin with 8CVs of lysis buffer, the stored supernatant from the *E. coli* cell lysis was added to the amylose resin and incubated on a roller rocker at 4°C for 45 min. All subsequent purification steps were performed at 10°C. The matrix was washed with 3CVs of column buffer followed by an elution step with 3CVs of the same buffer additionally containing 10 mM maltose. The fractions were collected in pre-chilled (4°C) falcon tubes to reduce protein aggregation and further analyzed by SDS-PAGE. The protein concentrations in the purified fractions were determined using a Nanodrop spectrophotometer at a wavelength of 280 nm. The protein concentration was determined according to the following formula:

$$C = \frac{A_{280} \times MW}{\epsilon \times d}$$

C = Protein concentration

A₂₈₀ = Specific absorption at 280 nm

MW= Molecular weight

ε = Extinction coefficient

d= Thickness of the cuvette

3.3.7. Purification of the p53 proteins

Purification of the p53 protein was carried out by affinity column chromatography using a GST matrix (Qiagen, Germany). After equilibration of the column resin with 6 CVs of lysis buffer, the stored supernatant from *E. coli* cell lysis was added to the GST resin and the column was incubated on a roller rocker at room temperature for 2hrs. All subsequent purification steps were performed at room temperature. The matrix was washed with 4CVs of column buffer followed by an elution step with 4 CVs of the elution buffer containing 25 mM reduced glutathione. The fractions were collected in falcon tubes and analyzed by SDS-PAGE. The protein concentration in the purified fractions was determined using a Nanodrop spectrophotometer at a wavelength of 280 nm.

3.3.8. Purification of the TEV protease

After cell disruption and centrifugation, the supernatant was incubated with previously equilibrated Ni-NTA agarose (Qiagen, Germany) at 4°C, with 4CVs of lysis buffer and incubated on a roller rocker at 4°C for 45min. All subsequent

purification steps were performed at 10°C. The matrix was washed with 4CVs of column buffer followed by an elution step using 4CVs of the same buffer containing additionally 250mM imidazole. The fractions were collected in pre-chilled (4°C) falcon tubes and analyzed by SDS-PAGE. The protein concentrations in the purified fractions were determined using a Nanodrop spectrophotometer at a wavelength of 280nm. Due to TEV protease instability against oxidation, the elution buffer was removed by dialysis and exchanged by TEV protease storage buffer containing 1 mM dithiothreitol (DTT) (Biomol, Germany). TEV protease was stored at -20 °C.

3.3.9. Regeneration of the amylose matrix

The amylose matrix was washed with 3CVs of water, then with 3CVs of 0.1% SDS solution, followed by 1CV of water and finally 5CVs of column buffer. For subsequent use, the matrix is stored in 20% (v/v) ethanol at 4°C. The matrix can be reused 3-5 times when regenerated promptly after use.

3.3.10. Regeneration of the GST matrix

This procedure was performed by applying 10ml of the regeneration solution 1 followed by washing with 10ml of the regeneration solution 2. The above was repeated by 2 cycles of washing and then the resin, for use, was equilibrated in binding buffer.

3.3.11. Regeneration of the Ni-NTA matrix

The reuse of Ni-NTA resin depends on the nature of the recombinant proteins. Ni-NTA matrix was washed first by applying 2CVs of regeneration buffer, then 5CVs of water and after that with 3CVs of 2% (w/v) sodiumdodecylsulfate (SDS) solution. An ethanol (Roth, Germany) gradient from 25% (1 CV per washing step) to 100% (5 CVs) and back to 25% was applied. To remove the ethanol, the resin was washed with 1CV of water. To complex Ni²⁺ ions, the matrix was incubated with 5CVs of 100mM ethylenediaminetetraacetic acid (EDTA), pH 8.0 (Biomol, Germany), containing buffer and was subsequently washed with 2CVs of water. The matrix was recharged 10 min with 2CVs of 100 mM NiSO₄ (AppliChem, Germany) containing buffer, washed with 2CVs of water, 2CVs of regeneration buffer and 1CV of water. For subsequent use, the matrix was equilibrated with protein buffer or stored in 20% ethanol at 4 °C.

3.3.12. Size-exclusion chromatography (SEC)

An ÄKTA purification system (ÄKTA Purifier P-901; GE Healthcare, UK) connected to a UV detector and a fraction collector was provided and maintained at 16 °C, which was used to purify the recombinant proteins. The device including the Hi Load 16/60 Superdex 200 column was previously washed with water and the respective buffer. Separation parameters were optimized by the accompanying UNICORN software, which also supported the chromatogram evaluation.

3.3.13. Protein quantification by absorption measurements

The protein concentration was determined by using a Nanodrop 2000c (Thermo Scientific, peqLab, Germany). 2µl of protein buffer were applied to the sensor, the lever arm was brought down and the measurement was blanked. For concentration determination, the procedure was repeated with the application of 2µl of protein solution. Measurements were carried out in duplicates. Values for the molar extinction coefficient (ϵ) and the molecular weight were entered and the protein concentration was displayed by the software, calculated on the basis of the **Lambert-Beer –law**.

$$A_{280} = \epsilon * b * c$$

A_{280} = absorption at 280 nm

ϵ = molar extinction coefficient [$\text{mol}^{-1} \text{cm}^{-1}$]

b = path length [cm]

c = protein concentration [mg/ml]

3.3.14. SDS-polyacrylamide gel electrophoresis (PAGE)

SDS-PAGE is a simple method used to determine size and purity of a protein sample under denaturing conditions. The separation of macromolecules in an electric field is called *electrophoresis*. A very common method for separating proteins by electrophoresis uses a discontinuous polyacrylamide gel as a support medium and sodium dodecyl sulfate (SDS) to denature the proteins. SDS (also called lauryl sulfate) is an anionic detergent maintaining a net negative charge within a wide pH range. A polypeptide chain binds the amounts of SDS in proportion to its relative molecular mass. The negative charges on SDS destroy most of the complex structure of the proteins and they are strongly attracted toward an anode (positively-charged electrode) in an electric field. Polyacrylamide gels restrain larger molecules, whereas smaller molecules migrate faster within the gel. Because the charge-to-mass ratio is

nearly the same among SDS-denatured polypeptides, the final separation of proteins is dependent almost entirely on their differences in relative molecular mass. Protein separation by SDS-PAGE can be used to estimate relative molecular mass, to determine the relative abundance of major proteins in a sample and to determine the distribution of proteins among distinct fractions. Protein samples were mixed with 2× concentrated sample buffer and incubated at 96°C for 10min for denaturation. The gel was vertically placed in a gel chamber (Hoefer Inc, USA) and connected to an EV 231 power supply (Peqlab, Germany) to adjust the electric field. Electrophoresis was terminated as soon as bromophenol blue reached the low end of the gel. The gel was stained for at least 2hrs in a coomassie staining solution and was subsequently destained in 20% (v/v) acetic acid until a sufficient contrast was visualized. The gels were documented by scanning the gel using a color scanner (Epson).

3.3.15. Dynamic Light Scattering (DLS)

Dynamic light scattering (also known as photon correlation spectroscopy or quasi-elastic light scattering) is a technique that can be used to determine the size distribution profile of small particles in suspension or polymers in solution [Berne and Pecora, 2000]. It can also be applied to probe the behavior of complex fluids such as concentrated polymer solutions. The dynamic light scattering (DLS) system spectroLIGHT 300 DLS instrument (Xtal concepts, Germany) is an instrument, which can be used to determine the size distribution profile of small particles in suspension or polymers in solution mentioned above (Fig. 10). A truly monodisperse sample would give rise to a single exponential decay to which the fitting of a calculated particle size distribution is relatively straightforward. The sample was irradiated by a red light class 3b laser ($\lambda = 690$ nm; laser power 10-50 mW) to detect isotropic scattering at an angle of 90 degree. In preparation, samples with a concentration between 1-2mg/ml were centrifuged at 4°C for 30min at 12.000rpm to remove high molecular weight aggregates and were analyzed in a quartz cuvette with a path length of 1cm at room temperature. Measurements were accumulated per sample using an autopilot function.

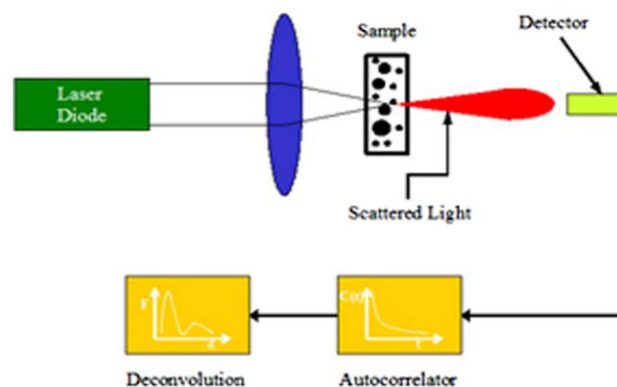


Figure 10: Schematic diagram of a dynamic light scattering instrument. [Particle Sizing Systems (PSS)] 2015 . Taken from <http://pssnicomp.com>.

The hydrodynamic radius of the particles is calculated using the Stokes-Einstein equation.

$$R_H = \frac{K_B T}{6\pi\eta D_T}$$

R_H is the hydrodynamic radius, which is determined by its dependence on viscosity η and the diffusion coefficient D_T . K_B is the Boltzmann's constant, and T is the absolute temperature.

3.3.16. Circular dichroism (CD) spectroscopy

CD spectroscopy is a spectroscopic technique used to determine the secondary structure contents of proteins and polypeptides in solution and a lower extend into the tertiary structure, as well as investigating the stability of proteins by measuring the melting temperature. It allows structural comparison of protein variants or proteins obtained from different expression systems. The CD spectrometer (J-815, Jasco, UK) equipped with a peltier element was calibrated according to the supplier's instructions. The peltier element allows precise investigations concerning the thermal stability of a certain protein fold. The *elasticity* of the sample was typically measured in a 1mm quartz cuvette with a wavelength interval ranging from 185-260 nm (*far-UV* spectrum) or in a 1cm cuvette for wavelength values from 260-320 nm (*near-UV* spectrum). The baseline recorded for the corresponding buffer was subtracted. The *elasticity* θ is defined as the difference in absorbance of clockwise and counter clockwise circular polarized light. Prior to the measurement, the sample solutions were centrifuged at 4°C for 30min at 12. 000rpm and were then measured in a quartz cuvette at room temperature.

$$\theta = \frac{180 * \ln 10}{4 * \pi} * (A_L - A_R)$$

From standard curves, secondary structure elements were determined. Typical curves for α -helical folding show minima at 208 and 220 nm and a maximum at 192 nm (see green curve in Figure 11), proteins with mainly β -sheet folding show a minimum at 215 nm and a maximum at 195 nm (see blue curve in Figure 11), whereas random coil structures lead to a minimum between 190 and 200 nm and a maximum at 220 nm (see red curve in Figure 11). All these values are not absolute, but show landmarks for CD spectra analyses.

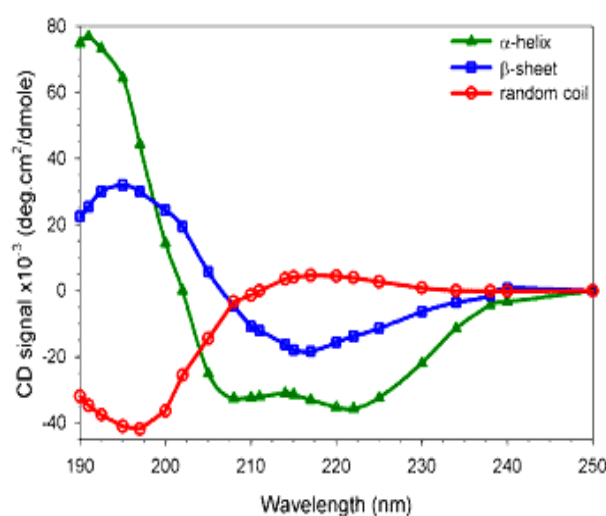


Figure 11: Standard curves for CD measurements of proteins. The CD signal for α -helices is depicted in green, β -sheets in blue and random coil in red. The figure is maintained by G. Nasir Khan, 2015 University of Leeds, Leeds. Taken from <http://www.fbs.leeds.ac.uk/facilities/cd>.

3.3.17. Mass spectrometry (MS)-based protein identification

Digestion by trypsin and mass spectrometry data collection was performed at University of Hamburg under the supervision of Dr. Maria Riedner. For protein identification, protein bands were manually excised from an SDS-PAGE gel and digested with trypsin. The samples were loaded onto a Zip tip by pipetting 20 times and washed 3 times with 10 μ l 0.2% formic acid. The tryptic fragments were eluted with 60% acetonitrile. Tryptic peptides of the digested protein were spotted onto an Anchor Chip target (Bruker Daltonik GmbH, Bremen, Germany) with α -Cyano-4-hydroxycinnamic acid as matrix. Analysis was performed by MALDI-TOF/TOF mass analysis using an ultrafleXtreme mass spectrometer (Bruker Daltonik) equipped with a smart beam-II laser possessing a repetition rate of 2 kHz. The acquisition software FlexControl (version 3.3) was used. Mass spectra were acquired in a reflector mode

and externally calibrated using a peptide calibration mixture II (Bruker Daltonik) with masses between m/z 1046 and m/z 3147. After baseline subtraction and peak picking within the processing software (FlexAnalysis, version 3.3, Bruker Daltonik), sequencing has been performed manually in FlexAnalysis with a mass accuracy of 0.5Da. The $(M+H)^+$ values for the peptide fragments produced by trypsin digestion were used for protein identification.

3.3.18. TEV protease digestion and separation of TEV cleaved proteins

TEV protease was used to remove His-tags from proteins when the cleavage site was cloned with a His-tag. The cleavage was achieved by incubating the HBx proteins with TEV protease at a molar ratio of 1:100 and 1:10, originated from purified aliquots at -80°C to test the cleavage. Digestion was carried out at room temperature for 4hrs and overnight at 4°C . Samples were collected and analyzed by SDS-PAGE to determine the cleavage progress. Due to the instability of the HBx proteins during cleavage, the cleaved proteins were dialyzed with a stabilizing buffer before TEV removal. After dialysis of the cleaved proteins, the mixture of TEV protease and proteins for His- tag removal were incubated with previously equilibrated Ni-NTA resin on a roller rocker at 4°C for 45min. The collected flow through contained the cleaved proteins, the TEV protease and cleaved His-tags bound to Ni-NTA matrix, which were eluted by a buffer containing imadizole.

3.4. Methods to analyze the 3D structure of proteins

3.4.1. Sample preparation for protein crystallization

Crystallography is one of the most widely used technologies for the determination of high resolution 3D-structures of proteins. Crystals of the protein of interest are grown and subsequently analyzed using X-ray radiation. Prior to crystallization experiments, the protein concentration needs to be adjusted. Therefore, a pre-crystallization test (PCT) (Hampton Research, USA) was performed to obtain the most suitable starting conditions for the crystallization experiments. After purification of the HBx fusion proteins, samples were concentrated and centrifuged in an ultracentrifuge at 100,000g for 1hour. Disparity was monitored by DLS measurements and samples were concentrated to their final concentration. For the screening of various buffer conditions, different sets of crystallization solutions were carried out using the Zinsser Pipetting robots Honeybee 961 (Zinsser Analytic GmbH, Germany)

and the Oryx 4 (Douglas, UK). When using the Pipetting Robot (Zinsser Analytic GmbH, Germany), protein and precipitant solutions were transferred to 96 well *Nextal Qial* plates (Qiagen, Germany) (Fig. 12). The commercially available screens *JCSG+*, *Classic*, *Cryos*, *ComPAS*, and *AmSO4 Suite* (all Qiagen, Germany), also *Morpheus*, *Stura*, and *PACT* (all Molecular Dimensions, UK) were used. 400 nl of protein solution were mixed with 400 nl of the respective precipitant solution in one well. The reservoir was filled with 55µl of precipitant solution. The plates were sealed and stored at 16°C.



Figure 12: Zinsser Pipetting Robot. Taken from Zinsser Analytic GmbH, Germany)

When preparing the LCP procedure, a small amount (few mgs) of cholesterol was weighted in a small (1-2 ml) amber glass vial with a Teflon-lined cap. Cholesterol was found to be the best lipid additive significantly improving the β_2 AR-T4L crystal size [Cherezov *et al.*, 2007; Hanson *et al.*, 2008]. Then 100 – 200 mg of monoolein (1-oleoyl-rac-glycerol) (Sigma, USA) was added to obtain the required concentration of the additive lipid. The lipids were then dissolved in ~200 – 400 µl chloroform. The solvent was evaporated using ice to keep the vial warm at ~37 °C and to prevent the lipid from freezing. After these steps, the chloroform was removed by using a vacuum (<100 mTorr) for at least 4 hours, preferably overnight. After this step, 15 – 50 mg of a host cubic phase lipid, e.g. monoolein or a lipid mixture, were transferred into a small 0.5 ml plastic vial and were melted at 37 °C. The molten lipid was transferred into a 100 µl gas-tight syringe by the plunger end, using an adjustable volume pipette (Fig. 13A). After lipid application, the plunger was inserted back and the lipid was slowly moved up in the syringe to remove any trapped air bubbles until the lipid reached the end of the coupler needle (Fig. 13B).

A 25 or 50 μl syringe with a flat tipped 26s gauge needle was used to transfer an appropriate amount of the protein solution into the second 100 μl gas-tight syringe to achieve 40% of protein solution to the final required mixture (Fig. 13C). Then the protein solution was moved up with the plunger as far as possible to minimize the air trapping after assembling the syringe mixer (Fig. 13D). The syringe, containing the protein solution, was then attached to the open end of the coupler, which is placed on the syringe containing the lipid. The protein solution and the lipid were moved back and forth through the coupler inner needle, from one syringe to another, by pushing alternatively on the corresponding plungers until the lipid mesophase in the syringe mixer becomes homogeneous and transparent (Fig. 13E). This movement mixes the lipid with the protein solution, a lipidic cubic phase is formed spontaneously and the protein becomes inserted into the lipid bilayer of the LCP.

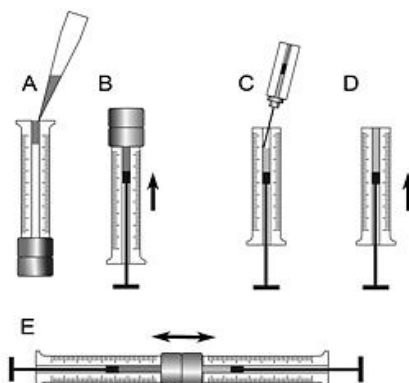


Fig 13: Schematic diagram of the loading procedure for sample preparation. (A) Lipid transmitting into the syringe. (B) Movement of the lipid into the syringe. (C) Protein transmitting into the second syringe. (D) Movement of the protein into the second syringe. (E) Sample (lipid, protein) mix. Taken from USC Dornsife, University of Southern California, Dept. of Chemistry.

The pipetting robot Oryx 4 (Douglas, UK) was used for this procedure. The protein mixture and precipitant solutions were transferred to 96 LCP (lipid cubic phase) sandwich set plates (Marienfeld, Germany) (Fig. 14). The commercially available screen *Cubic Phase-II-Suite* (Qiagen, Germany) was used. 200 nl of protein solution were mixed with 200 nl of the respective precipitant solution in one well. The reservoir was filled with 54 μl of the precipitant solution. The plates were sealed and stored at 20°C. All plates were monitored every week to identify crystallization hits.



Figure 14: Pipetting robot Oryx 4. Taken from Douglas instruments, UK.

3.4.2. Optimization of initial crystallization conditions

After obtaining initial crystallization conditions for the fusion protein crystals, they were optimized by varying the precipitant concentration around the condition found in the initial screen. In the presence of polyethylene glycols (PEGs) as precipitant, concentration was increased or decreased by 10% increments. Conditions were optimized in 24-well Linbro plates (Hampton Research, USA) using the hanging drop vapor diffusion method, consisting of 2 μ l protein solution and 2 μ l precipitant solution in the droplet and the reservoir was filled with 500 μ l precipitant solution. Conditions were also optimized in 48-well MRC sitting drop plates (Molecular Dimensions, UK). Droplets were made of 2 μ l protein solution plus 2 μ l precipitant solution and the reservoir was filled with 50 μ l of precipitant. Droplets were pipetted manually. Temperature was also varied and therefore, plates were either stored at 4°C or at 16°C in an air conditioned laboratory. Crystallization under oil and seeding techniques has also been considered. For crystallization under oil, a Terazaki plate (Nunc, Denmark) was previously treated with paraffin oil (Applichem, Germany) to fill all wells with oil. Then, 2 μ l of protein with 2 μ l of precipitant were pipetted into each well under the microscope, whereas the oil covered the droplet. Microseeding is a powerful tool to bypass spontaneous nucleation and to optimize the quality of the crystal. Seedstocks for the observed protein crystals were prepared, in the presence of a stabilizing solution, in a tube containing a glass ball according to the supplier's protocol (Jena BioScience, Germany). The seedstock was either diluted 1:10-1:100 with protein solution containing the protein at which the crushed crystal was obtained with the same concentration, or was used to draw streak lines using a horse-tail hair within droplets containing 2 μ l of the precipitant and 2 μ l of the protein solution.

3.4.3. Evaluation of the protein crystals

To distinguish between protein and salt crystals, droplets containing observed crystals were monitored using UV Crystal LIGHT 100 fluorescence (Xtal concepts, Germany) and SONICC (Benchtop, Formulatrix.Inc, USA), according to the manufacturer's specifications.

3.4.4. Negative staining electron microscopy (EM)

Negative staining electron microscopy (EM) is an established method, often used in diagnostic microscopy, for contrasting a thin specimen with an optically opaque fluid. In this technique, the background is stained, leaving the actual specimen untouched, and thus being visible [Cheng & Walz, 2009]. Negative stain EM is a powerful tool that can be used to study 3D structures of purified protein samples, such as using the random conical tilt method [Radermacher *et al.*, 1987]. This requires the collection of a pair of images within one specimen, one tilted to 60° and one from the same area but untilted, in order to calculate the 3D reconstructions of macromolecular complexes. In addition, negative staining EM can have many other applications, such as screening for two-dimensional (2D) crystals of membrane proteins [Zhao, 2010]. Visualizing protein samples by negative stain electron microscopy (EM) has become a popular structural analysis method. It is useful for quantitative structural analysis, such as calculating a 3D reconstruction of the molecules being studied, and also for qualitative examination of the quality of protein preparations. Negative staining is a simple sample preparation method in which protein samples are embedded in a thin layer of a dried heavy metal salt to increase the specimen contrast [Ohi *et al.*, 2004]. The enhanced contrast of negative stain EM allows the examination of relatively small biological samples. In addition to the determination of three-dimensional (3D) structures of purified proteins or protein complexes [Rabl, 2008], this method can be used for much broader purposes. For example, negative stain EM can be easily used to visualize purified protein samples, thus obtaining information such as homogeneity/heterogeneity of the sample, formation of protein complexes or large assemblies, or simply to evaluate the quality of a protein preparation. This procedure has been performed in the Max Planck Institute for Molecular Genetics, Berlin, under the supervision of Dr. Thorsten Mielke and was implemented by Mr. Jörg Bürger. This is principally done by first preparing the grids that will support the sample, then by filling a beaker with distilled water

containing a single drop of collodion (20 μ l, 2% in uranylacetate, Electron Microscopy Sciences, PA, USA) on the surface of the water. The collodion will spread to form a thin plastic layer at the water layer (Fig. 15A). A paper will be placed carefully on top of the grid (Fig. 15B), until the paper becomes completely wet (Fig. 15C). After a while, the /air surface. 50 -100 EM grids (mesh Gilder Cu grids, Ted Pella Inc., USA) will be placed onto the plastic layer floating on the water surface, with the shiny side of the grid facing down into the plastic paper will be removed and placed in a petri dish with the grids facing up for air drying (Fig. 15D). After these steps, the grids will be coated with carbon.

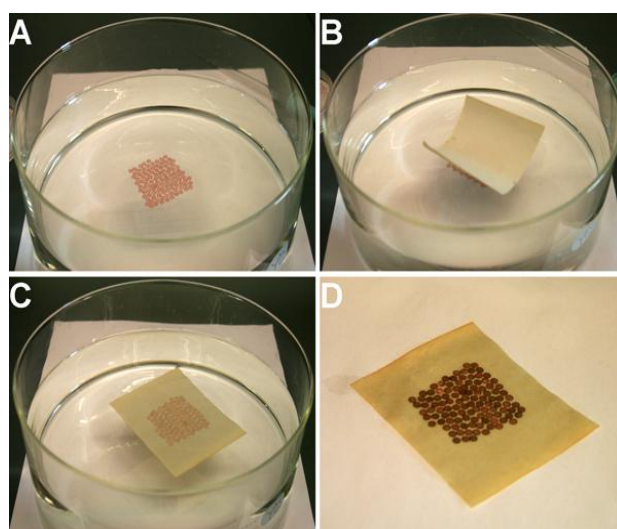


Figure 15: Preparation of carbon coated grids for negative stain EM. (A) EM grids are placed in a closed packing pattern on the surface of collodion film. (B) A piece of paper slightly larger than the area of the grids is placed upon. (C) After a period of time, the paper gets completely wet. (D) The paper together with the grids for air-drying. Taken from Booth, *et al.*, 2011, *Journal of Visualized Experiments*

The grids are discharged by the PELCO easiGlow GlowDischarge system (Ted Pella Inc., USA) for 30sec using a current of 15 mA. 1 μ l of the DHBx fusion protein solution with a concentration of 1mg/ml was used for this procedure. 3.5 μ l of the diluted protein were applied to the glow-discharged carbon-coated side grid and incubated at room temperature for 45sec. 1:40, 1:20, 1:15, and 1:7 dilutions of the protein were tested. The waiting time and the length of glow discharge both influence the concentration of the protein adsorbed in the grid. Very diluted samples require longer adsorption times. However, prolonged adsorption may change the buffer concentration since water vapors. After the incubation period, the grid will be blotted using filter paper. After this step, water is applied to the grid and blotted off with filter paper; this step will be repeated twice. A staining solution, 2% uranylacetate (Tab.

15), will also be applied to the grid and further incubated for 45sec at room temperature. The grid will be left to dry. The EM grid will be loaded in the single tilt standard specimen holder into the CompuStage of the 100 kV Philips CM100 equipped with a 1kx1k fastscan charge-coupled device (CCD) camera (TVIPS), using 21000x - 29500x magnification. The holder will be inserted into the column. The specimen will be focused and a desired defocus will be also be set, usually -1.5 μ m. Focusing can be achieved either manually using the minimum contrast method or by using the CCD camera to capture live images and to compute live Fourier power spectra. Images are recorded by using a CCD camera and collected to observe the negatively stained protein samples.

Electron imaging is considered a powerful technique for visualizing 3D structural details. However, because electrons interact strongly with matter, the electron path of the microscope must be kept under high vacuum to avoid unwanted scattering by gas molecules in the electron path. Consequently, the EM specimen has to be in the solid state for imaging, and special preparation techniques are necessary to either dehydrate or stabilize hydrated biological samples under vacuum [Jensen, 2010].



A



B

Figure 16: Equipment used for negative stain EM. (A) Tecnai T1 device Taken from FEI Company, used for observing the stained protein images on the grid. (B) A standard tilt specimen holder. Taken from *Nature methods*.

3.4.5. Small-angle X-ray scattering (SAXS)

Small-angle X-ray scattering (SAXS) is a small-angle scattering (SAS) technique where the elastic scattering of X-rays (wavelength 0.1-0.2 nm) by a sample which has in homogeneities in the nanometer range, is recorded at very low angles (typically 0.1

- 10Å) (Fig. 17). This angular range contains information about the shape and size of macromolecules, characteristic distances of partially ordered materials, pore sizes and other data. SAXS is capable of delivering structural information of macromolecules between 5 and 25 nm, of repeat distances in partially ordered systems of up to 150 nm [Glatter & Kratky, 1982]. SAXS is considered a universal technique applicable to a broad range of particle sizes, from small peptides to huge macromolecular machines with molecular weights from about 5kDa up to 100MDa.

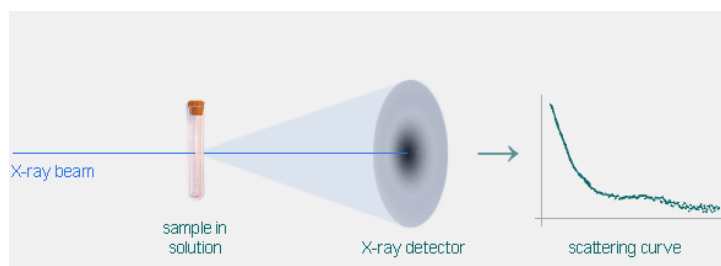


Figure 17: Schematic diagram of a SAXS experiment. Taken from Biosaxs.com 2014.

Biological SAXS has become a streamlined technique to rapidly characterize overall structural parameters comprising conformational changes of proteins, nucleic acids and macromolecular complexes in solution [Hura, 2013; Svergun, *et al.*, 2013]. However, for solutes containing aggregates, contaminating particles, partially dissociating complexes or oligomers, structural interpretation becomes difficult as most analysis methods for 3D structural analysis require monodisperse solutions [Jacques & Trewhella, 2012]. Complementary techniques, including size exclusion chromatography (SEC), are used to ensure sample quality in advance for a SAXS measurement. The integration of an in-line SEC separation step using size exclusion chromatography-small angle X-ray scattering (**SEC-SAXS**), where individual components are exposed to the X-ray beam while eluting from the column, provides evidence for data being collected from pure samples [Mathew, *et al.*, 2004].

The analysis of SEC-SAXS data is a major challenge regarding the large number of scattering curves measured at continuously varying sample concentrations. Knowledge of the solute concentration is significant for the proper analysis of experimental SAXS data that involves subtracting background scattering contributions and normalizing the resulting intensities against the sample concentration [Graewert, *et al.*, 2015]. In addition, knowledge of the solute concentration also permits determination of the solute species mean molecular weight

(MW). The set-up presented combines ultraviolet-visible light (**UV-vis**) and refractive index detectors to quantify the solute concentration of the flowing sample. In addition, the right angle light scattering (**RALS**) detector provides an independent means to estimate the MW of the eluted samples. The MW estimates, integrated over a peak volume, allow one to independently assess the oligomeric state of the eluting fraction, significantly improving the fidelity of subsequent interpretation steps. The combination of the biophysical and SAXS information allows a full automation of SEC-SAXS processing and analysis (Fig.18).

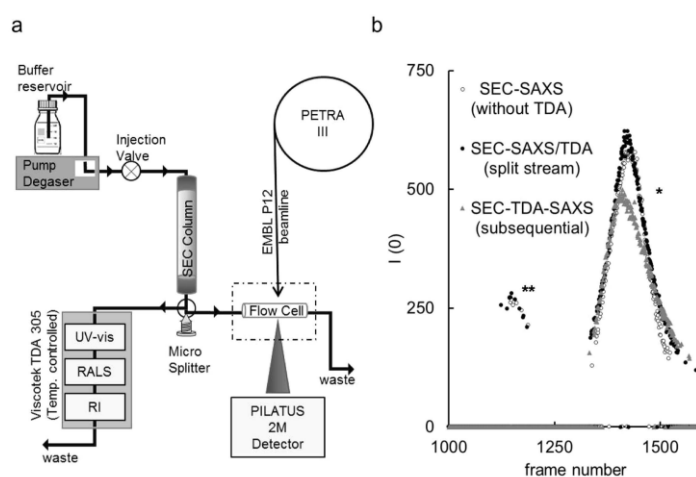


Figure 18: SEC-SAXS/TDA set-up at the EMBL-P12 synchrotron beamline (PETRA-III, EMBL/DESY, Hamburg). (a) Using a micro-splitter valve, the eluting stream is divided in equal parts enabling in-parallel SAXS and light-scattering measurements. (b) Automated SEC-SAXS pipeline trace of $I(0)$ vs. frame number. Bovine serum albumin was analyzed without TDA detectors (SEC-SAXS; ○), with a parallel SEC-SAXS/TDA split stream set-up (●) and in-line SEC-TDASAXS set-up (◆). *, ** indicate the peaks corresponding to the monomeric and dimeric fraction, respectively. Taken from Graewert1 *et al.*, 2015.

This procedure was implemented by Dr. Cy Jeffries at the EMBL-P12 synchrotron beamline (PETRA-3, EMBL/DESY, Hamburg). After purification of both DHBx and full human HBx fusion proteins, the proteins were dialyzed overnight in the same purification buffer containing 4mM DTT with 4% (v/v) glycerol to reduce the risk of radiation damage (Tab. 16). After this process, the proteins were concentrated to 3.5mg/ml. All samples were filtered and centrifuged prior loading onto the respective SEC column. BSA was subsequently used to calibrate the column for the batch measurements as well as for the data obtained from the SEC-SAXS/TDA experiments. 50-80 μ l of the concentrated proteins was loaded on the column after calibration. SEC experiments were performed at a flow rate of 0.5 ml/min at room temperature. A Superose 6 column (10/300, GE Healthcare) was used for this procedure. The separated sample components from in-line size exclusion

chromatography (**SEC**) were analyzed using combined right-angle light scattering (**RALS**), refractive index (**RI**) and UV-vis measurements (**UV**) made with a triple detector array (**TDA**, Viscotek model TDA 305; Malvern Instruments Ltd., Malvern, UK). The TDA data were processed using the integrated Omnisec software. The molecular weight (**MW_{RALS}**) of each species eluting from the SEC column was assessed using correlated concentration (*c*) measurements derived from base-line corrected RI in combination with base-line corrected RALS intensities calibrated against a bovine serum albumin narrow (monomeric) standard:

$$\mathbf{RALS} = c \cdot (\mathbf{dn/dc})^2 \cdot \mathbf{MW} \cdot \mathbf{k_{RALS}}$$

$$\mathbf{RI} = c \cdot (\mathbf{dn/dc}) \cdot \mathbf{k_{RI}}$$

dn/dc = The refractive index increment of unmodified protein

k_{RI} and **k_{RALS}** = The TDA instrument calibration constants

RI is used for estimating the protein concentration. It has advantages over UV absorption methods; it can also be used as a very sensitive tool to monitor baseline fluctuations for the selection of a suitable region for SAXS background subtractions.

3.4.6. Determination of protein-protein interaction

Protein–protein interactions (PPIs) refer to intentional physical contacts that are established between two or more proteins as a result of biochemical events and/or electrostatic forces. The function and the activity of a protein are often modulated by other proteins with which it interacts. Protein complex assembly can result in the formation of homo-oligomeric or hetero-oligomeric complexes. Interactions can also be established between domain-domain and domain-peptide contacts. Moreover, interactions can be classified into stable or transient, and also according to the nature of the chemical bonds that are established between the proteins. The interaction of HBx fusion proteins (full length and Tr-mini) with p53 proteins (full length and C-terminal) was tested by incubating HBx-tagged proteins in the presence of p53-tagged proteins after dialyzing both proteins overnight at 4°C with Tris/HCl buffer, pH 8.0. The molar ratio, as well as the incubation time and the temperature, were varied. Affinity chromatography was used for examination [Truant, *et al.*, 1995]. The mixtures were subsequently applied onto an amylose matrix. Samples of the washing step and of the specific elution fractions were collected and analyzed by SDS-PAGE

to determine the interaction of the target proteins. Another approach was used to determine the interaction between the HBx fusion proteins with the P53 proteins by applying the Octet HTX System, provided by Dr. Holger Nickel (Pall Life Science) and implemented by Mr. Hendrik Wuensche (Fig. 19). This method is used for analysis of bimolecular interactions, for quantization and kinetic characterization. The Octet HTX instrument monitors up to 96 biosensors simultaneously, enabling label-free detection for protein quantization and kinetic characterization at unmatched speed. The system's ability to read 8, 16, 32, 48 or 96 wells in parallel is used to maximize the analytical throughput or sensitivity. Rapid whole-plate detection is accomplished using the 96 biosensor mode, providing either quantitation data for 96 samples in as little as 2 minutes or full plate kinetic screening in minutes instead of hours. The Octet-HTX is equipped with disposable fiber optic sensors that use biolayer interferometry (**BLI**) detection. There are different biosensors used during the measurements. The 8 and 16 biosensor modes provide high sensitivity for measuring small molecule binding interactions and protein quantitation to 50ng/mL. The 32 or 48 biosensor modes enable larger complex assays such as epitope binning or multi-step quantitation to be analyzed in the shortest amount of time.



Figure 19: Octet HTX system. Taken from Forte` Bio, Pall Corp 2013, Germany.

The interaction between HBx fusion proteins (full length and Tr-mini) with the full p53 protein using the Octet HTX System was tested by dialyzing, both fusion proteins and the full p53 protein with PBS buffer pH 7.5. To analyze this procedure, 500µl of the HBx fusion proteins (full length and Tr-mini) were used, with a concentration of 0.5mg/ml and labeled with the Ez-link NHS-PEG4-Biotin linker (Thermo Scientific, USA). 8x 2mg aliquots were prepared for this procedure. The amount of Biotin applied to the HBx fusion proteins was at a 1:1 molar ratio of Biotin per HBx molecule. The prepared mixtures were incubated for 30min at room temperature. After the incubation period, a 2ml Zeba Spin desalt column with a 7kDa

MWCO (Thermo Scientific, USA), was used to remove any free biotin. The column was rinsed 3 times with PBS buffer before applying the biotinylated HBx sample. After applying the sample, the column was centrifuged for 2min at 1000 x g at room temperature. Samples were subsequently collected for the measurement.

4. Results and Discussion

4.1. Amplification of the HBx genes by PCR

Applying PCR techniques, the DHBx gene was amplified from a pRSET-A plasmid, while the human mini-HBx and the full-length human HBx genes were amplified from pTRIEX plasmids. The DNA template for the DHBx was provided by department 'General Virology' of the Heinrich Pette Institute, headed by Prof. Dr. Hans Will. The template for the gene sequences including both full human and mini HBx were approved the group 'Hepatology and Cell Transplantation' at the Center for Internal Medicine at the University Hospital Hamburg under the direction of Dr. rer. nat. Maura Dandri. All three genes were modified using primers that contained restriction sites for the endonucleases *Bam*H1 (5' end) and *Hind*III (3' end) when cloning into the pMAL-c2x vector, as well as a recognition sequence for the TEV protease (5' end). When cloning into the pMAL-p5x vector, genes were modified using primers that contained restriction sites for the endonucleases *Bam*H1 (5' end) and *Eco*RI (3' end), as well as a recognition sequence for the TEV protease (5' end). Applying agarose gel electrophoresis (data not shown), single DNA bands were consistently detected that corresponded well to the expected size of the genes (~ 400bp for DHBx; slightly more than 400bp for human mini-HBx and ~ 500bp for human full-length HBx). All PCR fragments were isolated using a DNA purification kit to remove the salts and unwanted macromolecules.

4.2. Cloning of the HBx genes into the expression pMAL vectors

The PCR amplification products and the expression vector pMAL-c2x were treated with the restriction endonucleases *Bam*HI and *Hind*III. When using the pMAL-p5x vector, PCR amplification products and the expression pMAL vector were treated with the restriction endonucleases *Bam*HI and *Eco*RI to generate overlapping termini of the DNA molecules. For purification and to determine the cleavage efficiency, the digested vectors and the HBx DNA fragments were applied to a preparative 1% (w/v) agarose gel (data not shown.).

All detected single bands consistently corresponded well to the expected values: The vectors with an approximate size between 4000-10000 bp, the DHBx DNA fragment with a size of 400bp, the human mini-HBx DNA fragment with slightly more than 400bp and the human full-length HBx fragment with an approximate size of 500bp. Thus, all fragments were cut out of the gel and purified using a specific

Results and Discussion

DNA gel extraction kit (Macherey-Nagel, Düren, Germany). After determination of the DNA concentration in the purified solutions, all HBx DNA fragments were ligated into the pMAL bacterial expression vectors using an insert/vector ratio of 5:1. The ligation mixtures were transformed into competent *E. coli* DH5a cells for amplification of the new plasmids. After overnight incubation at 37°C, several colonies grew on LB-agar plates that contained ampicillin as a selection marker. For plasmid preparation, the individual colonies from the plates were transferred into liquid cultures. The presence of plasmids containing HBx DNA inserts within the selected *E. coli* colonies were verified by PCR using HBx-specific primers. The subsequent analysis of the PCR reaction by agarose gel electrophoresis revealed for all test colonies the presence of a single DNA fragment that corresponded well to the expected size (Fig.20). Additionally, DNA sequencing of all plasmids revealed that the ligation of the HBx genes into the *E. coli* expression vectors was successful. After the identification of the positive colonies, test expression experiments were performed.

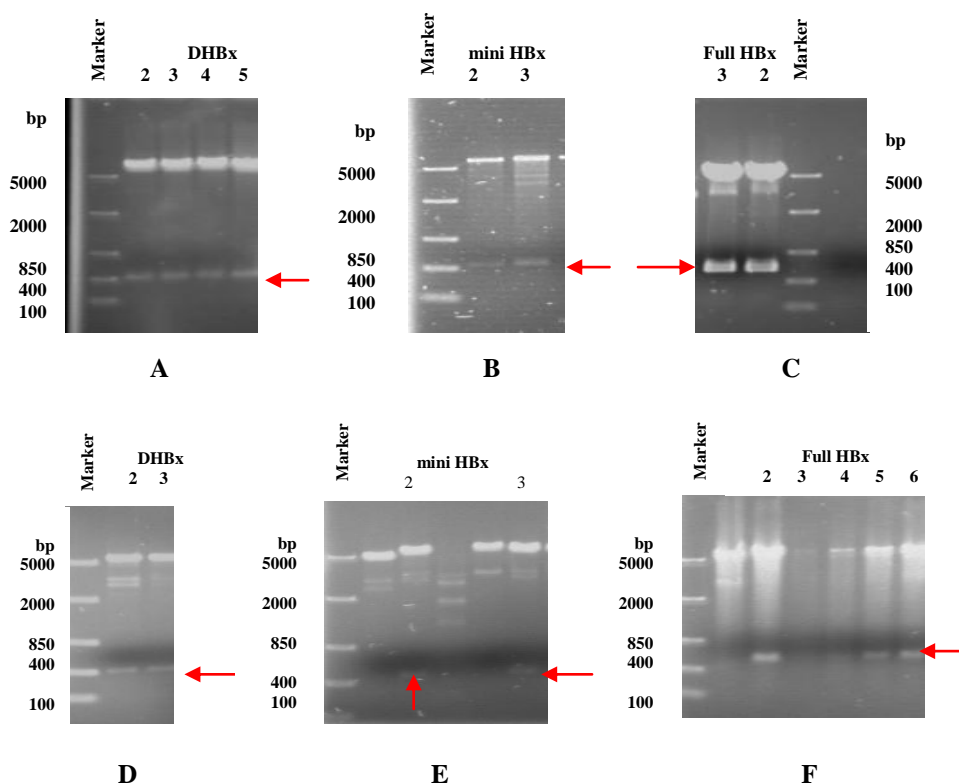


Figure 20: Agarose gelelectrophoretic analysis of the amplification of the HBx genes by PCR after ligation into the *E. coli* expression pMAL vectors. (A) Lane 2 to 5: Amplification products of selected *E. coli* clones after transformation with the ligation mixture containing the DHBx gene in pMAL-c2x. (B) Lane 2 and 3: Amplification products of selected *E. coli* clones after transformation with the ligation mixture containing the mini HBx gene in pMAL-c2x. (C) Lane 2 and 3: Amplification products of selected *E. coli* clones after transformation with the ligation mixture containing the full human HBx gene in pMAL-c2x. (D) Lane 2 to 3: Amplification products of selected *E. coli* clones after

transformation with the ligation mixture containing the DHBx gene in pMAL-p5x. (E) Lane 2 and 3: Amplification products of selected *E. coli* clones after transformation with the ligation mixture containing the mini HBx gene in pMAL-p5x. (F) Lane 2 to 6: Amplification products of selected *E. coli* clones after transformation with the ligation mixture containing the full human HBx gene in pMAL-p5x. Marker: *Fast Ruler Middle Range Ladder*.

4.3. Expression of the HBx fusion proteins in different *E. coli* strains

The cultivation of the *E. coli* strains was performed in LB media supplemented with 100mg/ml of the antibiotic ampicillin. The expression of recombinant proteins in the selected *E. coli* strains was induced by the addition of 1mM IPTG (isopropyl- β -D-thiogalactopyranoside). An improved solubility of the target proteins can be achieved by lowering the concentration of the inducer. Also, the cultivation temperature plays an important role for the solubility of the produced recombinant protein. Usually, a cultivation temperature of 37°C is applied for large-scale protein expression in *E. coli*, but lowering the temperature is known to result in an improved solubility of the target protein. Furthermore, determination of the optimal time point for induction of the recombinant protein expression is important and depends on the cell density in the culture medium that can be determined by measuring the optical density at a wavelength of 600nm (OD₆₀₀). Consequently, the cultivation temperature, the inducer concentration and the OD₆₀₀ at the time point of induction were varied during the test expression experiments.

Within the first experiments to express DHBx in the *E. coli* strains BL21 star and BL21 DE3, cells were induced at an OD₆₀₀ of approx. 0.6 with 0.03mM and 0.1mM IPTG, respectively, and a cultivation temperature of 37°C was applied. The fusion proteins were expressed for 3hrs. When using the shuffle cells, the DHBx fusion protein was induced with 0.5mM IPTG and incubated overnight with a cultivation temperature of 37°C. The cells were harvested by centrifugation and the amount of recombinant expressed DHBx fusion protein was analyzed by 10% SDS-PAGE. For the strain BL21 DE3, the expression level of the target protein was relatively high when using 0.03mM IPTG (Fig. 21A). The fusion protein consisting of DHBx and MBP has a calculated molecular weight of 57 kDa, corresponding to a protein band that appears after induction of the recombinant protein expression. If an IPTG concentration of 0.1mM was used for induction, the expression level of the target protein was relatively low at the same incubation temperature. For the strain BL21 star, no significant expression of the target protein was detected at 37°C after induction with both IPTG concentrations (data not shown). For the shuffle cells, the

Results and Discussion

expression level of the target protein was relatively low with an IPTG concentration of 0.5mM and a cultivation temperature of 37°C (Fig. 21B). Also a decrease of the incubation temperature to 18°C did not result in significant protein expression in both strains, independent of the IPTG concentration (data not shown).

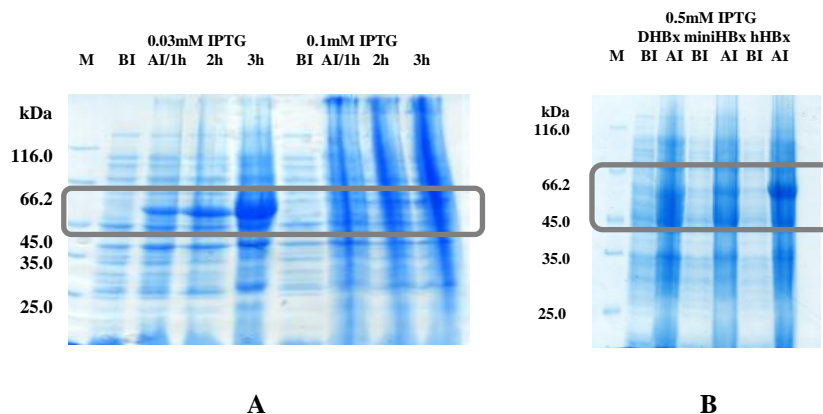


Figure 21: SDS-PAGE analysis of the DHBx fusion protein expression at 37°C (A, B). (A) Recombinant protein expression in strain BL21 DE3 at different IPTG concentrations. (B) Recombinant protein expression in shuffle cells.

For both the human full-length and the mini-HBx fusion proteins, expression was performed using *E. coli* strains BL21 star, BL21 DE3 and BL21 AI, induced also at an OD_{600} of approx. 0.6 with 0.03mM and 0.1mM IPTG. After 3hrs of protein expression, the cells were harvested by centrifugation. When using the shuffle cells, the fusion proteins were induced with 0.5mM IPTG and incubated overnight with a cultivation temperature of 37°C. The amount of recombinant expressed full-length and mini-HBx fusion proteins was analyzed by 10% SDS-PAGE. For the strain BL21 DE3 incubated at 37°C, the expression level of the target proteins was observed to be high when both 0.03mM and 0.1mM IPTG were used for induction (Fig. 22A, B). The fusion protein consisting of MBP and mini-HBx has a calculated molecular weight of 57kDa, while the molecular weight of the hHBx fusion protein has been calculated to be 59kDa. These values correspond well to the protein bands that appeared after induction of the recombinant protein expressions. A similar positive expression of the target proteins in BL21 star cells was observed at 37°C after induction with both 0.03mM and 0.1mM IPTG concentrations (Fig. 22C, D). Using the strain BL21 AI, positive expression was only detected for the mini-HBx target protein with arabinose as an inducer (Fig. 22E), whereas the hHBx fusion protein showed no expression (data not shown). For the shuffle cells incubated at 37°C, the expression level of the hHBx fusion protein was observed to be high when 0.5mM

Results and Discussion

IPTG was used for induction and low for the mini HBx fusion protein when using similar conditions (Fig. 23B). Decreasing the incubation temperature to 18°C for both mini HBx and hHBx resulted in weak expression in both BL21 DE3 and BL21 star cells (data not shown) independent of the IPTG concentration, whereas BL21 AI cells were still negative (data not shown).

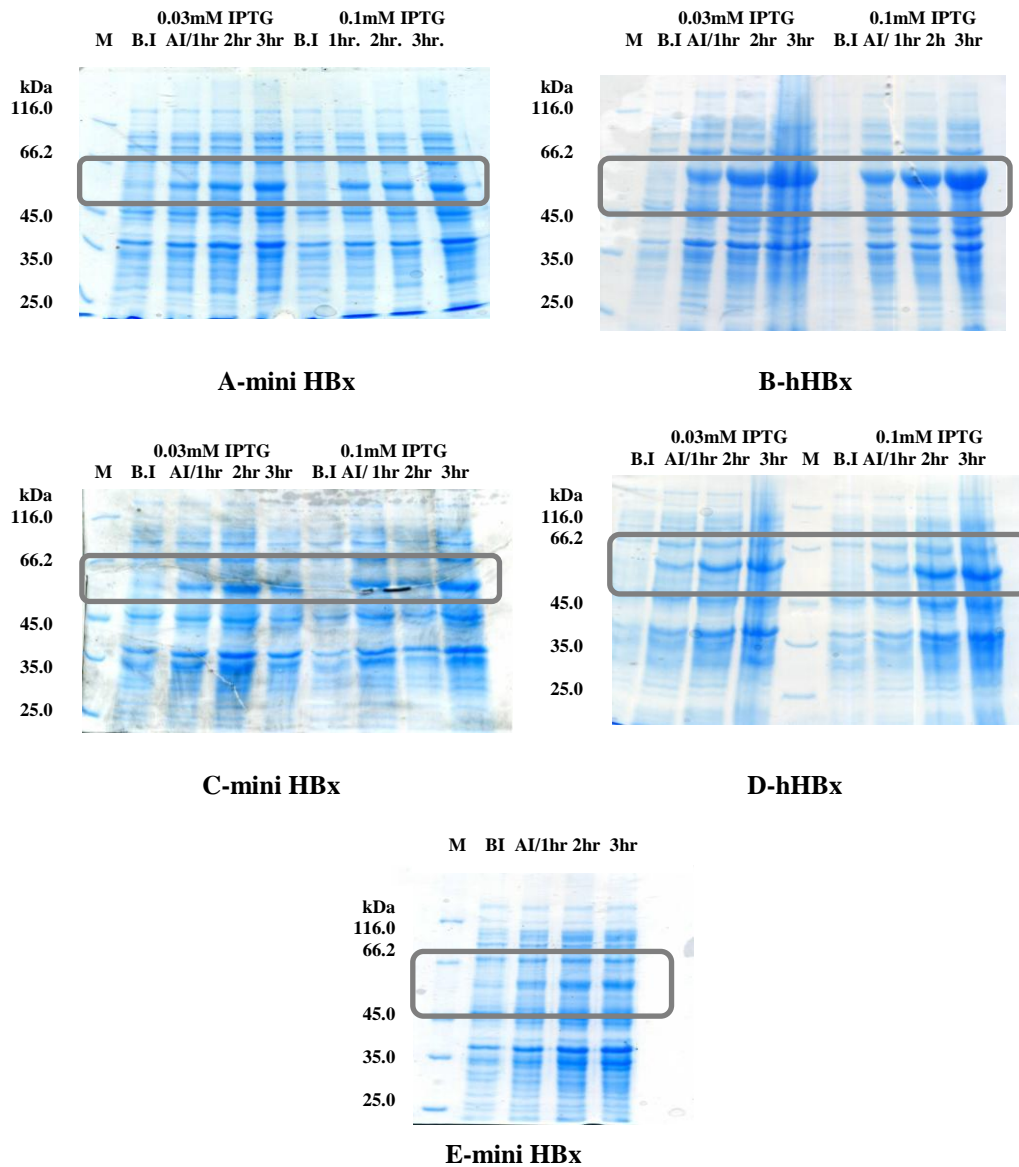


Figure 22: SDS-PAGE analysis showing the expression of human mini and hHBx fusion proteins in *E. coli* at a cultivation temperature of 37°C. (A, B) Recombinant protein expression in strain BL21DE3 at different IPTG concentrations. (C, D) Recombinant protein expression using BL21 star at different IPTG concentrations. (E) Recombinant protein expression using the BL21AI strain BI: before induction; hrs: hours after induction. M: molecular weight marker.

These experiments were performed with the HBx proteins cloned in the pMAL c2x vector. For the HBx proteins cloned in the pMAL-p5x vector, expression was carried out with *E. coli* strains BL21 DE3 and shuffle cells, induced also at an OD₆₀₀

Results and Discussion

of approx. 0.6 with 0.03mM IPTG when using the BL21 DE3 strain. After 3hrs of protein expression, the cells were harvested by centrifugation. Using the shuffle cells, the fusion proteins were induced at an OD₆₀₀ of approx. 0.6 with 0.5mM IPTG and were further incubated overnight with a cultivation temperature of 37°C. After overnight expression, the cells were harvested by centrifugation. The amount of recombinant expressed HBx fusion proteins was analyzed by 10% SDS-PAGE. For the strain BL21 DE3 incubated at 37°C, the expression levels of both mini HBx and hHBx fusion proteins were observed to be high when 0.03mM IPTG was used for induction (Fig. 23A, B), as compared to the DHBx fusion protein, which was observed to be negatively expressed when using similar conditions (Fig. 23A). Regarding the shuffle cells incubated at 37°C, the expression level of the hHBx fusion protein was observed to be high when 0.5mM IPTG was used for induction (Fig. 23B) and low for the mini HBx fusion protein when using similar conditions (Fig. 23A), while no significant expression of the DHBx fusion protein could be detected (Fig. 23A). The obtained results indicated that the optimal expression of HBx fusion proteins among the tested conditions was obtained when using the *E. coli* strain BL21 DE3 at 37°C and 0.03mM IPTG for induction. To improve the solubility of the target proteins, the expression was further performed at 37°C followed by cultivation at 30°C for 5hrs using the BL21 DE3 strain.

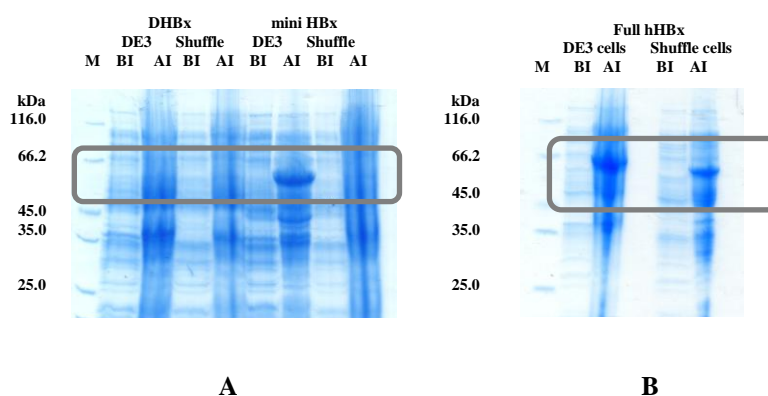


Figure 23: SDS-PAGE analysis showing the expression of HBx fusion proteins in *E. coli* at a cultivation temperature of 37°C. (A, B) Recombinant protein expression in strain BL21DE3 and in shuffle cells. BI: before induction; AI: after induction. M: molecular weight marker.

4.4. Expression of TEV protease

For the TEV protease, expression was performed at 37°C followed by cultivation at 30°C and an induction at an OD₆₀₀ of approx. 0.6 using an IPTG concentration of

Results and Discussion

1mM. After 4hrs of protein expression, the cells were harvested by centrifugation and the amount of the recombinant expressed TEV protease was analyzed by 15% SDS-PAGE. The detected expression level of the TEV protease was relatively high when 1mM IPTG was used. After induction of the recombinant protein, the expression protein band appeared in the SDS-PAGE that consistently corresponded to the protein with a calculated molecular weight of approx. 27kDa (Fig 24).

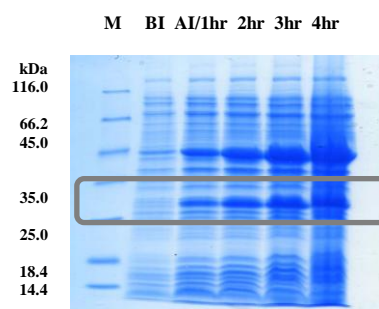


Figure 24: SDS-PAGE analysis of the expression of TEV protease at a cultivation temperature of 37-30°C. BI: before induction; AI: after induction; M: molecular weight marker.

4.5. Solubility of HBx fusion proteins

After determining of the optimized conditions for expression of the HBx fusion proteins, a solubility test was performed. Following separation of the soluble from the insoluble proteins by centrifugation, both the pellet and the supernatant fractions were analyzed by SDS-PAGE. The DHBx fusion protein is present in both a soluble and an insoluble form when expression is performed in BL21 DE3 at 37°C induced by addition of 0.03mM IPTG (Fig. 25A). This was also observed for the mini- and hHBx fusion proteins in BL21DE3 cells at 37°C, 0.03mM or 0.1mM IPTG (Fig. 25B, C), as well as for the mini HBx fusion protein in BL21 AI cells (Fig. 25D). However, when the human HBx fusion proteins were expressed in BL21 star cells at 37°C with 0.03mM and 0.1mM IPTG (Fig. 25C), the full hHBx fusion protein was again present in a soluble and insoluble fraction, whereas the mini HBx fusion protein formed only insoluble protein aggregates (data not shown). These results were observed for HBx proteins cloned in the pMAL-c2x vector.

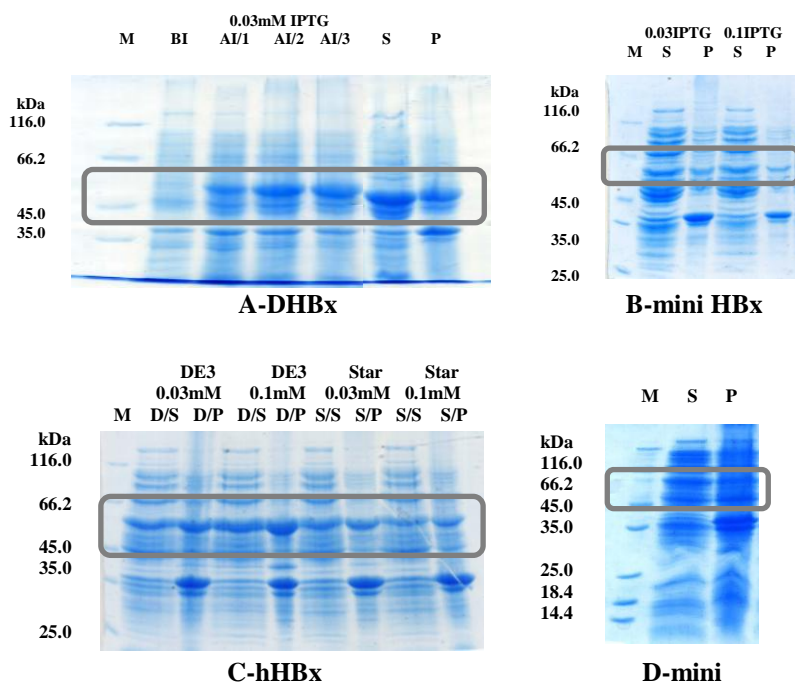


Figure 25: SDS-PAGE analysis shoeing the solubility test: Expression and solubility profile for HBx fusion proteins expressed in *E. coli* strains at a cultivation temperature of 37°C. (A) Expression and solubility profile of DHBx fusion protein expressed in *E. coli* BL21DE3, induced with 0.03mM IPTG. (B) Solubility profile of mini-HBx fusion protein expressed in *E. coli* BL21DE3, induced with 0.1mM and 0.03mM IPTG. (C) Solubility profile of hHBx fusion protein expressed in *E. coli* BL21DE3and BL21 Star, induced with 0.1 and 0.03mM IPTG. (D) Solubility profile of mini HBx fusion protein expressed in *E. coli* BL21AI, induced with arabinose.

The mini and full hHBx fusion proteins are present in a soluble form when expression is performed in BL21 DE3 strain at 37°C induced by addition of 0.03mM IPTG (Fig.31). This was also observed for the hHBx fusion protein when expressed in shuffle cells at 37°C with 0.5mM IPTG (Fig. 26), whereas the mini HBx fusion protein was only weakly expressed when using the shuffle cells (Fig. 26). These results were observed for HBx proteins cloned in the pMAL-p5x vector.

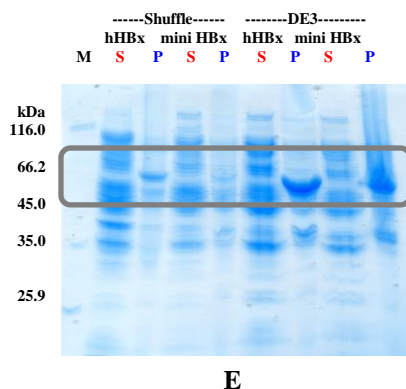
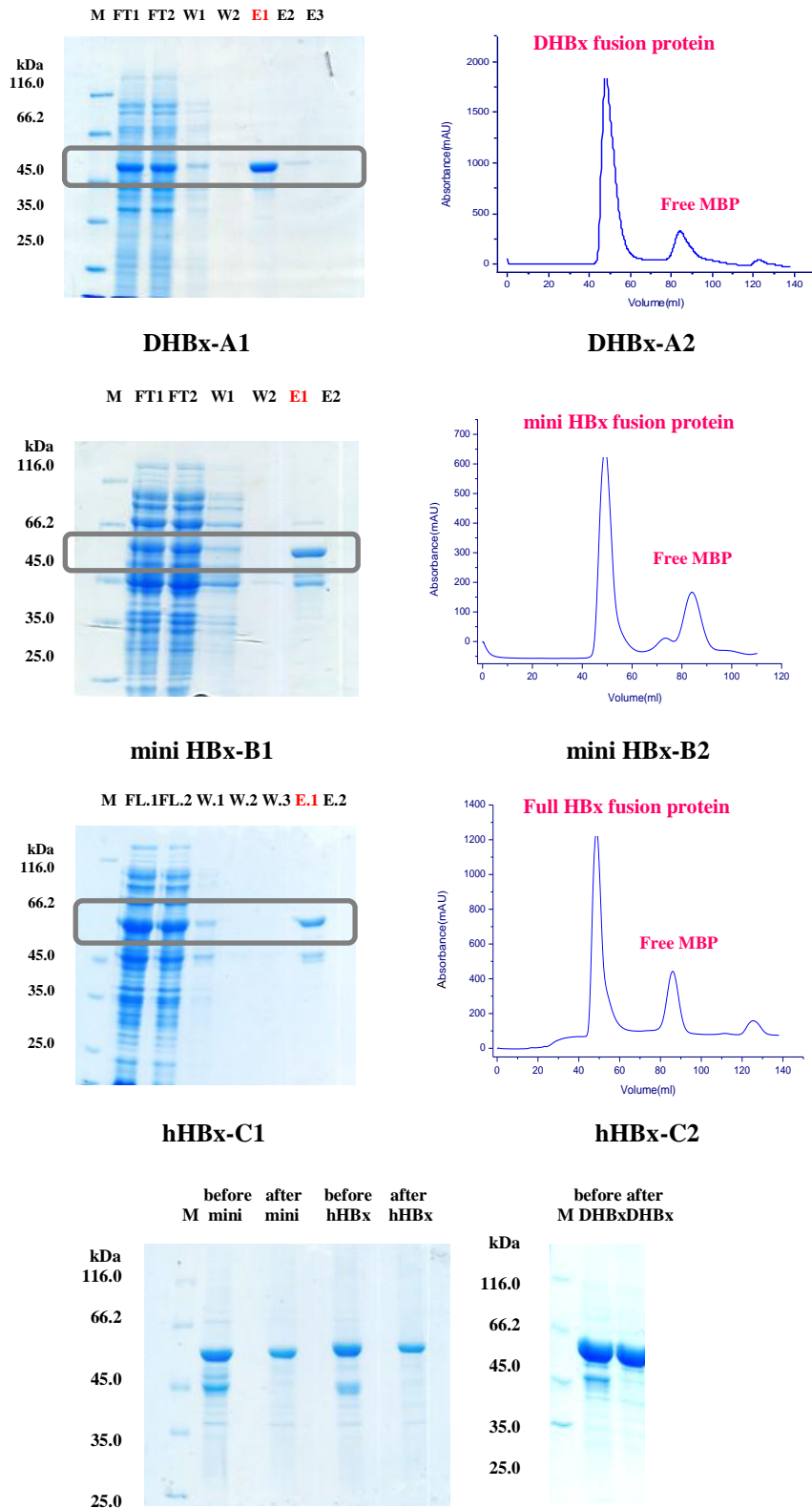


Figure 26: SDS-PAGE analysis of the solubility test. Expression and solubility profile for HBx fusion proteins expressed in *E. coli* strains at a cultivation temperature of 37°C. (E) Solubility profile of full and mini HBx fusion proteins clones in pMALp5x and expressed in *E. coli* BL21DE3, induced with 0.03mM IPTG. Also expressed in shuffle cells, induced with 0.5mM IPTG.

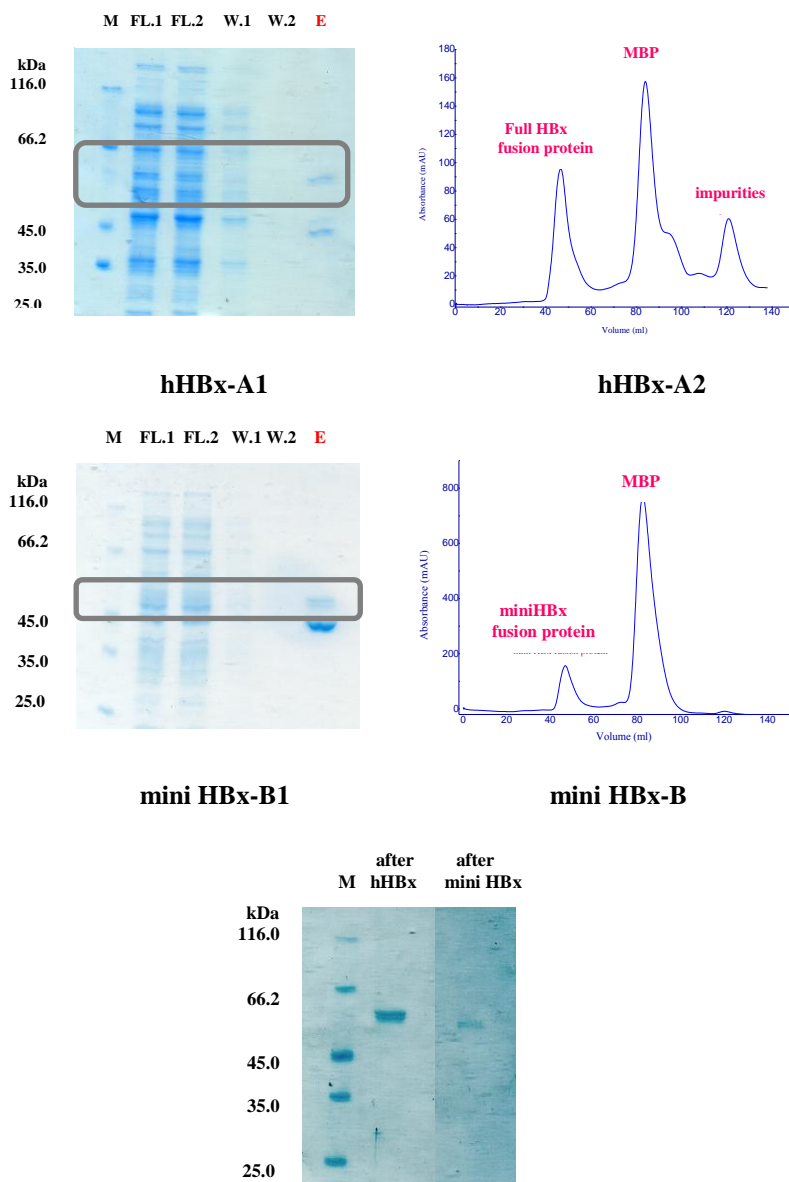
4.6. Purification of the HBx fusion proteins

For purification of the soluble HBx fusion proteins, affinity chromatography using an amylose matrix column was applied, since the MBP part of the fusion protein binds to amylose with high affinity. After equilibration of the column using the appropriate buffer (Tab. 16), the soluble proteins in the supernatant fraction of the centrifuged lysed cells were applied onto the column. The high affinity of the maltose-binding protein tag to the matrix resulted in a high specific binding of the protein at the resin. After several washing steps using the appropriate buffers to remove unspecific bound proteins, the fusion proteins were eluted manually with maltose and the fractions were analyzed by 10% SDS-PAGE. The gel electrophoretic analysis showed that the HBx fusion proteins in the pMAL-c2x vector eluted in almost pure forms (Fig. 27A1, B1, C1), with a slight elution fraction for the HBx fusion proteins in the pMAL-p5x vector (Fig. 27A1, B1). A single protein band was consistently identified at a molecular weight between 45kDa and 66kDa, corresponding well with the calculated MW of the target proteins: 57kDa for the DHBx (Fig. 27A1), 57kDa for the -mini HBx (Fig. 27B1, 28B1) and 59kDa for the hHBx (Fig. 27C1, 28A1) fusion proteins. Subsequently, a second purification step using a Superdex G-200 size exclusion chromatography column (Hi-Load 16/60 Superdex 200) was performed to obtain pure protein (Fig. 27A2, B2, C2/ 28A2, B2). This revealed two well defined peaks corresponding to an oligomeric and a monomeric state in solution, for the HBx fusion proteins and MBP, respectively, which co-elutes from the affinity chromatography column. Size exclusion chromatography revealed a co-existence of an oligomeric state of the HBx fusion proteins in solution. Regarding the obtained results, the study was continued by using the proteins cloned into the pMAL-c2x vector, due to the low production of proteins cloned into the pMAL-p5x vector. As can be seen on the gels, the proteins eluted from the SEC were highly concentrated for observation, compared to the proteins cloned into the pMAL- c2x vector.

Results and Discussion



D
Figure 27: SDS-PAGE and gel filtration analysis of the HBx fusion proteins purification cloned in the pMAL-c2x vector. (A1, B1, C1) Analysis of HBx fusion proteins purification using affinity chromatography. FT1/2, first and second flowthrough fraction; W1/2/3, first, second and third wash fraction; E1/2/3, elution fractions; M, molecular weight marker. (A2, B2, C2) Purification of the HBx fusion proteins using a Superdex G-200 SEC column. The first peak of the chromatogram that shows the absorbance at 280 nm represents the HBx fusion proteins, the second peak free MBP, which co-eluted from the affinity chromatography column. (D) Analysis of HBx fusion proteins before and after SEC column.



C
 Figure 28: SDS-PAGE and gel filtration analysis of the HBx fusion proteins purification cloned in the pMAL-p5X vector. (A1, B1,) Analysis of HBx fusion proteins purification using affinity chromatography. FT1/2, first and second flowthrough fraction; W1/2, first and second wash fraction; E, elution fractions; M, molecular weight marker. (A2, B2,) Purification of the HBx fusion proteins using a Superdex G200 SEC column. The first peak of the chromatogram that shows the absorbance at 280 nm represents the HBx fusion proteins, the second peak free MBP, which co-eluted from the affinity chromatography column, the third peak for the full Hbx fusion protein shows impurities. (C) Analysis of HBx fusion proteins after SEC column.

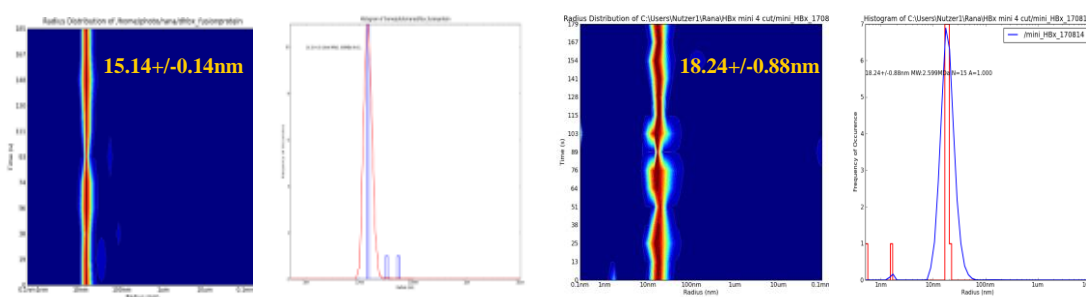
4.7. Dynamic light scattering (DLS) of the HBx fusion proteins

To further characterize the stability of the HBx fusion proteins' particles in solution and to analyze the influence of buffer conditions on the aggregation behavior of the HBx fusion proteins and their high molecular weight oligomers, dynamic light scattering techniques was applied. This method is used to determine the size

Results and Discussion

distribution profile of small particles in suspension or polymers in solution. It can also be applied to probe the behavior of complex fluids such as concentrated polymer solutions. It is based on the scattering of a red-light laser that is focused on the sample. The fluctuation of the scattering intensity due to Brownian motion of the molecules in solution is correlated with the hydrodynamic radius (R_H) of a particle, allowing the molecular weight estimation in homogenous solutions. Pure fractions separated by size exclusion chromatography were investigated in comparison to a mixture of oligomeric states obtained directly after affinity chromatography.

After purification of the fusion protein using size exclusion chromatography, the DLS histograms (Fig. 29A, B, C) indicated a radius distribution of the HBx fusion proteins in a range from 10 nm to 30 nm in the corresponding buffer. The oligomeric state of the HBx fusion proteins was characterized by a hydrodynamic radius (R_H) of $=15.1\pm 0.14\text{nm}$ for the DHBx, $18.2\pm 0.88\text{nm}$ for the mini HBx and $20.0\pm 0.78\text{nm}$ for the full HBx fusion proteins. These results indicate the polydispersity of the HBx fusion protein particles in solution, compared to the free MBP which observes a monodisperic state with a hydrodynamic radius (R_H) of $3.47\pm 0.54\text{nm}$ (Fig. 29D). These observations suggested the presence of differently sized aggregates of the HBx fusion proteins in solution. However, the later methods observe the HBx fusion proteins corresponding to higher oligomeric states. The presence of 1mM DTT and EDTA maintained the stability of the HBx fusion proteins in the corresponding buffer despite the presence of large aggregates.



A-DHBx fusion protein

B-mini HBx fusion protein

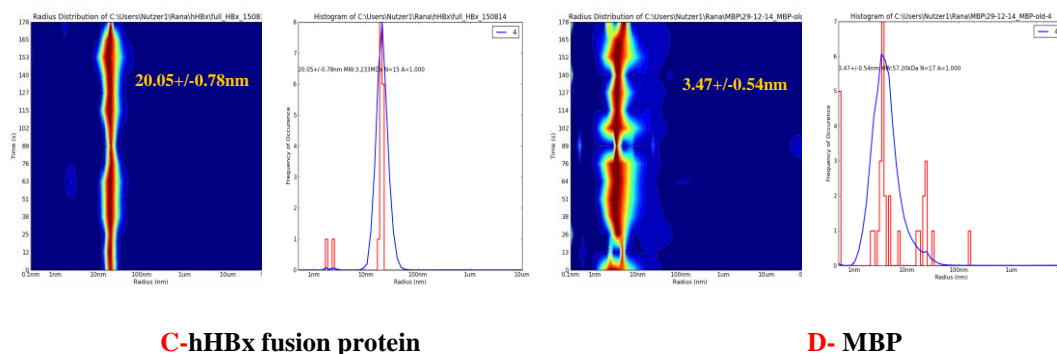


Figure 29: DLS histograms (blue) and statistical distribution of the measured radius in the histogram (red). (A) Sample of the DHBx fusion protein. (B) Sample of the mini HBx fusion protein. (C) Sample of the hHBx fusion protein. (D) Sample of MBP.

4.8. Secondary structure determination for the HBx fusion proteins

To compare the secondary structure composition of the HBx fusion proteins, circular dichroism (CD) spectroscopy was applied. All measurements were performed using 20mM Tris, pH 7.4, 50mM NaCl, 1mM EDTA and 1mM DTT (Tab.16) at room temperature. The samples were measured with the presence of the MBP tag. Figure (30) shows the CD spectrum of the purified DHBx fusion protein. The spectrum revealed one strong positive peak in the vicinity of 197nm and two minima at 212 and 227nm. Fractions of β -sheets are indicated by a single minimum at 215nm; the two minima are characteristic for a largely α -helical structure which is indicated at 209nm and 220nm. The results obtained from the CD spectra analysis revealed that the secondary structure of the DHBx fusion protein is predominantly composed of α -helices and β -sheets. A similar CD spectrum was obtained for the mini HBx fusion protein, which shows the spectrum revealing one strong positive peak in the vicinity also of 197nm and two minima at 215nm and 225nm. Small Fractions of β -sheets are indicated by a single minimum at 212nm and the two minima are characteristic for a large α -helical structure, which is indicated at 210nm and 225nm.

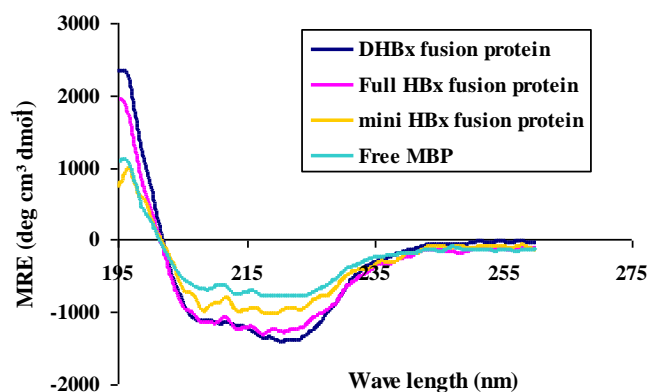


Figure 30: Secondary structure estimation for the purified HBx fusion proteins with free MBP by using CD spectroscopy.

The secondary structure spectrum for the full hHBx revealed one strong positive peak in the vicinity of 196nm and two minima at 212nm and 232nm. Fractions of β -sheets are indicated by a single minimum at 210nm and the two minima are characteristic for a largely α -helical structure, indicated at 209nm and 222nm. Comparing the results obtained from both full and the mini HBx fusion proteins, which observed differences in the folding stage of both structures, suggest that the mini HBx is partially folded which correlates to the observations that the mini-HBx is a hybrid type in which a disordered region and a globular region coexists [Lee, *et al.*, 2012]. Further conclusions suggest that the disorder of the full HBx points to the fact that the N-terminal ~50 residues in full HBx encompass the putative dimerization domain of full HBx [Lin and Lo, 1989], whereas the N-terminal ~30 residues in mini-HBx are disordered.

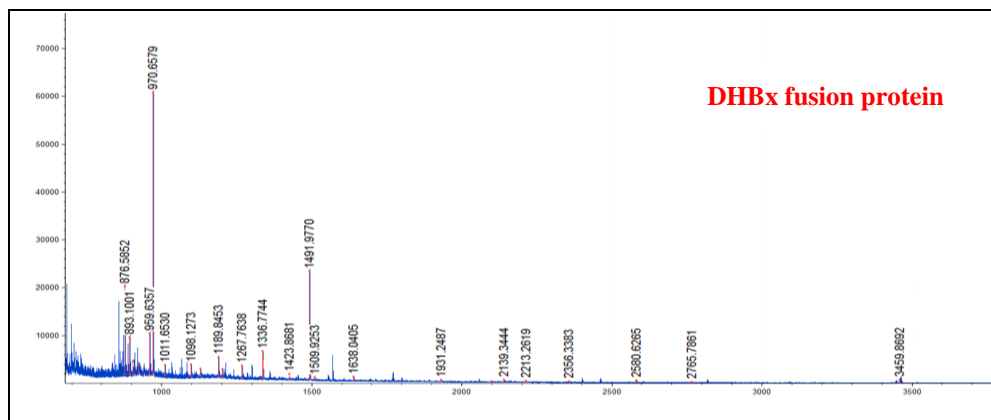
For the free MBP, the spectrum revealed one strong positive peak in the vicinity of 196nm and two minima at 210nm and 230nm. Fractions of β -sheets are indicated by two minima at 212nm and 216nm. The two minima are characteristic for a largely α -helical structure, which are indicated at 210nm and 221nm. Regarding the obtained results, the MBP was, in following, used as a control to observe the differences in the HBx proteins' structures and the effect of the presence of the MBP on the folding of the observed structures.

4.9. Identification of HBx fusion proteins by MADI TOF/TOF mass spectrometry

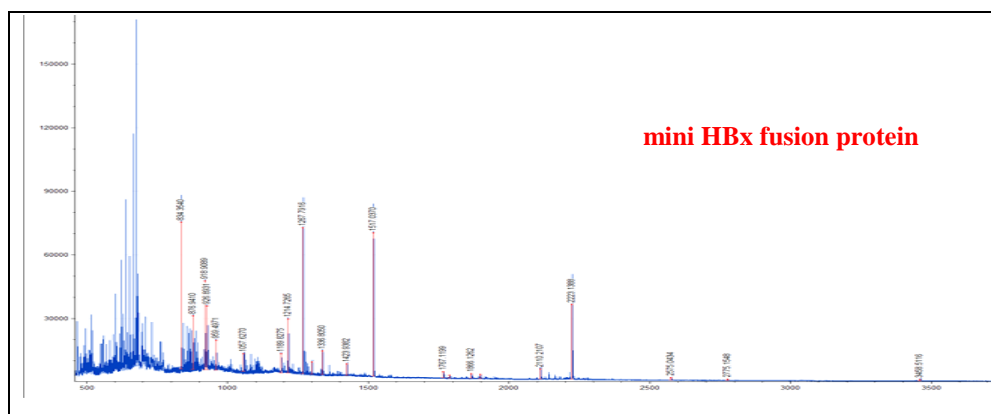
Mass spectrometry is an analytical technique that is used to identify the amount and type of chemicals present in a sample by measuring the mass-to-charge ratio and abundance of gas-phase ions. The ions are detected by a mechanism capable of

Results and Discussion

detecting charged particles, such as an electron multiplier. The atoms or molecules in the sample can be identified by correlating known masses to the identified masses or by a characteristic fragmentation pattern. Tryptic digestion combined with MALDI-TOF mass spectrometry was used to verify the identity of the single protein bands corresponding to the molecular weight of the HBx fusion proteins. The following bands could be detected: One at approx. 57kDa, which is assigned to the DHBx, again one at 57kDa in correlation to the mini HBx and a 59kDa band for the full hHBx fusion protein. Peptides were identified with mass values corresponding well to that expected for the DHBx (Fig. 31A), mini HBx (Fig. 31B) and the full hHBx (Fig. 31C). The identified peptide masses were compared with that of calculated peptides that mimic a theoretical trypsin digestion. Database searches using peptide masses and amino acid sequences for each spectrum showed that most peptide masses matched with the predicted ones, identifying the corresponding peptides as a part of the respective protein. The similarities and differences between both mini and full hHBx proteins regarding eliminated and mutated parts of the mini HBx were also determined (Fig. 31D).



A



B

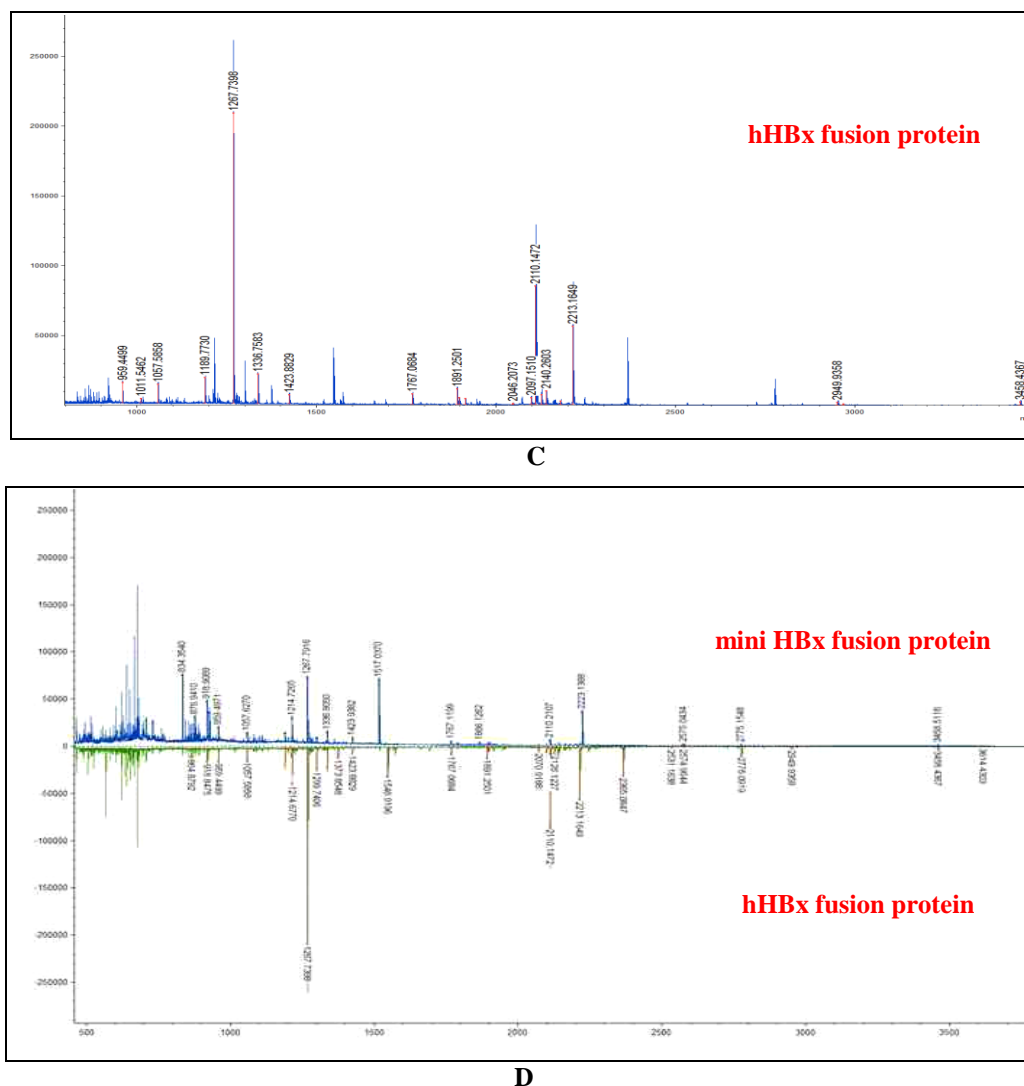


Figure 31: Tryptic peptide identification after mass spectrometry of DHBx (A), mini HBx (B) and full hHBx fusion proteins (C), as well as comparison of the peptide masses between both mini and full hHBx fusion proteins (D).

4.10. Cleavage of the HBx fusion proteins by TEV protease

After purification and concentration of the HBx fusion proteins, the proteins were incubated with TEV protease to establish the cleavage of the MBP-tag and to finally obtain the tag-free HBx proteins in a pure form. The progress of the TEV digestion was analyzed by 15% SDS-PAGE. For the mini HBx, a single protein band was detected after 1h of TEV cleavage at a molecular weight of approx. 15kDa, corresponding to the free mini HBx protein (Fig. 32A). The intensity of this protein band increased during incubation up to 4 hrs. Moreover, a new protein band appeared at a molecular weight of approx. 45 kDa, corresponding to the free MBP. Since an intense band of the fusion protein is found to be absent after 4 hrs of digestion, the cleavage of the MBP tag was suggested to be complete. To separate the TEV protease

Results and Discussion

from the cleaved mini-HBx protein, Ni-NTA affinity chromatography as well as a G-200 SEC was applied. The elution fractions were collected and analyzed using 15% SDS-PAGE. From the observed results it appears that the mini-HBx is eluted together with the free MBP within the exclusion volume of the G-200 SEC column, despite the complete cleavage (Fig. 32B). This result indicates that the free mini-HBx strongly interacts with the free MBP, forming aggregates that exceed the separation limit of a G-200 column.

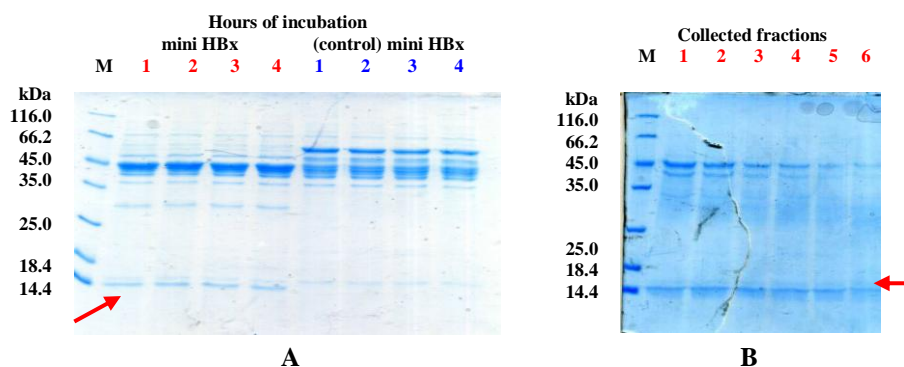


Figure 32: SDS-PAGE analysis of the mini HBx fusion protein cleavage by TEV protease. (A) M, molecular weight marker; (1, 2, 3, 4) fusion protein before cleavage; (1, 2, 3, 4) hrs after TEV cleavage with control protein without TEV cleavage. (B) Analysis of the mini HBx purification by SEC column after TEV cleavage. M, molecular weight marker; 1 to 6: collected fractions of the free mini-HBx protein from the SEC column.

Both DHBx and full hHBx proteins were also incubated with TEV. The digestion process was analyzed by SDS-PAGE. A single band was detected for both proteins after 1hr of TEV cleavage at a molecular weight of slightly less than 14 kDa and 17kDa corresponding to the free DHBx (Fig. 33C) and full hHBx (Fig. 34E) proteins, respectively. However, the intensity of the bands did not increase during incubation up to 4 hrs. Moreover, a new protein band appeared at a molecular weight of approx. 45 kDa, corresponding to the free MBP. Since an intense band of the fusion proteins is still present even after 4 hrs of digestion, the cleavage of the MBP tag from both DHBx and full hHBx proteins was found to be incomplete. This might be attributed to the strong aggregation of the molecules of the fusion proteins in solution, blocking the access to the TEV cleavage sites within the aggregates.

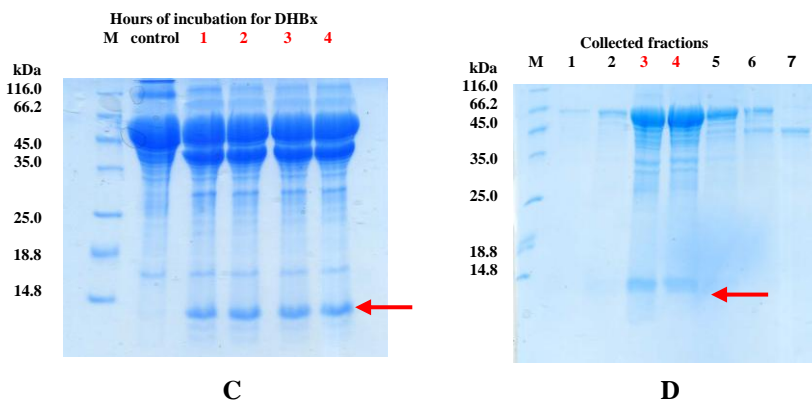


Figure 33: SDS-PAGE analysis of the DHBx fusion protein cleavage by TEV protease (C) M, molecular weight marker; (control) fusion protein before cleavage; (1, 2, 3, 4) hrs after TEV cleavage with control protein without TEV cleavage. (D) Analysis of the DHBx purification by SEC column after TEV cleavage. M, molecular weight marker; 1 to 7: Collected fractions from SEC column of the free DHBx protein, (3, 4) incomplete separation by the SEC column.

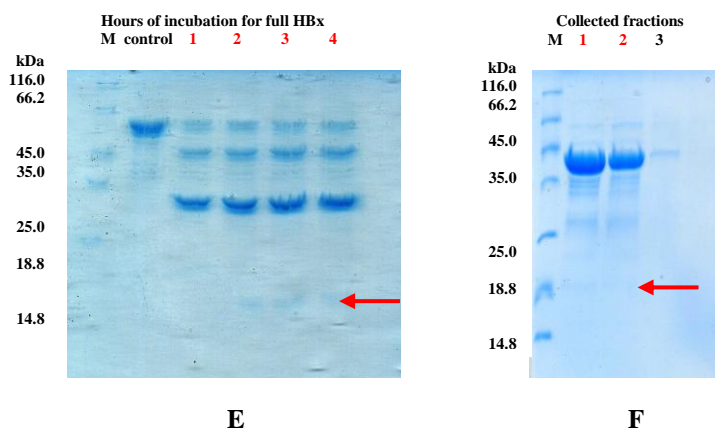


Figure 34: SDS-PAGE analysis of the full HBx fusion protein cleavage by TEV protease (E) M, molecular weight marker; (control) fusion protein before cleavage; (1, 2, 3, 4) hrs after TEV cleavage with control protein without TEV cleavage. (F) Analysis of the full HBx purification by SEC column after TEV cleavage. M, molecular weight marker; 1 to 3: Collected fractions from the SEC column of the free full HBx protein, (1, 2) incomplete separation by the SEC column.

However, since significant amounts of free DHBx and full hHBx proteins have been detected after TEV cleavage, the purification of free DHBx and full hHBx was investigated. A G-200 size exclusion chromatography column was applied to separate the cleaved HBx proteins from the uncleaved fusion protein and from the free MBP. The eluted fractions were analyzed on a 15% SDS-PAGE for both DHBx (Fig. 33D) and full hHBx (Fig. 34F), which revealed the co-existence of cleaved HBx proteins and uncleaved fusion proteins that eluted in a mixed fraction at the exclusion volume of the column. The free MBP was separated which eluted in subsequent fractions. This result indicates that both free DHBx and full hHBx strongly interact with the DHBx and full hHBx fusion proteins, forming large aggregates that exceed the separation limit of the G-200 column.

4.11. Crystallization experiments for the HBx fusion proteins

After observing the difficulties in removing the MBP tag from the HBx fusion proteins after cleavage, different experimental crystallization trials for the HBx fusion proteins were determined to find the proper conditions to obtain high quality protein crystals. For obtaining regular X-ray-suitable crystals, many optimization steps were required. Besides the purity of the proteins, many factors have to be considered that facilitate the crystal growth such as protein concentration, precipitant, pH, temperature etc. Crystallization depends on protein solution conditions, the molecular structure may be affected along with a subsequent change in the particle size. Thus monitoring the size of a protein molecule is one way of observing stability in the protein solution under its native conditions. Proteins can aggregate to heterogeneous complexes thus preventing crystallization. Performing DLS is essential to determine the size distribution profile of the protein particles in solution and the monodisperse nature of the protein solution.

After demonstrating the homogeneity of the protein solutions, the next step was to determine the precipitant which will be used in crystallization by using different crystallization conditions. For initial crystallization experiments, HBx fusion protein solutions were centrifuged at 20,000 x g and 4 °C for 1 h. The protein solutions were concentrated to 5-5.5 mg/ml using a centrifugal filter device with a MW cut-off of 3,000 kDa (Millipore, USA). In total, initial robot-assisted crystallization trials including different crystallization conditions were performed, some of these conditions resulted in a few promising observations. 400 nl of the protein solutions were mixed with 400 nl of the precipitant solution using the Zinsser Pipetting Robot (Zinsser Analytic GmbH, Germany) in 96-well sitting drop plates (NeXtalQIA1 uplates, Qiagen, Germany). The reservoir was filled with 55 µl of precipitant solution. Several promising conditions were obtained within the initial screening approach for both DHBx (Fig. 35) and mini HBx (Fig. 36) fusion proteins, nevertheless negative results were obtained for the full HBx fusion proteins. The conditions observed for the DHBx fusion protein originated from the Morpheus suite condition (C1), which consists of 10% (w/v) PEG 20000, 20% (v/v) PEG MME 550, 0.03M of each NPS (sodium nitrate, disodium hydrogen phosphate, ammonium sulfate), and 0.1M MES/Imadizole pH6.5 (Fig. 35A). A second promising condition came from the Pact

Results and Discussion

suite condition (E2), which consists of 20% (w/v) PEG 3350 and 0.2M sodium bromide as a precipitant (Fig. 35B).

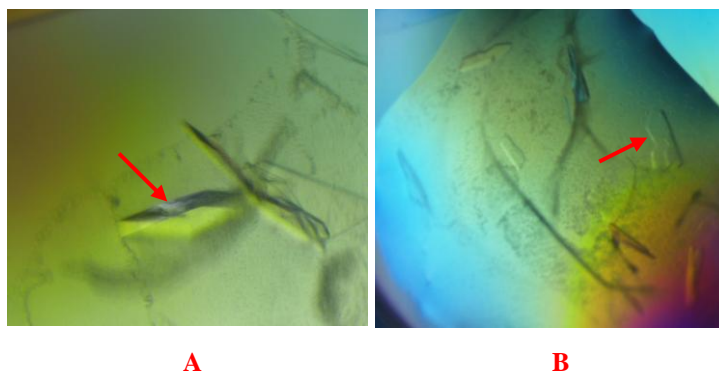


Figure 35: Observed crystals of the MBP-DHBx fusion protein from the screening plates with dimensions of approx. 134 μm and 115 μm growing from the (A) Morpheus suite condition (C1), and with a size of approx. 132 μm to 130 μm originating from the (B) Pact suite condition (E2).

The conditions observed for the mini HBx fusion protein were from the Campus suite condition (G11), which consists of 1.4M trisodium citrate, 0.1M HEPES pH7.5 (Fig. 36A). A second promising condition from the same suite is (A11), which consists of 18% (w/v) PEG8000, 0.1M sodium acetate pH 7.5 and 0.1M HEPES (Fig. 36B). For the third condition that is from the Classic suite condition (F8), it consists of 0.2M magnesium acetate, 0.1M sodium cacodylate pH 6.5 and 30% (w/v) PEG 4000 (Fig. 36C).

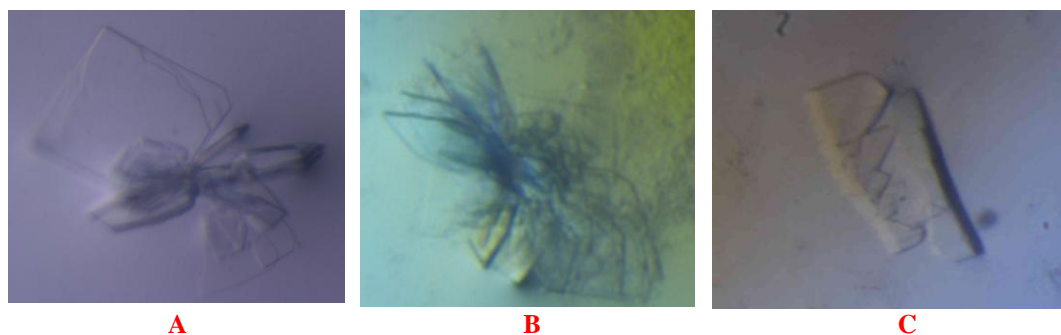


Figure 36: Observed crystals of the mini HBx fusion protein from the screening plates with dimensions of approx. 110 μm and 12 μm originating from the (A) Campus suite (G11) and the size of approx. 130 μm to 80 μm grown from the (B) Campus suite (A11), and finally an approx. 150 μm to 120 μm (C) for the Classic suite condition (F8).

Considering that the structure of both DHBx and mini HBx fusion proteins are so far unknown and is assumed to be highly flexible, the crystallization of the DHBx and mini HBx fusion proteins were suggested to be difficult or even impossible despite the known structure of the free MBP. The crystals obtained so far were not suitable for diffraction analysis. Due to this, manual screening techniques, e.g. hanging-drop, sitting-drop and micro-seeding approaches were performed to obtain better crystals.

Results and Discussion

The previous mentioned conditions were optimized varying PEG and salt conditions around the initial concentration in 24-well hanging drop CPL-130 plates (Jena Bioscience, Germany) by mixing 2 μ l of previously clarified (80,000 x g, 4°C, 1hr) protein solution and 2 μ l of the respective precipitant solution. Centrifugation at 80,000 x g was obtained to remove larger aggregates. Despite the optimization, the crystals remained weak and not suitable for diffraction analysis (Fig. 37). Other approaches such as sitting-drop and micro-seeding also obtained weak crystals.

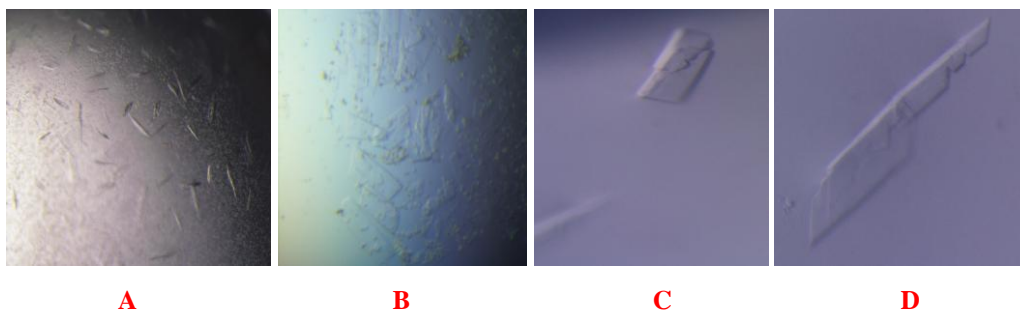


Figure 37: Observed crystals of the MBP-DHBx fusion protein (A, B) and mini HBx fusion protein (C, D) after optimization using a hanging drop system.

Another approach using LCP (lipid cubic phase) was observed to obtain protein crystals for the HBx fusion proteins. The fusion protein solutions were also centrifuged at 20,000 x g and 4 °C for 1 h. The protein solutions were concentrated to 15-25 mg/ml using a centrifugal filter device with a MW cut-off of 3,000 kDa (Millipore, USA). Initial robot-assisted crystallization trials including different crystallization conditions were performed, some of these conditions resulted in a few promising observations. 200 nl of the protein solutions were mixed with 200 nl of the precipitant solution by the Pipetting robot Oryx 4 (Douglas instruments, UK) in 96-well sitting drop plates (LCP sandwich plates, Marienfeld, Germany). The reservoir was filled with 54 μ l of precipitant solution. Several promising conditions were obtained within the initial screening approach for both DHBx (Fig. 38A, B) and mini HBx (Fig. 38C, D) fusion proteins, and again negative results for the full HBx fusion proteins. The conditions observed for both DHBx and mini HBx fusion proteins originated from the *Cubic Phase-II-Suite* (Qiagen, Germany). For the DHBx fusion protein, the first condition (F4) consists of 4% (w/v) PEG 3350, 1M sodium malonate and 0.1 M MES pH 5.8 (Fig. 38A). A second promising condition from the same suite is (C5), which consists of 12% (w/v) PEG 2000 MME, 0.2 M sodium chloride pH 5.8 and 0.1M MES (Fig. 38B). For the mini HBx fusion protein, the first condition (H4) consists of 4% (w/v) PEG 6000, 0.5M sodium malonate pH 5.8 and 0.1M MES (Fig.

38C). The second observed condition for the mini HBx (F2) consists of 12% (w/v) PEG 3350, 0.2 M sodium malonate pH 4.6 and 0.1M sodium acetate (Fig. 38D).

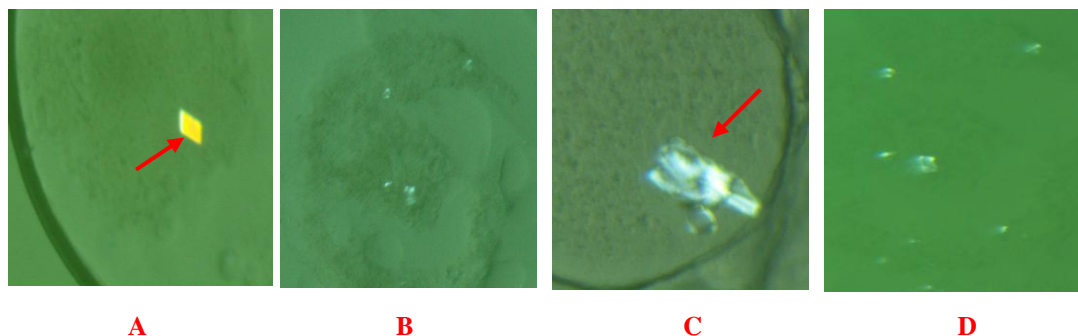


Figure 38: Observed crystals, under polarized light, for MBP-DHBx fusion protein (**A, B**) and mini HBx fusion protein (**C, D**) from the LCP screening plates with dimensions of approx. 30 μm and 30 μm for (**A**). For mini HBx fusion protein, the dimensions are approx. 142 μm and 51.4 μm for (**C**).

Despite this new method for crystallizing both DHBx and mini HBx fusion proteins, the crystals were also found to be not suitable for diffraction analysis due to the limited extraction success and the paucity of well-ordered 3D crystals.

4.12. Negative staining electron microscopy (EM) of DHBx fusion protein

Negative staining is considered an easy, rapid, qualitative method for examining the structure of isolated organelles, individual macromolecules and viruses at the EM level. This method involves the addition of a heavy metal salt solution that forms an electron-dense mould around individual macromolecular complexes. Normally, this mould is formed by simply air drying the EM grid. The resulting samples can be stored for long periods. In the electron microscope, this mould produces a high contrast image and is resistant to radiation damage. Thus, negative staining is the preferred method for screening samples and can also be used for low-resolution structure determination of the molecular envelope. The structures of flexible macromolecules are difficult or oft even impossible to examine by crystallography or NMR spectroscopy. Progress can be made by electron microscopy, but electron cryo-microscopy of unstained, hydrated specimens is limited to larger macromolecules because of the inherently low signal-to-noise ratio [Burgess, *et al.*, 2004].

This method was used to investigate the structure and action of the DHBx fusion protein. Investigations using many techniques provide the evidence or yielded information for a considerable flexibility within this protein [van Hemert, *et al.*, 2011]. Negative staining EM was applied to visualize the structure particles of the DHBx fusion protein and moreover, the particle shape of the protein was determined.

Results and Discussion

The EM negative stain images displayed in the figures shown are representative for the quality of all images for the DHBx fusion protein (Fig.39). The corresponding radii of the protein aggregates were significantly observed while visualized by EM (Section 4.7). However, it has to be mentioned that the visible size of a particle in EM depends on the capability to visualize it by negative stain, which is associated with the charge and the density of the molecule. The apparent size of negatively stained particles is also influenced by drying and the associated flattening of particles. Therefore, the molecular size as measured by EM can differ slightly from that determined in solution.

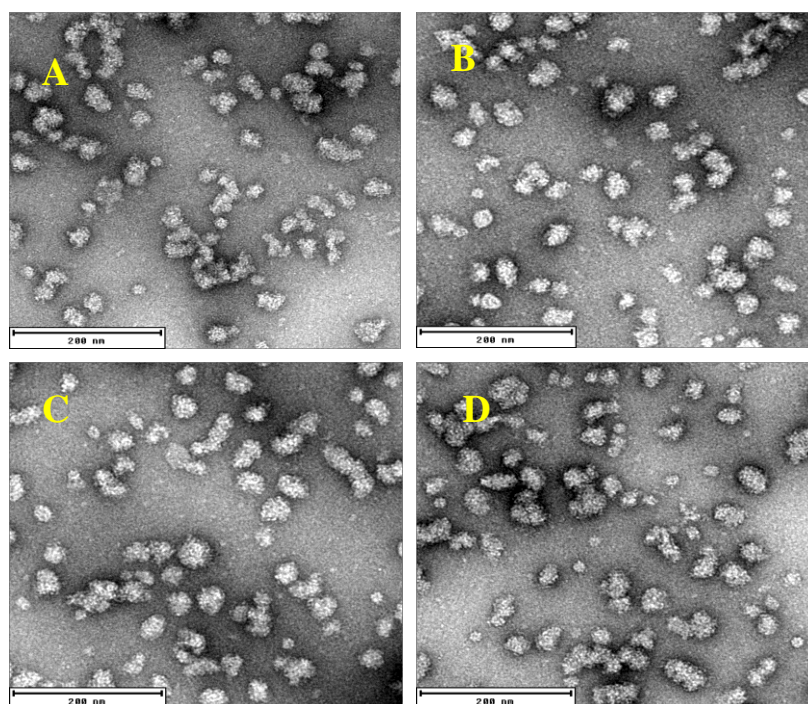


Figure 39: Negative staining images of DHBx fusion protein oligomerized molecules. The figures A, B, C, D, show different particles of the protein with slightly different shapes.

These measurements revealed the existence of particles characterized by an almost globular or a cylindrical shape, which assessed to be 20-40nm in length (Fig. 40B), also a side view of a kidney like with a length of 40-50nm (Fig. 40C). Most of these particles tend to connect with each other to form a complex and a long chain like particle, showing differences in size (Fig. 40A). Images of a biological complex in solution reflect the different states of the complex captured during verifications [Orlova, & Saibil, 2010]. The shapes seem to be flexible allowing the image processing strategy to be customized to suit molecules with unusual shapes and behaviors. The background seems to be significantly clean, indicating a high purity of the sample. The kidney shape seems to contain one extended and flexible structure

Results and Discussion

called the stalk, which emerges from a globular-like head (Fig. 40C). From the two parts, the stalk is the smaller one and is predicted to contain the C-terminal part of the DHBx, while the N-terminal part is connected to the MBP, which forms the globular shape. Stalks were subsequently found to flex independently of the globular shape (Fig. 40C) producing many different flexible structures. This problem is compounded by the alignment which, for each orientation of the globular shape, fails to achieve a precise alignment to all the other shapes including the kidney shapes. Understanding this structure is vital to understand the mechanism of the DHBx protein. Currently, the three-dimensional structure of the entire DHBx protein molecule is unknown and the mechanism of this protein is poorly understood. What follows is a description of the image processing strategies used to align, classify and analyze images of negatively stained DHBx fusion protein molecules.

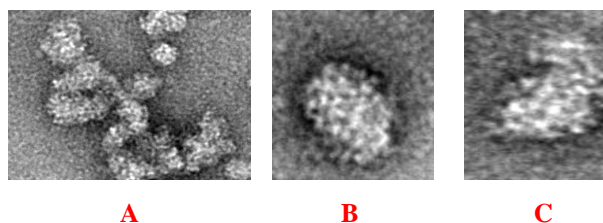


Figure 40: Negative staining images of DHBx fusion protein oligomerized molecules. (A) Represents the formation of a complex and a long chain like particle, (B) Represents a globular shape, (C) Represents the Kidney like-shape.

The images show that the particles are within the size of an oligomer, as was already detected whilst running the sample on a native gel, which shows that all the HBx fusion proteins appear to maintain a molecular weight higher than 700kDa (Fig. 41). The resolution limit of negative staining EM towards molecular details was evaluated using the following features, (i) the flexibility of the DHBx protein (ii) the solubility and stability of the DHBx protein without the MBP and (iii) the formation of the complex with the presence of MBP. After asymmetric single particle observation, it became clear that symmetry could not be applied due to the differences in the particles, which prevented the formation of a tomographic model. Nevertheless, the resulting two-dimensional images have provided new insights into the DHBx fusion protein structure and mechanism.

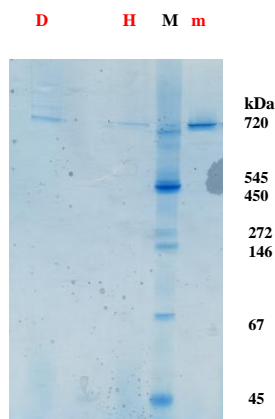


Figure 41: Native gel analysis of the HBx fusion proteins using a native gel from SERVAGelTM MN 3-12, Vertical Native Gel 3-12%. **(D)** DHBx, **(H)** full HBx, **(m)** mini HBx fusion proteins, **(M)** molecular weight marker.

Structural details of the DHBx fusion protein show molecular complexes of different sizes. The size of the complex seems to be significant regarding the structural difference. The larger the differences, the better the resolution in negative staining. Nevertheless, larger complexes produce more trustworthy results, as differences can already be examined on the single particle level. But due to the heterogeneity of the particles, the molecular details were not clearly resolved and it was not possible to determine the exact amino acids responsible for the formation of the complexes. Sample heterogeneity can arise from several sources: (i) partial occupancy of a ligand in a molecular complex [Halic, *et al.*, 2004], (ii) structural dynamics that are reflected in a few distinct reaction states or by a gradual transformation through intermediate states [Heymann, *et al.*, 2003; Fischer, *et al.*, 2010] and (iii) multiple oligomeric states of a different symmetry and/or size [Tilley, *et al.*, 2005; White, *et al.*, 2006]. As the X protein from the DHBV has a protein sequence, it was interesting to see whether or not it possesses a defined structure. In negative staining, the shape of the particle was observed; nevertheless it was not possible to observe the structure. This was expected as changes on the secondary structure level can not be visualized by negative staining. Negative staining EM provides different techniques to explore the structure of single molecules. Several challenges arise whether the object exists in several discrete structural states in solution. If a small number of different conformations would exist, these could be identified during preliminary processing and it would be possible to derive a 3D structure of each conformer [Schoehn, *et al.*, 2000]. However, this approach fails when the molecule is flexible, due to the presence of a continuum of flexible

conformers, which are referred as fleximers. Caution should be taken when interpreting the apparent flexibility seen in molecules adsorbed to a substrate, since distortion during specimen preparation may have contributed to it or even caused it. Therefore, it may not represent the true flexibility of the molecule in solution. Nevertheless, these images may still be useful because distortions by external forces still show the locations within the molecule where flexibility is most likely to occur.

Following adsorption onto carbon, negative staining has implications that the structure seen is distorted or disrupted by the preparative procedure. For example, interactions between protein and the charged surface of the substrate may distort the protein conformation. Further, distortion may occur as the concentration of salts and stains increase during drying with the additional possibility of a drying induced collapse of the structure. Nevertheless, even large complexes that might be expected to collapse can show a surprising degree of fidelity between the negative stained structure and that determined by other techniques [Frank, *et al.*, 1991]. Using this method to observe flexible molecules may be useful in revealing the location of weak points that deform under stresses *in vivo*. Secondly, adsorption to the substrate may perturb a flexible molecule in a way that provides important structural insights; also changes in flexibility can be detected by comparing molecules prepared under different conditions [Burgess, *et al.*, 2004]. Despite the progress in cryo-electron microscopy, negative staining will continue as a useful additional technique for the study of macromolecular functions.

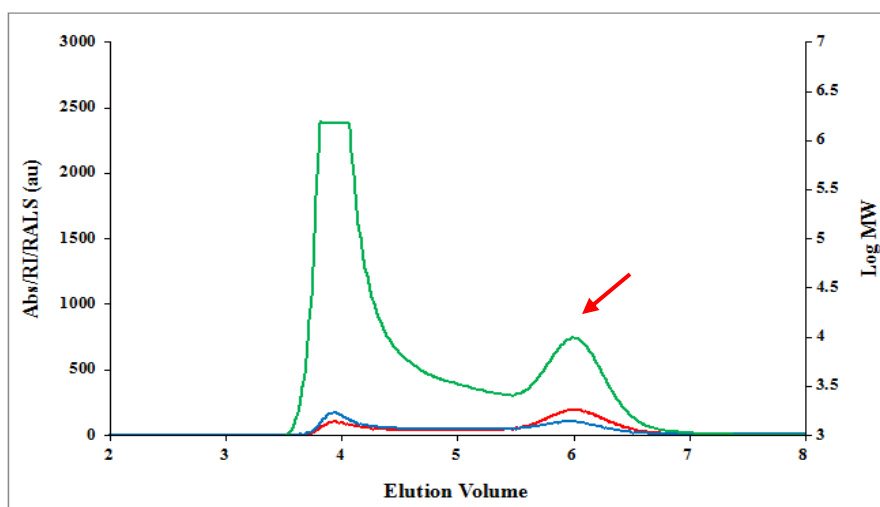
4.13. DHBx and full HBx fusion proteins SEC-SAXS structure

To verify that both DHBx and full HBx fusion proteins are oligomeric in solution, SEC-SAXS measurements were carried out at the EMBL-P12 synchrotron beam line (PETRA-III, EMBL/DESY, Hamburg). Both DHBx and full HBx fusion proteins were purified and centrifuged at 100,000 x *g* for 1hr at 4°C. Solutions were prepared at a concentration of 3.5mg/ml. A dialysis buffer (20mM Tris, pH 7.4, 200 mM NaCl, 1mM EDTA, 4mM DTT, Tab.16) was used, with the addition of 4% (v/v) glycerol to reduce the effects of radiation damage [Jeffries, *et al.*, 2015]. The fusion proteins, (approx. 75 µl) were applied to the SEC column (Superose 6) at a flow rate of 0.5 ml/min. The integration of an in-line SEC separation step (SEC-SAXS) immediately

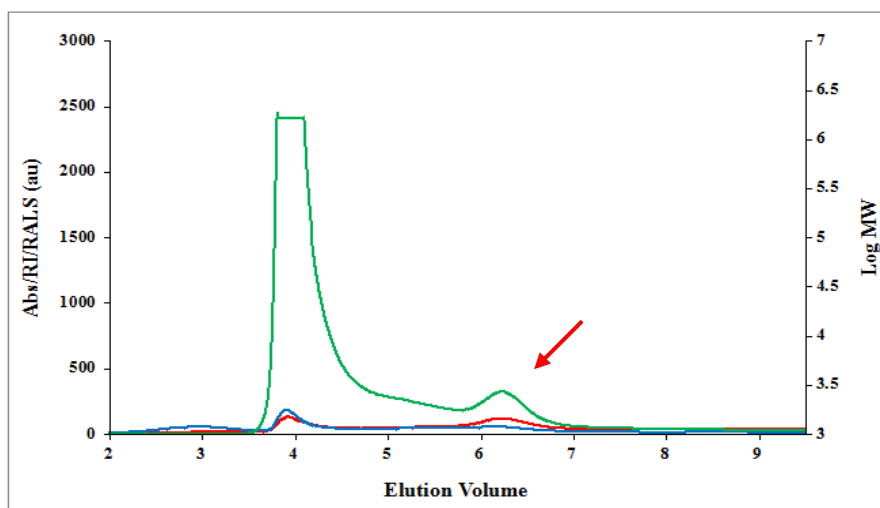
Results and Discussion

up-stream of the X-ray beam enables the analysis of the individual components of both DHBx and full HBx fusion protein samples as they elute from the column.

The SEC-SAXS setup [Graewert, *et al.*, 2015] utilizes a modular triple detector array (TDA, Viscotek model TDA 305, Malvern Instruments) that extracts MW estimations of SEC-separated components by correlating the index (RI) and/or UV-vis concentrations with RALS data. A simple in-series SEC-TDA-SAXS configuration was used by attaching the TDA between the exit of the SEC column and the entry to the SAXS sample capillary. Several dilutions of the eluting samples and also peak broadening were observed during this process. Different software modules were added to the beamline for data analysis and modeling pipelines. After synchronized data collection for both HBx fusion proteins, data frames containing the SAXS intensities of buffer were identified, averaged and subtracted from each acquired data frame to produce net scattering from the solution. Using $\text{Auto}R_g$, [Petoukhov, *et al.*, 2012] the forward scattering extrapolated to zero angle, $I(0)$, which is proportional to the concentration and volume squared (i.e., MW) of the eluting species, were determined using an automated least-squares which fits to Guinier plots of the data ($\ln I(s)$ vs s^2) in the linear region of the plots at very-low scattering angles ($sR_g < 1.3$). The radius of gyration (R_g) was also extracted for each subtracted frame, based on the slope of the Guinier plot (where the slope is proportionate to R_g^2). Each reduced SAXS profile is normalized to concentration and those frames with consistent R_g values are evaluated statistically similar across the entire s -range (0.03 - 4.0 nm^{-1}) [Franke, *et al.*, 2015] and averaged to produce the final SAXS scattering curves corresponding to the separated sample components (Fig.42).



A



B

Figure 42: Schematic diagrams of the collected fractions for both DHBx (A) and full HBx (B) fusion proteins. The first peaks represent the aggregation particles. The second peaks represent the collected fractions used for data analysis and model processing.

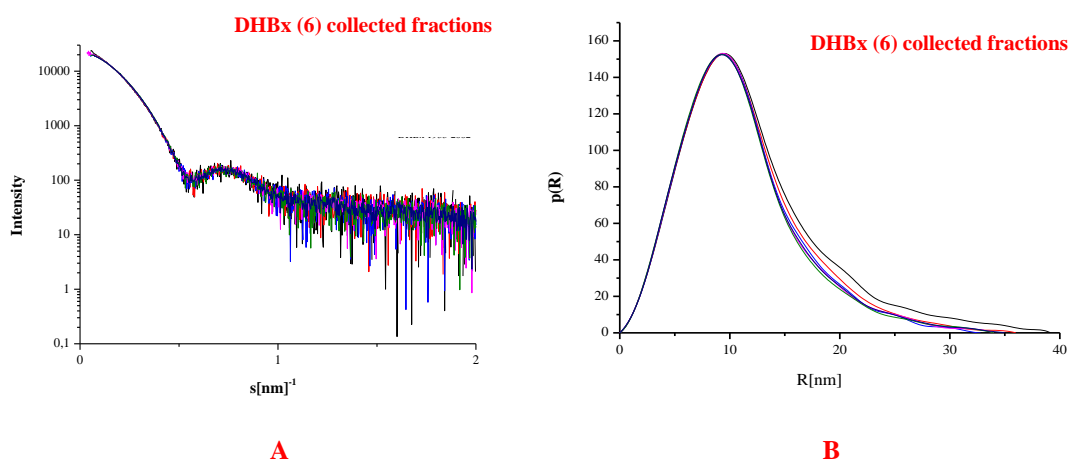
It can be observed from the SEC elution trace recorded by the TDA that both proteins form extremely large aggregates (> 4 MDa) that elute in the void volume of the SEC column which is observed as the first elution peak, followed by a smaller component (Fig. 42A, B). The MW estimation for the components of the second major elution peak for the DHBx fusion protein (based on RI/RALS data), lies within the range of 765-858 kDa, with an average of 800kDa. The second elution peak for the full HBx fusion protein, corresponds to species between the range of 650-700kDa, with an average of 660kDa. Considering that the monomer molecular weights for both proteins are 57kDa and 59kDa, for the DHBx and full HBx fusion proteins, respectively, the combined TDA results clearly indicate that both proteins have a propensity to spontaneously self assemble into high molecular weight oligomers.

With respect to the SAXS data analysis of the second major elution peaks observed for DHBx and full HBx fusion proteins, it must be noted, that as the RALS intensities do not return to baseline between the first aggregate peak and the second major peak. This indicates that both full HBx and DHBx fusion proteins, in the initial samples, exist as a continuum of highly polydisperse high-molecular weight oligomers. These oligomers may not be fully separated from the second major elution peak for both fusion proteins and likely contribute to the SAXS data. However, it is possible to select SAXS data frames corresponding to sections of the second peak for both full HBx and DHBx fusion proteins that have a consistent R_g and statistical equivalency

Results and Discussion

across the scattering profiles. This enables to obtain insights into the global shapes of the 800 kDa DHBx and 660 kDa full HBx fusion protein assemblies.

The software package *GNOM* [Svergun, 1992] was used to compute the inverse indirect fourier transform of the SAXS data from which the probable real-space atom-pair distance distribution, or $p(r)$ vs r profile, was calculated (Fig. 43A-B, 44A- B). This distribution reflects the frequency of distances between scattering centres within the DHBx and full HBx fusion proteins assemblies and is therefore characteristic of the shapes of the assemblies in solution. For both fusion proteins, the R_g extracted from the first peak of $p(r)$ vs r for the DHBx fusion protein assembly, was in the range of 16.0-19.5 nm with a maximum particle dimension, D_{max} , of 62-82 nm. For the full HBx fusion protein assembly, the R_g was between 18.5-20.9 nm and the D_{max} between 65-78 nm, these results observe large aggregates. The R_g extracted from the second moment of $p(r)$ vs r for the 800 kDa DHBx fusion protein assembly was in the range of 8.2-8.9 nm with a maximum particle dimension, D_{max} , of 35-39 nm. For the full HBx fusion protein 660 kDa assembly, the R_g was between 9.5-10.1 nm and the D_{max} between 45-50 nm. With respect to visualizing the global shapes of the assemblies derived from $p(r)$ vs r for the second major peaks, the *ab initio* bead modeling program *DAMMIF* [Franke & Svergun, 2009] was employed to restore the shapes of both DHBx and full HBx fusion proteins (Fig. 43C and 44C).



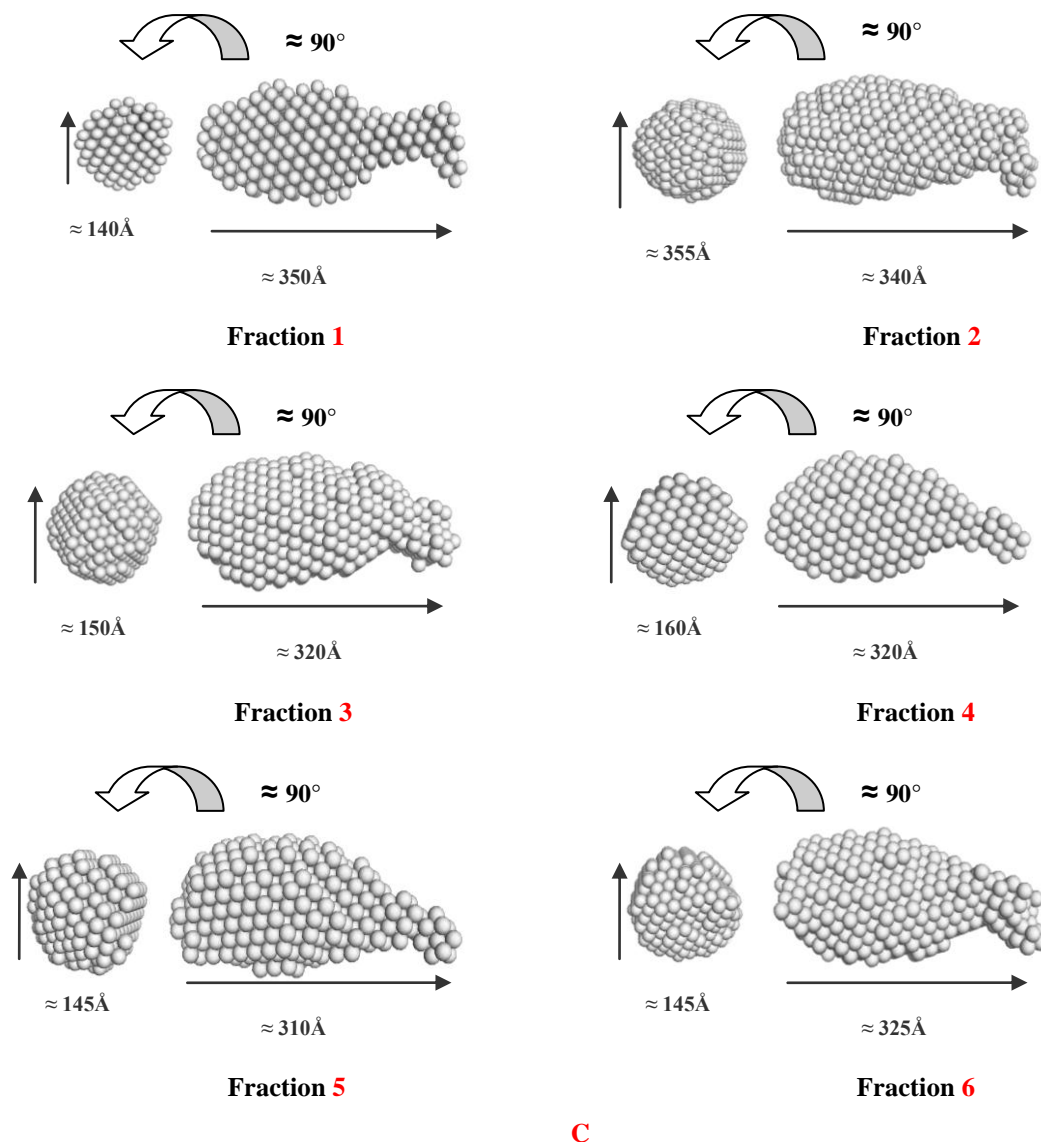


Figure 43: Processed solution SEC-SAXS scattering data for the DHBx fusion protein used for *ab initio* modeling (A-left panel), and the fit graph of the models (B-right panel), all generated by DAMMIF. (C) Represents the average models observed from DAMMFILT. The fit graph demonstrates that the SEC-SAXS scattering data is well interpreted.

The average and volume-corrected *ab initio* models calculated for the DHBx fusion protein (Fig. 43C) appear as an elongated ellipsoidal shape with a thickened globular end possessing a small curved extension. The individual models used to calculate the average representation fit the experimental data well, with a χ^2 between (1.06-1.2; APP. Fig 58). The shape of the DHBx obtained from SAXS is in overall agreement with the negative staining EM results, which also indicate that the assembly adopts an ellipsoidal ‘kidney like’ shape (Section 4.12, Fig. 40C). For the full HBx fusion protein, the models contain a thickened globular end and a small globular lengthening ($\chi^2 = 1.38-1.41$; APP. Fig.59), (Fig. 44C). It must be cautioned, due to the poor resolving power of the SEC column, that this lengthening of the full

Results and Discussion

HBx fusion protein's shape may be caused by contributions from larger molecular weight species overlapping into the second elution peak of the full HBx fusion protein sample. However, and in general, both the DHBx and full HBx fusion protein assemblies have similar overall shapes in solution that are primarily characterized as anisotropic ellipsoids, the results of which are supported by the EM observations especially for the DHBx fusion protein.

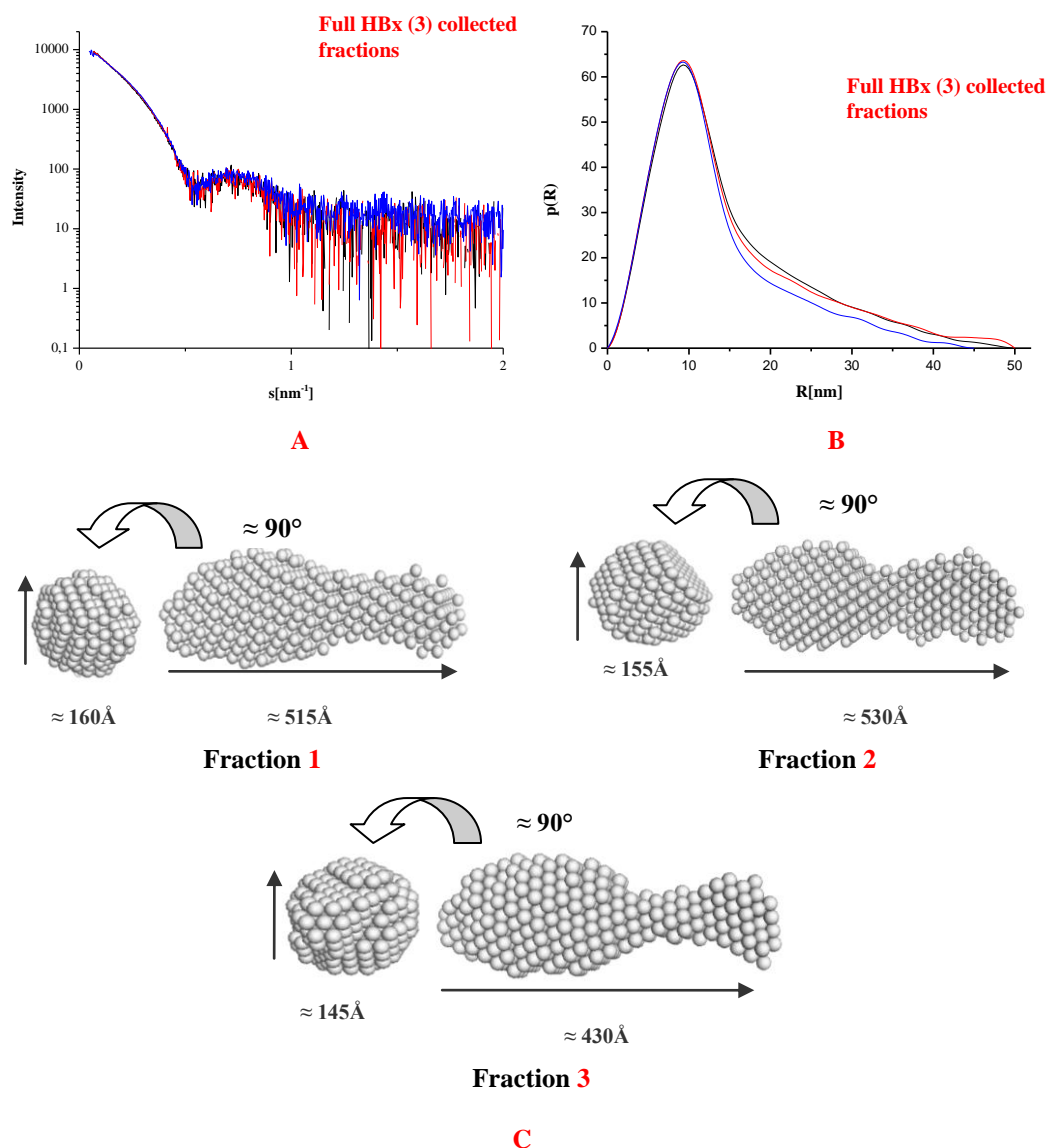


Figure 44: Processed solution SEC-SAXS scattering data for the full HBx fusion protein used for *ab initio* modeling (A-left panel) and the fit graph of the models (B-right panel), all generated by *DAMMIF*. (C) Represents the average models observed from *DAMMIFILT*. The fit graph demonstrates that the SEC-SAXS scattering data is well interpreted.

From the observed *ab initio* models for both HBx fusion proteins, the MBP reflecting the N-terminal part is the thickened globular end, which is considered the stable part of the structure, whereas the C-terminal part of the models, which obtain the small curved lengthening or a small globular lengthening, represent the DHBx and

full HBx, respectively. The C-terminal part of the models is the unstable part of the structure, which was observed for the DHBx fusion protein, as the protein tends to form complexes by interacting with each other when performing negative staining EM (Section 4.12, Fig.40A). The bending or the curved lengthening of the C-terminus part of the DHBx fusion protein would additionally enable this part to interact with other molecules and form a complex, also a long chain like particle (Section 4.12, Fig.40A). This is also assumed for the full HBx fusion protein, although the *ab initio* model is more elongated than that of the DHBx fusion protein, the bending of the C-terminus part is similarly conceivable. The differences of the models originated are due to the differences between the structures of both HBx fusion proteins. In conclusion to this study, SEC-SAXS/TDA system was developed for parallel SAXS and biophysical measurements to validate and correlate the molecular weights of separated sample components for automated data analysis and modeling of polydisperse macromolecular samples. SEC-SAXS is highly beneficial and indispensable in analyzing particularly partly flexible multi-domain proteins. In this project, SEC-SAXS was used to analyze and observe the structure of HBx fusion proteins, having in mind that the structure of these proteins is unknown. Significantly, the SEC-SAXS data are entirely consistent with the observations made from the EM results.

4.14. Expression of p53 proteins

The p53 genes containing full-length p53 (393 amino acids), truncated N-terminal p53 (1-160) and the truncated C-terminal p53 (160-393) were provided by PD Dr. rer. nat. N. Fischer, Center for Diagnostic, Department of Medical Microbiology, Virology and Hygiene, University Medical Center Hamburg-Eppendorf (UKE). The genes were already cloned into the pGEX2-T vector that provides an N-terminal GST-tag. Expression for the three constructs was performed at of 37°C, followed by cultivation at 30°C using the *E. coli* strain BL21 DE3 and all were induced at an OD₆₀₀ of approx. 0.6-0.7 with 1mM IPTG. After 5hrs of protein expression, the cells were harvested by centrifugation and the amount of the recombinant expressed p53 proteins was analyzed by 15% SDS-PAGE. The detected expression level of the p53 proteins was relatively high when 1mM IPTG has been used. After induction of the recombinant proteins, expression protein bands appeared on the SDS-PAGE that consistently correspond to the protein consisting of full-length p53 and GST with a

Results and Discussion

calculated molecular weight of approx. 79kDa (Fig. 45A) to the truncated N-terminal p53 (1-160)-GST protein with a calculated molecular weight of approx. 43kDa (Fig.45A) and to the truncated C-terminal p53 (160-393)-GST protein, which corresponds to 52kDa (Fig.45B).

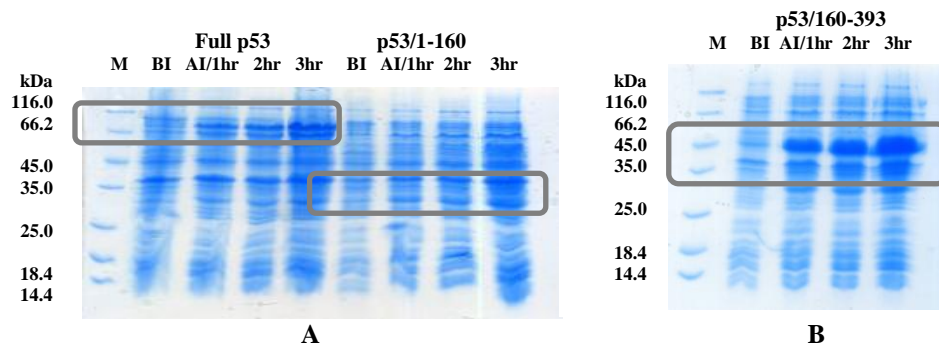


Figure 45: SDS-PAGE analysis of the expression of full-length p53, as well as truncated N-terminal p53 (1-160) (A) and C-terminal p53 (160-393) proteins (B) in *E. coli* at a cultivation temperature of 37-30°C. BI: before induction; AI: after induction; M: molecular weight marker.

4.15. Solubility of p53 proteins

After determination of the optimized conditions for the p53 genes expressed in *E. coli* cells, the solubility of the recombinant proteins was tested. Following separation of the soluble from the insoluble proteins by centrifugation, both the pellet and the supernatant fractions were applied to SDS-PAGE analysis. Both full length and C-terminal p53 proteins were present in a soluble and in an insoluble form when gene expression is performed in BL21 DE3 cells at 37°C and 30°C, respectively. By induction with 1mM IPTG (Fig.46), the N-terminal p53 protein formed only insoluble protein aggregates (Fig. 46). Due to these results, the test experiment was continued by using both full length and C-terminal p53 proteins, which were observed to be purified in a soluble form.

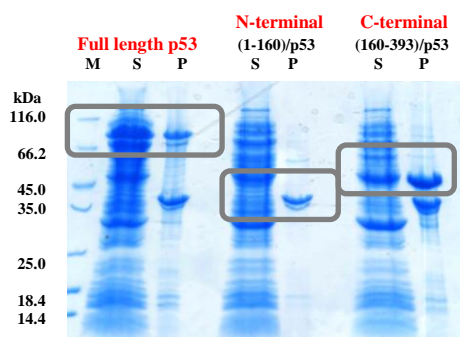


Figure 46: SDS-PAGE analysis of the solubility test of GST-p53 proteins after gene expression in *E. coli* strain BL21 DE3, induced with 1mM IPTG at a cultivation temperature of 37 and 30°C; M, molecular weight marker; S, supernatant; P, pellet.

4.16. Purification of full-length and C-terminal p53 proteins

Affinity chromatography, using a GST matrix column, was applied for the purification of full-length and C-terminal GST-p53 proteins. After equilibration of the column using the appropriate buffer (Tab.16), the soluble proteins in the supernatant fraction that was separated by centrifugation of the lysed cells, were applied onto the column. After several washing steps using the appropriate buffer to remove unspecific bound proteins, the proteins were eluted manually with reduced glutathione and the collected fractions were analyzed by SDS-PAGE. The gel electrophoretic analysis showed that the p53 proteins eluted in a purified state (Fig. 47A, B). A single protein band was identified between the molecular weight markers of 66kDa and 116kDa, corresponding well with the calculated MW of 79kDa for the full-length GST-p53 target protein (Fig. 47A). For the C-terminal p53 protein, a band corresponding well with the calculated MW of 52kDa was identified between the 45kDa and 66kDa molecular weight markers (Fig. 47B).

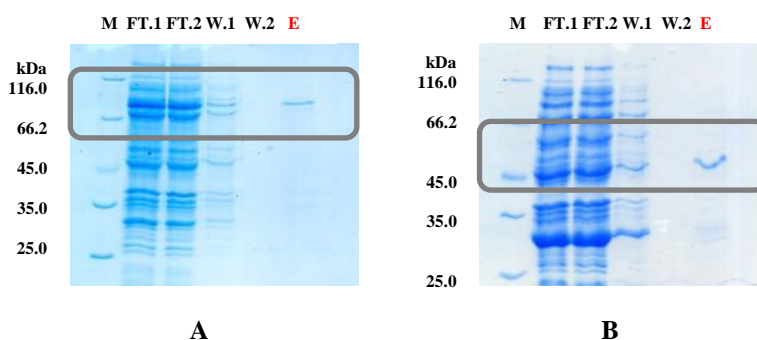


Figure 47: SDS-PAGE analysis of the purification of full-length (A) and C-terminal p53 proteins (B). FT1/2, first and second flow through fraction; W1/2, first and second wash fraction; E, elution fraction 1. M, molecular weight marker. The boxes highlight the eluted full-length and C-terminal p53 fusion proteins.

After cleavage of both p53 proteins by Thrombin (Fig. 48A, B), the free tagged proteins were separated from the GST tag by affinity chromatography using a GST matrix. The free tagged proteins appeared in the flow through. The samples were collected and analyzed by SDS-PAGE.

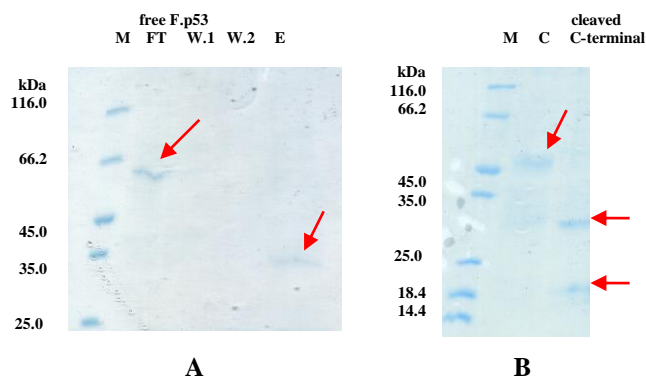
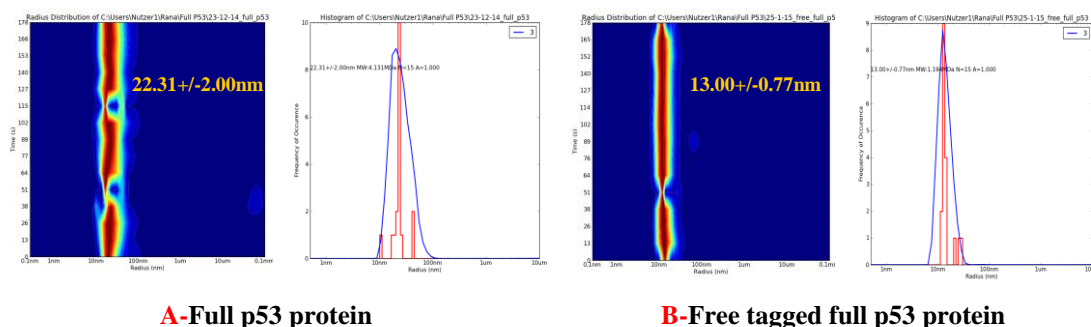


Figure 48: SDS-PAGE analysis of the separation of full-length P53 protein after cleavage (A) and complete cleavage of C-terminal p53 protein (B). FT, flow through fraction; W1/2, first and second wash fraction; E, elution fraction. C, control M, molecular weight marker.

4.17. Dynamic light scattering (DLS) for the p53 proteins

Dynamic light scattering (DLS) is a non-invasive, well-established technique for measuring the size distribution of molecules and particles typically in the submicron region. The radius distribution of the p53 proteins, both full length and C-terminal, was determined after purification using size exclusion chromatography (Fig. 49A, B, C, D). The oligomeric state of the p53 proteins, with and without the presence of the GST tag, was characterized by a hydrodynamic radius of $R_H=22.3\pm 2.00\text{nm}$ for the full p53 in the presence of the GST tag (Fig. 49A). When removing the GST tag, the hydrodynamic radius decreased to $13.0\pm 0.77\text{nm}$, which indicates that the protein is more stable with the absence of the GST tag (Fig. 49B). The hydrodynamic radius for the C-terminal p53 in the presence of GST tag is of $R_H=17.2\pm 3.21\text{nm}$ (Fig. 49C). When removing the GST tag, the hydrodynamic radius increased to $28.53\pm 5.75\text{nm}$, which shows that the absence of the GST tag affects the stability of the C-terminal p53 protein that induced the formation of large aggregates (Fig. 49D).



A-Full p53 protein

B-Free tagged full p53 protein

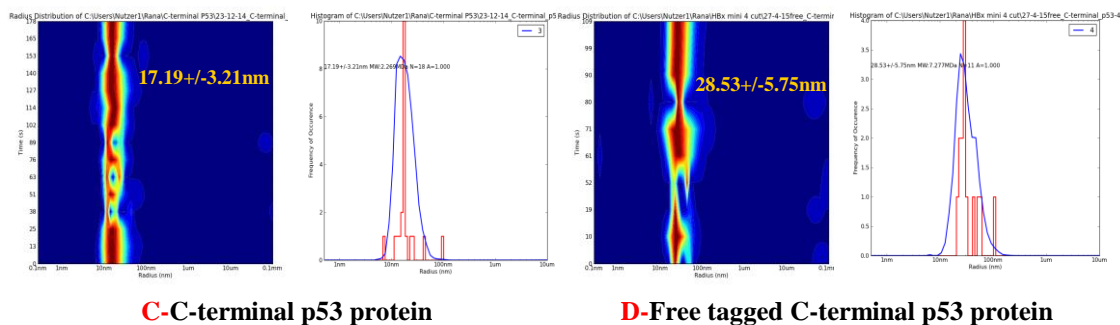


Figure 49: DLS histograms (blue) and statistical distribution of the measured radius in the histogram (red). (A) Sample of the full p53 protein. (B) Sample of the free tagged full p53 protein. (C) Sample of the C-terminal p53 protein. (D) Sample of the free tagged C-terminal p53 protein.

4.18. Secondary structure determination for the p53 proteins

To compare the secondary structure composition of the p53 proteins with and without the presence of the GST tag, circular dichroism (CD) spectroscopy was applied. All measurements were performed using 50mM Tris, pH 8.0, 50mM NaCl (Tab.16) at room temperature. The samples were measured with the presence and absence of the GST tag. Figure 50 shows the CD spectrum of the purified full p53 protein. The spectrum revealed one strong positive peak in the vicinity of 195nm and two minima at 212nm and 225nm. Fractions of β -sheets are indicated by a single minimum at 213nm; the two minima are characteristic for a largely α -helical structure as indicated at 210nm and 222nm. Another CD spectrum was obtained for the free tagged full p53 protein, the spectrum revealed one strong positive peak also in the vicinity of 195nm and two minima at 212nm and 222nm. Fractions of β -sheets are indicated by a single minimum at 213nm; the two minima are characteristic for a largely α -helical structure and are indicated at 215nm and 220nm. The results obtained from the CD spectra analysis revealed that the secondary structure of the full p53 proteins, with the presence and absence of the GST tag, is predominantly composed of α -helices and β -sheets. . They additionally demonstrate the influence of the presence and absence of the GST tag on the secondary structure of the protein, which shows high percentage of β -sheets for the free full p53 protein and this is known to form a tetramer [Friedman, *et al.*, 1993], as compared to the full p53 protein, which obtains high percentage of α -helices due to the presence of GST.

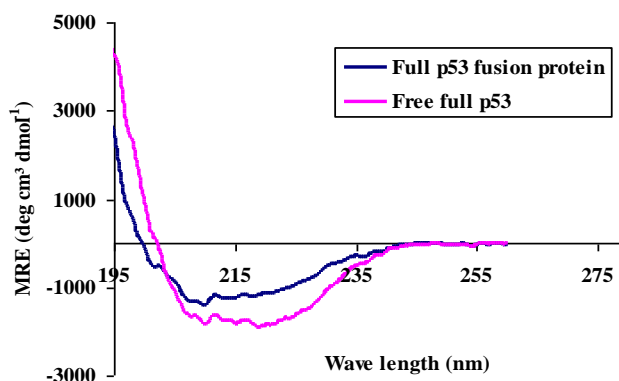


Figure 50: CD spectra of the purified full p53 protein and free tagged full p53 protein.

A similar CD spectrum was obtained for the C-terminal p53 protein, for which the spectrum revealed one strong positive peak in the vicinity of 195nm, also two minima at 212nm and 220nm. Small fractions of β -sheets are indicated by a single minimum at 213nm and the two minima are characteristic for a large α -helical structure is indicated at 215nm and 218nm (Fig. 51). The CD spectrum for the free tagged C-terminal p53 protein revealed two strong positive peaks in the vicinity of 197nm, two minima at 212 and 225nm. Small fractions of β -sheets are indicated by a single minimum at 215nm and the two minima are characteristic for a large α -helical structure, indicated at 216nm and 222nm. Here both structures also differ, due to the presence of the GST tag, which is highly observed between both spectrums. The free C-terminal p53 protein is known to form a dimer [Truant, *et al.*, 1995; Ou, *et al.*, 2007], containing high percentage of β -sheets, compared to the C-terminal protein, which shows high percentage of α -helices instead of β -sheets.

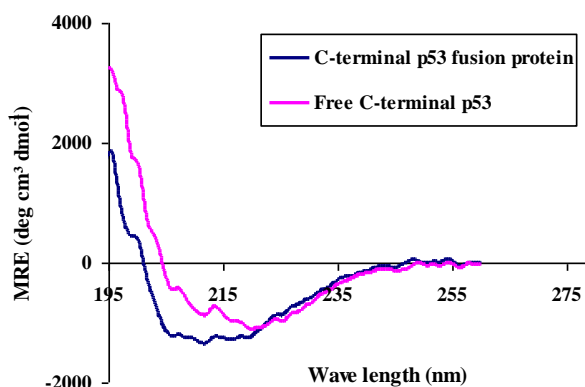
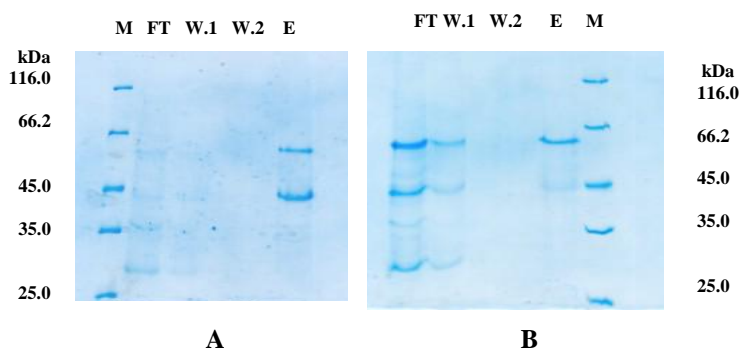


Figure 51: CD spectra of the purified C-terminal protein and free tagged C-terminal p53 protein.

4.19. Interaction of full and mini HBx fusion proteins with p53 proteins

Protein affinity chromatography was used to detect whether human p53 proteins could directly or selectively bind to the HBx fusion proteins [Truant, *et al.*, 1995]. This procedure was performed after purification of both fusion proteins with the p53 proteins. The proteins were mixed at a molar ratio of 1:1 (HBx fusion proteins: p53 proteins) and incubated over night at room temperature and at 4°C. Subsequently, the protein mixtures were applied to the amylose matrix. Collected fractions of the flow through and the specific elution were tested for the presence or absence of the HBx fusion proteins and p53 proteins. A binding test was first performed for the full-length hHBx fusion protein and the C-terminal p53 protein at room temperature and at 4°C. Figure 52A shows that both proteins were present in the elution fraction after overnight incubation at room temperature, indicating a positive interaction between the proteins. For the same mixture incubated at 4°C, only a weak interaction could be detected, since only a part of the full-length hHBx was present in the elution fraction, while the other part was present in the flow through fraction (Fig. 52B). This result was also observed when analyzing the interaction between mini HBx fusion protein and C-terminal p53 protein at 4°C (Fig. 52D). The binding test of both mini HBx fusion protein and C-terminal p53 protein at room temperature showed an obvious band in the elution step and only a very slight lower band of the C-terminal p53, which indicates the expected molecular weight maintained in the flow through (Fig. 52C). These results indicate that the interaction of both HBx fusion proteins with the p53 proteins is stronger at room temperature as compared to 4°C. Figures 52E, F show positive interaction for the mini HBx (Fig. 52E) and full-length hHBx (Fig. 52F) fusion proteins, with full-length p53 protein being present in the elution step after over night incubation at room temperature.



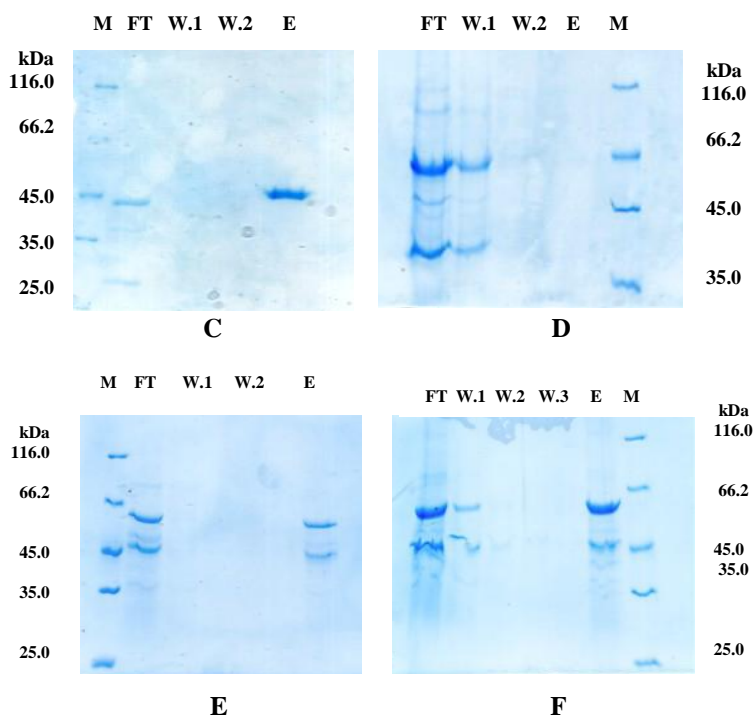


Figure 52: Interaction test of HBx fusion proteins and p53 proteins. (A, B) SDS-PAGE analysis of the binding test between full hHBx fusion protein and C-terminal P53 protein at room temperature (A) and at 4°C (B). (C, D) SDS-PAGE analysis of binding test between mini hHBx fusion proteins and C-terminal P53 protein at room temperature (C) and at 4°C (D). (E, F) SDS-PAGE analysis of the binding test between mini HBx fusion proteins and full p53 protein. (E). And also between full hHBx fusion protein and full P53 protein at room temperature (F). FT, flow through fraction; W1/2, first and second wash fraction; E, elution fraction; M, molecular weight marker.

In order to observe the possibility of both full and C-terminal p53 proteins to interact with the amylose matrix by absence of the HBx fusion proteins, both p53 proteins were applied to this matrix. After sample collection, the probes were run on SDS-PAGE. The results showed that both p53 proteins are present in the flow through and washing step, and negatively observed in the elution step, indicating a negative binding of both p53 proteins to the amylose matrix (APP. Fig- 57A, B). Another binding test was performed after purification of the HBx fusion proteins and cleavage of the p53 proteins from the GST tag. After this procedure, the proteins were also mixed at a molar ratio of 1:1 (HBx fusion proteins: free tagged p53 proteins) and incubated over night at room temperature. Subsequently, the protein mixtures were applied to the amylose matrix. Collected fractions of the flow through and the specific elution were tested for the presence or absence of the HBx fusion proteins and the free tagged p53 proteins. The first binding test was performed for the full-length hHBx fusion protein and for the free tagged C-terminal p53 protein, both at room temperature. Figure 53A shows that the full-length hHBx fusion protein was present in the elution fraction, while the free tagged C-terminal protein, which indicates the

Results and Discussion

expected molecular weight, maintained in the flow through after overnight incubation at room temperature, indicating a negative interaction between both proteins. This result was also observed when analyzing the interaction between mini HBx fusion proteins with free tagged C-terminal p53 protein after performing the same procedure (Fig. 53C). These results indicate that the binding was performed in the presence of GST tag. The binding test of both full-length hHBx fusion protein and free tagged full p53 protein after overnight incubation at room temperature showed an obvious band in both flow through and the elution step (Fig. 53B). This result was also observed when analyzing the interaction between the mini HBx fusion protein and the free tagged full p53 protein after overnight incubation at room temperature (Fig. 53D). Both bands observed in the elution step were sent for MS analysis to observe the presence or the absence of the free tagged full p53 protein. The MS results indicated the absence of free tagged full p53 protein in the elution step (data not shown) with the presence of the HBx fusion proteins only. These results conclude a negative interaction between the HBx fusion proteins and the free tagged full p53 protein. This shows that the trans-activation domain for the free tagged full p53 protein is dispensable for HBx-binding [Lin, *et al.*, 1997].

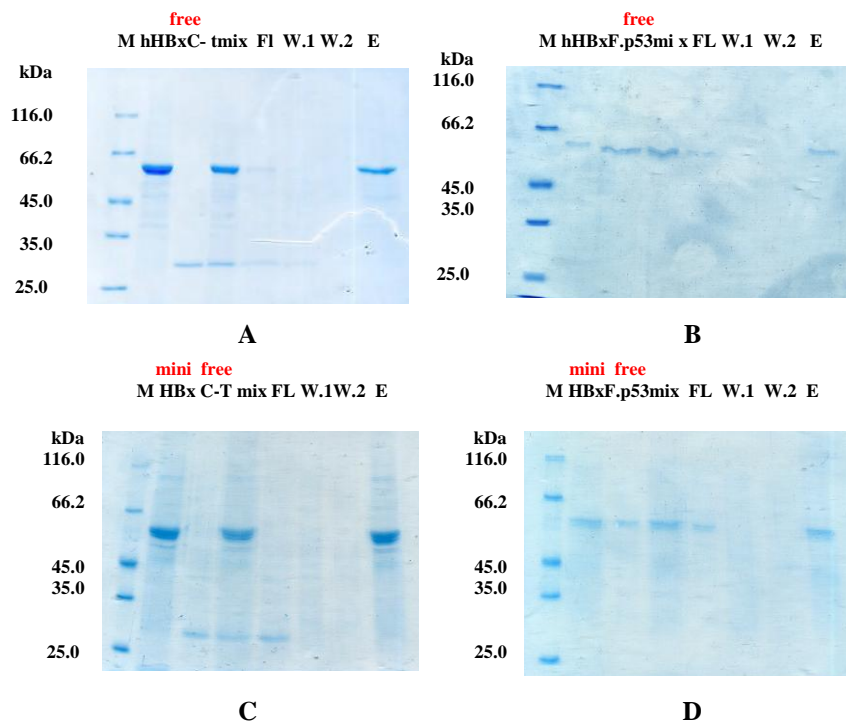


Figure 53: Interaction test of HBx fusion proteins and free tagged p53 proteins. (A) SDS-PAGE analysis of binding test between full hHBx fusion protein and free tagged C-terminal P53 protein at room temperature. **(B)** SDS-PAGE analysis of binding test between full hHBx fusion protein and free tagged full P53 protein at room temperature. **(C)** SDS-PAGE analysis of binding test between mini hHBx fusion protein and free tagged C-terminal P53 protein at room temperature. **(D)** SDS-PAGE analysis of binding test between mini hHBx fusion protein and free tagged C-terminal full P53 protein at room temperature.

Results and Discussion

FT, flow through fraction; mix, mix fraction for both proteins; W1/2, first and second wash fraction; E, elution fraction; M, molecular weight marker.

The N-terminal domain of full p53 protein is very acidic [Fields and Jang, 1990], which showed negative interaction. Nevertheless, the interaction between HBx fusion proteins and free tagged full p53 activation domain may be quite weak, since it could not be detected [Truant, *et al.*, 1995]. The interaction between HBx fusion proteins (full length and mini) with the full-length p53 protein were confirmed by using an Octet HTX system device. This system is used for analysis of bimolecular interactions and binding kinetics, which shows both proteins interacting at different concentrations. The results show an interaction between the HBx fusion proteins with full length p53 protein and are negative with free tagged full length p53. These experiments were performed using different concentrations of both HBx fusion proteins with full length p53 (with the absence and presence of GST tag).

The first experiment was performed with the presence of the mini HBx fusion protein with the full length p53 protein. In this experiment, 8 sensors were used with different concentrations of the mini HBx fusion protein. The presence of PBS buffer in the last sensor was used as a control instead of the mini HBx fusion protein, while maintaining the same concentration for the full p53 protein in all 8 sensors. The results show an interaction between the mini HBx fusion protein and the full length p53 protein, which is highly observed when using a low concentration of mini HBx fusion protein (Fig. 54A). The interaction decreases when the concentration of the mini HBx fusion protein is increased. The dissociation constant (K_D) value observed was $14.40 \pm 6.8 \text{ nM}$. The last sensor, which contains the full p53 protein with buffer instead of the mini HBx fusion protein, also shows binding activity, which clarifies the unspecific interaction between both proteins due to the presence of GST tag.

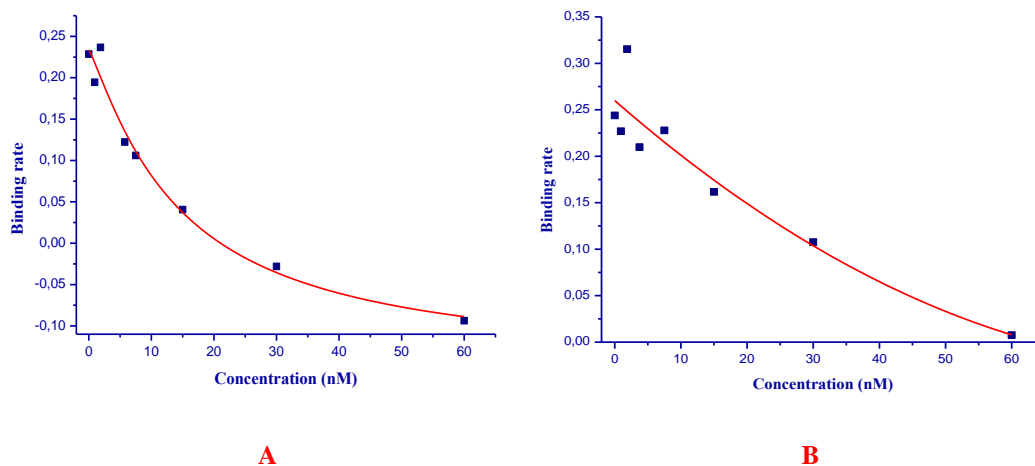


Figure 54: Conformation analysis of the interaction between mini HBx fusion protein with full P53 protein (A), and full length HBx fusion protein (B) using the Octet device.

To determine the effect of the GST tag, full p53 protein was replaced with free tagged full p53 protein. Negative binding was observed in the presence of the mini HBx fusion protein at different concentrations (data not shown). Another experiment was performed between the full length HBx fusion protein and the full p53 protein. The results also show interaction between both proteins. Lower concentrations of the full length HBx fusion protein with a constant concentration of the full p53 protein show increment interaction between both proteins, which decreased gradually by increasing the concentration of the full HBx fusion protein (Fig. 59B). The dissociation constant (K_D) value was $55.18 \pm 22 \text{ nm}$ which is relatively high as compared to the mini HBx fusion protein interaction procedure. The last sensor, which contains the full p53 protein with PBS buffer instead of the full HBx fusion protein, shows unspecific binding due to the presence of the GST tag. When comparing both interactions from the figures, it appears that the interaction between both proteins in the presence of the mini HBx fusion protein is more accurate than that with the full HBx fusion protein, which is observed in the K_D value. This might be the fact due to the structural formation of the mini HBx, which could result in modifying its binding activity. When replacing the full p53 protein, the free tagged full p53 protein showed negative binding to the full HBx fusion protein. Subsequently, these results confirm the negative interaction of HBx fusion proteins to the N-terminal domain of the free tagged full p53 protein, due to the weak binding, which is not able to be detected [Truant, *et al.*, 1995]. The results also reveal that the interaction was achieved in the presence of the GST tag.

Several results regarding the interaction function between HBx and p53 proteins, using different methods, have been demonstrated. Most results indicate that the HBx-binding sites are located within the oligomerization domains and specific DNA-binding domains of p53, but the trans-activation domain is dispensable for HBx binding [Truant, *et al.*, 1995]. The p53 binding site was confined to be a small region in the HBx trans-activation domain [Lin, *et al.*, 1997]. Also, p53 possesses two independent HBx-binding sites located in the specific DNA-binding domain and oligomerization domain, respectively. The p53 and HBx proteins interfere with each other's trans-activation function. However, HBx trans-activation was detected in the p53-negative site and HBx trans-activation is distinct from its p53-binding domain [Lin, *et al.*, 1997]. Several studies also confirm that both HBx and p53 proteins directly interact with each other *in vitro*, which was shown by different techniques. The proteins used in these methods are observed as tagged-proteins [Feitelson, *et al.*, 1993; Lee, *et al.*, 1995], similar as in our experiment studies. Other studies show that both proteins also interact functionally *in vivo*. A study reported that p53 protein has no detectable effect on the reporter. However, the HBx trans-activation activity was severely repressed by the p53 protein in a dose-dependent manner. A similar effect was observed when p53 and HBx proteins were co-expressed, which constitutes the trans-activation domain of HBx. The repression by p53 protein could be alleviated by an excess amount of HBx. The ability of HBx to interfere with the p53 trans-activation was mapped to the p53-binding region of HBx, suggesting that the interference may be the direct result of p53 binding to HBx. The direct interaction of p53 and HBx may prevent the p53 protein from accessing the regulation element of the p53-responsive genes [Wang, *et al.*, 1994; Truant, *et al.*, 1995]. It is clear that the HBx trans-activation is distinct from the p53-binding function, although the HBx trans-activation could be affected by an excess of p53.

5. Summary

HBV is one of several liver-specific viruses that cause different severe inflammation of this central metabolic organ. HBV has been implicated in causing severe disease since 1947, yet despite the discovery of the HBx protein in the early 1980s, controversy remains questioning its function in both the viral lifecycle and the progression of HBV-associated HCC. Chronic hepatitis B virus (HBV) infection affects over 2 billion people worldwide, 400 million are chronically infected with this virus and over 1 million patients die annually of HBV-related chronic liver disease. Although many individuals eventually achieve a state of non-replicative infection, the prolonged immunologic response to infection leads to the development of cirrhosis, liver failure, or hepatocellular carcinoma (HCC) in up to 40% of individuals with chronic HBV infection. The prevalence of chronic HBV infection varies widely in different parts of the world. In endemic areas, where carrier rates are >5%, most individuals are infected perinatally, by vertical transmission, or in early childhood. A variety of host factors (age at infection, gender, immune status), viral factors (viral load, genotype mutation) and external factors (concurrent viral infections, alcohol consumption, chemotherapy) influence disease progression. Several variables (age at infection, gender, ethnicity, immune status) also influence the risk of chronic infection. Immunization is the most effective mean of preventing HBV infection because till now there is no specific treatment for acute hepatitis B. Therefore, care is aimed to maintain comfort and adequate nutritional balance, which includes replacement of fluids lost from vomiting and diarrhea. Chronic hepatitis B infection can be treated with drugs, including oral antiviral agents. Treatment can slow the progression of cirrhosis, reduce the incidence of liver cancer and improve long term survival.

HBV X protein (HBx protein) is a multifunctional regulator that plays a crucial role in hepatocarcinogenesis. The enigmatic HBx protein is a trans-activator which can activate various viral and cellular promoters and enhancers, these activities are necessary for viral replication. HBx protein is highly conserved among the different subtypes of the virus. It is present in the cytoplasm and, to a lesser extent in the nucleus of hepatocytes. The HBx protein is essential for establishing natural viral infection and has been implicated in the development of liver cancer associated with chronic infection. This protein has been reported to exhibit a variety of different

activities in tissue culture cells, including induction of cell death and stimulation of HBV replication. The HBx structural studies have been hampered by expression difficulties and as a result, no X-ray or NMR data are available for HBx up to date. Furthermore, the role that HBx plays in liver disease has been negatively affected by reliance on transfection-based over-expression systems and physiologically irrelevant cellular models. These methodologies may have inadvertently introduced numerous artefactual findings into the field.

The work presented in this thesis adds to the growing body of knowledge and expands the methods used to study the function/s of HBx, with particular emphasis on generating soluble protein within prokaryotic cells. In addition this work provides a solid argument in explaining some of the controversies around HBx proteins and delivers an enlightening description of the complex HBx protein. The bacterial strains are established systems that have been used by researchers to express a multitude of proteins of biomedical and biotechnological importance. The expression and purification of HBx proteins in bacterial strains was guided by previous studies. The cloning of these proteins using vectors containing an MBP tag was explored. This allowed purification of HBx to a high degree, including major improvements in the solubility of the proteins. The oligomeric structure determination of the fusion proteins was confirmed in solution by EM and SEC-SAXS. The proteins were expressed in the *E.coli* (DE3) strain in a soluble form with approximate molecular weights of 57, 57, 59 kDa for the DHBx, mini HBx and full HBx fusion proteins, respectively, after observation on SDS-PAGE. The proteins were purified with two chromatography steps using an amylose resin and a SEC superdex-200 column. Dynamic Light Scattering (DLS) was performed to characterize the proteins solutions. Single bands were observed with a hydrodynamic radius (R_H) of 15.1, 18.2, and 20.0 nm for the DHBx, mini HBx and full HBx fusion proteins, respectively, corresponding to the molecular weights of the proteins and the existence of polydisperse particles in solution was demonstrated. Evidence of disorder in the secondary structure of HBx proteins using CD spectroscopy, with soluble, pure and *E. coli* derived HBx fusion proteins could not be detected due to the presence of the MBP tag, which showed stability of the HBx fusion proteins. Negative observations concerning the separation of the proteins after cleavage from the MBP suggested that the fusion proteins were only partially stable after cleavage from the tag. Several attempts to crystallize the proteins were undertaken. The protein crystals were

observed to be weak, which reflects the merely partial stability of the HBx protein structures. Negative staining EM was used to examine flexible macromolecules posing special difficulties regarding structure determination by crystallography or NMR. This procedure was performed for the DHBx fusion protein. The results show the presence of different shaped particles, which tend to form a complex and long chain like particles, which are within the size of an oligomer, as detected when running the sample on a native gel. These results were confirmed by the SEC-SAXS for both DHBx and full HBx fusion proteins, which resulted in *ab initio* models containing an unstable part of the structure in the HBx proteins. The calculated averaged molecular weights for both fusion proteins based on RI/RALS data were 800 and 660kDa for both DHBx and full HBx fusion proteins, respectively. The R_g values from the DHBx collected fractions from the second major peaks were 8.2-8.9 nm and D_{max} of 35-39 nm. Also for the full HBx, the data showed R_g values of 9.5-10.1 nm and D_{max} of 45-50 nm. The R_g values from the DHBx collected fractions from the first peaks were 16.0-19.5 nm and D_{max} of 62-82nm. For the full HBx fusion protein, R_g values were 18.5-20.9 nm and D_{max} of 65-78nm.

Another attempt was performed in this study by examining the interaction between the HBx proteins with p53 binding partners. This procedure was performed between both full and mini HBx fusion proteins with full length and C-terminal p53 proteins. The results indicate an interaction between both HBx and p53 proteins in the presence of both protein tags; this was observed when performing an affinity chromatography technique and following observation of the interacting proteins in the elution step. The results were confirmed by using an octet device, which is used for analysis of bimolecular interactions and binding kinetics. The K_D value observed for the interaction between mini HBx and full p53 proteins was 14.40 ± 6.8 nM, as well as 55.18 ± 22 nM for the interaction between both full HBx and full p53 proteins. Negative interactions were observed when obtaining free tagged p53 proteins, which showed no interaction to the HBx fusion proteins. These observations indicated that the interaction between both proteins was observed due to the presence of the GST tag.

6. Zusammenfassung

HBV gehört zu einer Familie von leberspezifischen Viren, die zu verschiedenen schweren Entzündungen dieses zentralen Stoffwechselorgans führt. HBV wird seit 1947 mit diesen Erkrankungen in Verbindung gebracht, doch trotz Entdeckung des HBx Proteins in den frühen 1980er Jahren, bleibt seine Funktion sowohl im viralen Lebenszyklus, als auch im Verlauf von HBV-assoziiertem HCC umstritten. Das chronische Hepatitis B-Virus (HBV) infiziert mehr als 2 Milliarden Menschen weltweit, 400 Millionen sind chronisch mit diesem Virus befallen und über eine Millionen Patienten sterben jährlich an einer HBV-Infektion, in Zusammenhang mit chronischen Lebererkrankungen. Obwohl viele Personen schließlich den Zustand einer nicht-replikativen Infektion erreichen, resultiert die verlängerte Immunantwort oftmals in der Entwicklung einer Leberzirrhose, einem Leberversagen oder in einem Leberzellkarzinom (HCC) und bis zu 40% der Patienten leiden an chronischer HBV-Infektion. Die Prävalenz der chronischen HBV-Infektion ist sehr unterschiedlich in den verschiedenen Teilen der Welt. In endemischen Gebieten, in denen Trägerraten von > 5% existieren, sind die meisten Menschen perinatal infiziert, hervorgerufen entweder durch vertikale Übertragung oder einer Infektion in der frühen Kindheit. Eine Vielzahl von wirtsspezifischen Faktoren (Alter bei der Infektion, des Geschlechts, des Immunstatus), viralen Faktoren (Viruslast, Genotyp, Mutation) und externen Faktoren (gleichzeitige virale Infektionen, Alkoholkonsum, Chemotherapie) beeinflussen den Krankheitsverlauf. Mehrere Variable (Alter bei der Infektion, des Geschlechts, der ethnischen Zugehörigkeit, des Immunstatus) beeinflussen ebenfalls das Risiko einer chronischen Infektion. Die Immunisierung ist das wirksamste Mittel zur Verhinderung von HBV-Infektionen, da bis heute keine spezifische Behandlung für akute Hepatitis B existiert. Daher wird darauf ausgerichtet, auf eine angemessene Ausgewogenheit der Ernährung zu achten, um den Ersatz von Flüssigkeiten aufrechtzuerhalten, die durch Erbrechen und Durchfall verloren gegangen sind. Chronische Hepatitis B-Infektion kann mit Medikamenten, einschließlich mit oralen antiviralen Mitteln behandelt werden. Die Behandlung kann das Fortschreiten der Leberzirrhose verlangsamen, das Auftreten von Leberkrebs reduzieren und zu langfristigem Überleben beitragen.

Das HBV X-Protein (HBx Protein) ist ein multifunktionaler Regulator, welcher eine entscheidende Rolle bei Hepatokarzinogenese spielt. Das HBx Protein ist ein

Transaktivator, der verschiedene virale und zelluläre Promotoren und Enhancer aktivieren kann, dessen Aktivitäten für die virale Replikation notwendig sind. Das Protein ist innerhalb den verschiedenen Subtypen des Virus stark konserviert. Es ist im Cytoplasma vorhanden und in geringerem Maße auch im Kern von Hepatozyten. Das HBx Protein ist für die Festlegung der natürlichen Virusinfektion von Bedeutung und wird mit der Entwicklung von Leberkrebs und chronischer Infektion in Verbindung gebracht. Von diesem Protein wurde berichtet, dass es eine Vielzahl von verschiedenen Aktivitäten in Gewebekulturzellen besitzt, einschließlich der Induktion von Zelltod und dass es eine Stimulation der HBV-Replikation bewirkt. Strukturelle Studien von HBX wurden bisher durch Schwierigkeiten während der Expression erschwert und als Folge sind bis heute keine Röntgendiffraktions- oder NMR-Daten für HBx erhältlich. Darüber hinaus wurde die Rolle, die HBx bei Lebererkrankungen spielt, durch transfektions-basierte Überexpressions-Systeme und physiologisch irrelevante zelluläre Modellen fälschlich interpretiert. Diese Methoden wurden versehentlich eingeführt und haben zu zahlreichen Artefakten in diesem Bereich beigetragen.

Die in dieser Arbeit vorgestellten Ergebnisse ergänzen das wachsende Wissen über HBx und ergänzen auch die eingesetzten Methoden, um die Funktion/en von HBx zu untersuchen. Ein besonderer Schwerpunkt liegt in der Erzeugung von löslichem Protein aus prokaryotischen Zellen. Weitergehend bietet diese Arbeit solide Argumente um einige der Kontroversen rund um HBx Proteine aufzuklären und liefert zusätzlich eine aufschlussreiche Studie des komplexen HBx Proteins. Die verwendeten Bakterienstämme sind etablierte Systeme, die von unterschiedlichsten Forschern eingesetzt wurden, um eine Vielzahl von Proteinen die Bedeutung in der Biomedizin und Biotechnologie haben, zu exprimieren. Die Expression und Reinigung von Proteinen in HBx-Bakterienstämmen wurde in dieser Arbeit im Einklang zu früheren Untersuchungen durchgeführt. Die Klonierung dieser Proteine wurde mittels Verwendung von Vektoren durchgeführt, die eine MBP-Markierung besitzen. Dies erlaubt die Reinigung von HBx zu einem hohen Grad, weiterhin führt es zu erheblichen Verbesserungen in der Löslichkeit der Proteine. Die oligomere Struktur der Fusionsproteine wurde in Lösung von EM- und SEC-SAXS-Messungen bestätigt. Die jeweiligen DHBx-, Mini-HBx- und Voll-HBx-Fusionsproteine wurden im *E. coli* (DE3)-Stamm in einer löslichen Form exprimiert, mit ungefähren Molekulargewichten von 57, 57 und 59 kDa, wie durch Beobachtung mittels SDS-

PAGE gezeigt werden konnte. Die HBx-Proteine wurden mittels zwei Chromatographieschritten, unter Verwendung von Amylose-Harz einerseits und einer SEC Superdex-200-Säule andererseits, gereinigt. Dynamische Lichtstreuung (DLS) wurde verwendet, um die Proteine in Lösung zu charakterisieren. Einzelne Banden wurden mit einem hydrodynamischen Radius (R_H) von 15.1, 18.2 und 20.0 nm jeweils für die DHBx, mini HBx und voll HBx Fusionsproteine bestimmt, entsprechend dem jeweiligen Molekulargewicht. Außerdem wurde das Vorliegen polydisperser Teilchen in Lösung beobachtet. Eine Beeinflussung der Sekundärstruktur der HBx-Proteine aufgrund der Anwesenheit des MBP-Tags wurde mit Verwendung von CD-Spektroskopie beobachtet, und zwar für lösliche, reine und *E. coli*-abgeleitete HBx Fusionsproteine. Dies zeigt Auswirkungen auf die Stabilität der HBx Fusionsproteine. Nach der Abspaltung des MBP-Tags wurde beobachtet, dass die Fusionsproteine nur noch teilweise stabil waren. Mehrere Versuche wurden unternommen um die Proteine zu kristallisieren. Erhaltene Proteinkristalle zeigten auch nach einer Optimierung nur schwache Röntgendiffraktion, was die nur teilweise stabile Struktur der HBx Proteine reflektiert. Negative Färbung EM wurde verwendet, um diese flexiblen Moleküle zu untersuchen, da sie kaum oder nicht geeignet sind für die Strukturbestimmung durch Kristallographie oder NMR. Dieses Verfahren wurde mit den DHBx Fusionsproteinen durchgeführt. Die Ergebnisse zeigen die Anwesenheit von verschiedenen geformten Teilchen, die einen Komplex bilden und zu langkettigen Partikeln neigen, die die Größe eines Oligomers besitzen, wie auch durch native Gelelektrophorese gezeigt werden konnte. Dies wurde außerdem bei der Durchführung von SEC-SAXS, sowohl für die ab initio-Modelle von DHBx, als auch für Voll-HBx-Fusionsproteine, die einen instabilen Teil der Struktur beinhalten, bestätigt. Die berechneten gemittelten Molekulargewichte ergaben für beide Fusionsproteine, auf Basis von RI/RALS-Messungen 800 und 660 kDa für jeweils das DHBx und für das Voll-HBx Fusionsprotein. Die R_g -Werte aus den DHBx gesammelten Fraktionen betrugen 8,2 bis 8,9 nm und der D_{max} betrug 35-39 nm. Für das Gesamt-HBx-Protein ergaben die Daten R_g -Werte von 9,5 bis 10,1 nm und einen D_{max} von 45-50 nm. Die R_g -Werte aus den DHBx gesammelten Fraktionen von den ersten Peaks betrugen 16,0 bis 19,5 nm und der D_{max} betrug 62-82 nm. Für das Gesamt-HBx-Protein ergaben die Daten R_g -Werte von 18,5 bis 20,9 nm und einen D_{max} von 65-78 nm. In dieser Studie wurde ein weiterer Versuch durchgeführt, der die Beobachtung der Wechselwirkung zwischen den HBx Proteinen und deren p53 Bindungspartnern betrifft. Diese

Experimente wurden mit Voll- und Mini-HBx Fusionsproteinen mit voller Länge und C-terminalen p53-Fusionsproteinen durchgeführt. Die Ergebnisse deuten auf eine Wechselwirkung zwischen den beiden HBx- und p53-Proteinen in der Gegenwart von beiden Protein-Tags hin. Dies wurde bei der Durchführung mittels einer speziellen Affinitätschromatographie beobachtet, mit gezielter Beobachtung der Protein-Wechselwirkungen im Elutionsschritt. Diese Ergebnisse wurden durch die Verwendung eines Oktett-Geräts, welches für die Analyse von bimolekularen Wechselwirkungen und Bindungskinetiken verwendet wird, bestätigt. Der für die Interaktion zwischen mini und vollen HBx p53 proteinen beobachtete K_D -Wert betrug $14,40 \pm 6,8\text{nm}$ bzw. $55,18 \pm 22\text{ nm}$ für die Wechselwirkung zwischen den beiden vollen HBx und vollen p53 proteinen. Keine Wechselwirkung konnte zwischen unmarkierten p53-Proteinen und HBx-Fusionsprotein beobachtet werden, was darauf hindeutet, dass die Wechselwirkung zwischen den beiden Proteinen durch die Anwesenheit des GST-Tags zu erklären ist.

7. References

- Abbas, N., Ahmed, A., and Shakoori, A F. (2007). Overexpression and purification of PreS region of hepatitis B virus ntigenic surface protein adr subtype I *Escherichia coli*. Journal of Biochemistry and Molecular biology; 40:6, 1002-1008.
- Alberti, A., Trevisan, A., and Fattovich, G. (1984). The role of hepatitis B virus replication and hepatocyte membrane expression in the pathogenesis of HBV-related hepatic damage. In Advances in Hepatitis Research, Chisari FV, Ed. New York: Masson Publishing; p.134.
- Alter, M. (2003). Epidemiology of hepatitis B in Europe and worldwide. J Hepatol; 39: S64-S69.
- Amann, E. (1985). Gene; 40, 183–190.
- Arauz-Ruiz, P., Norder, H., Robertson, B. H., and Magnius, LO. (2002). Genotype H: a new Amerindian genotype of hepatitis B virus revealed in Central America. J Gen Virol; 83(8): 2059-2073.
- Assogba, B. D., Choi, B. H., and Rho, H. M. (2002). Transcriptional activation of the promotor of human cytomegalovirus immediate early gene (CMV-IE) by thee hepatitis b vitus x protein through the NF—KB site. Virus res; 84, 171-179.
- Avantaggiati, M. L., Natoli, G., Balsano, C., Chirillo, P., Artini, M., D.C Marzio, E., Collapardo, D., and Levrero, M. (1993). The hepatitis B virus (HBV) pX transactivates the *c-fos* promotor through multiple cis-acting elements. Oncogene; 8, 1567-1574.
- Ayadi, W., Karray-Hakim, H., Khabir, A., Feki, L., Charfi, S., and Boudawara, T.(2008). Aberrant methylation of p16, DLEC1, BLU and E-cadherin gene promoters in nasopharyngeal carcinoma biopsies from Tunisian patients. Anticancer Res; 28(4B): 2161-2167.
- Balsano, C., Avantaggiati, M. L., Natoli, G., De Marzio, E., will H., Perricaudet, M., and Levrero, M. (1991). Full-length and truncated versions of hepatitis b virus (HBV) X protein (pX) transactivate the cmyc proton co-gene at the transcriptional level. Biochem. Biophys.Res. comm; 176, 985-992.
- Bancroft, W.H., Snitbhan, R., Scott, R.M., Tingpalapong, M., Watson, W.T., and Tanticharoenyos, P. (1977). Transmission of hepatitis B virus to gibbons by exposure to human saliva containing hepatitis B surface antigen. J Infect Dis; 135:79-85.
- Barnbas, S., Hai, T., and Andersani, O. M. (1997). The hepatitis B virus X protein enhances the DNA binding potential and transcription efficacy of bZIP transcription factors. J. boil. Che; 272, 20684-20690.

References

- Barrera, A., Guerra, B., Notvall, L. and Lanford, R.E. (2005). Mapping of the hepatitis B virus pre-S1 domain involved in receptor recognition. *J Virol*; 79:9786-98.
- Beasley, R.P.H., Wang, L.Y., Lin, C.C., and Chien, C.S. (1981). Hepatocellular Carcinoma and Hepatitis B virus. A prospective study of 22,707 men in Taiwan, *Lancet*; 2: 1129-133.
- Benhenda, S., Cougot, D., Buendia, M. A., and Neuveut, C. (2009). Hepatitis B virus X protein molecular functions and its role in virus life cycle and pathogenesis. *Adv Cancer Res*; 103:75-109.
- Benhenda, S., Cougot, D., Neuveut, C., and Buendia, M. A. (2009). Liver Cell Transformation in Chronic HBV Infection. *Viruses*; 1, p630-646.
- Benn, J., Su, F., Doria, M., and Schneider, R. J. (1996). Hepatitis B Virus HBx Protein Induces Transcription Factor AP-1 by Activation of Extracellular Signal-Regulated and c-Jun N-Terminal Mitogen-Activated Protein Kinases. *Journal of Virology*; 4978–4985.
- Berne, B. J., and Pecora, R. (2000). *Dynamic Light Scattering*. Courier Dover Publications ISBN; 0-486, 41155-9.
- Bontron, S., Lin-Marq, N., and Strubin, M. (2002). Hepatitis B Virus X Protein Associated with UV-DDB1 Induces Cell Death in the Nucleus and Is Functionally Antagonized by UV-DDB2. *J.Biol.Chem*; 2002, 277:38847-38854.
- Bouchard, M. J., Wang, J. L., and Schneider, R. J. (2004). The entimatic X gene of hepatitis B virus. *J. Virol*; 78: 12725- 12734.
- Bruix, J., Sherman, M. (2011). American Association for the Study of Liver Diseases. Management of hepatocellular carcinoma: an update. *Hepatology*; 53:1020-2.
- Burgess, S. A., Walker, M. L., Thirumurugan, K., Trinick, J., and Knight, P. J. (2004). Use of negative stain and single-particle image processing to explore dynamic properties of flexible macromolecules. *Journal of Structural Biology*; 147: 247–258
- Chami, M., Ferrari, D., Nicotera, P., Paterlini-Brechot, P., and Rizzuto, R.(2003). Caspase-dependent alterations of Ca²⁺ signaling in the induction of apoptosis by hepatitis B virus X protein. *J.Biol.Chem*; 278:31745-31755.
- Chang, S. F., Netter, H. J., Bruns, M., Schneider, R., Froeich, K., and Will, H. (1999). A new avian hepadnavirus infecting snow geese (*Anser caerulescens*) produces a significant fraction of virions containing single stranded DNA. *Virology*; 262:39–54.

References

- Chang, S., Netter, H. J., Hildt, E., Schuster, R., Schaefer, S., Hsu, Y., Rang, A., and Will, H. (2001). Duck Hepatitis B virus Expresses a Regulatory HBx – like protein from a hidden open reading frame. *J. Virol*; 161-170.
- Chang, S.F., Chang, S.H., Li, B.C., Will, H., and Netter, H.J. (2004). Characterization of nonconventional hepatitis B viruses lacking the core promoter. *Virology*; 330: 437-46.
- Chans, S. F., Netter, H. J., Bruns, M., Schneider, R., Froeich, K., and Will, H.(1999). A new avian hepadnavirus infecting snow geese (*Anser caerulescens*). Produces a significant fraction of various containing single stranded DNA. *Virology*; 262: 39-54.
- Chen, C. J., Yang, H. I., Su, I., Jen, C. L., You, S. L., Lu, S. I. N., Huang, G. T., and Iioje, U. H. (2006). Risk of Hepatocellular Carcinoma across a biological gradient of serum hepatitis B virus DNA level. *J Virol*; 295: 65-73.
- Chen, B.J., and Lamb, R.A. (2008). Mechanisms for enveloped virus budding: can some viruses do without an ESCRT? *Virology*; 15: 372(2):221-32.
- Cheng, Y., and Walz, T. (2009). The advent of near-atomic resolution in single-particle electron microscopy. *Annu. Rev. Biochem*; 78, 723-742.
- Cherezov, V., Rosenbaum, D.M., Hanson, M.A., Rasmussen, S.G., Thian, F.S., Kobilka, T.S., Choi, H.J., Kuhn, P., Weis, W.I., Kobilka, B.K., and R.C. Stevens. (2007). High-resolution crystal structure of an engineered human β 2-adrenergic G protein-coupled receptor. *Science*; 318: 1258-1265.
- Chisari, F.V. (1995). Hepatitis B virus immunopathogenesis. *Ann Rev Immunol*; 13:29-60.
- Cho, G., Na, S., Suh, S. W., and Jung, G. (2000). Expression of recombinant HBV PPL proteins in HEPG2 cell. *Journal of biochemistry and Molecular Biology*; 33:6, 440:447.
- Chongsrisawat, V., Thawornsuk, N., Theamboonlers, A., Louisirirothanakul, S. and Poovorawan, Y. (2006). Hepatitis B virus DNA in unusual serological profiles of hepatitis B surface antigen-positive sera. *Viral Immunol*; 19: 623-9.
- Chouteau, P., Le Seyec, J., Cannie, I., Nassal, M., Guguen-Guillouzo, C. (2001). A short N-proximal region in the large envelope protein harbors a determinant that contributes to the species specificity of human hepatitis B virus. *J Virol*; 75: 11565-72.
- Clippinger, A. J., Gearhart, T. L., and Bouchard, M. J. (2009). Hepatitis B Virus X Protein Modulates Apoptosis in Primary Rat Hepatocytes by Regulating both NF-B and the Mitochondrial Permeability Transition Pore. *Journal of Virology*; p. 4718–4731.

References

- Courouce-Pauty, A.M., Lemaire, J.M., and Roux, J.F. (1978). New hepatitis B surface antigen subtypes inside the ad category. *Vox Sang*; 35: 304-8.
- de Franchis, R., Hadengue, A., Lau, G., Lavanchy, D., Lok, A., McIntyre, N., Mele, A., Paumgartner, G., Pietrangelo, A., Rodés, J., Rosenberg, W., Valla, D., and Jury, E. (2003). EASL International Consensus Conference on Hepatitis B. 13-14 September, 2002 Geneva, Switzerland. Consensus statement (long version). *Journal of Hepatology* 39 Suppl; 1, S3-25.
- de Moura, P. R., Rui, E., De Almeida Goncalves, K., and Kobarg, J. (2005). The cysteine residues of the Hepatitis B virus Oncoprotein HBx are not required for its interaction with RNA or with human p53. *Virus Res*; 108, 121-131.
- Deng, Y.B., Nagae, G., Midorikawa, Y., Yagi, A., Tsutsumi, S., and Yamamoto, S. (2010). Identification of genes preferentially methylated in hepatitis C virus-related hepatocellular carcinoma. *Cancer Sci*; 101(6):1501 – 1510.
- Dewantoro, O., Gani, R.A., and Akbar, N. (2006). Hepatocarcinogenesis in viral Hepatitis B infection: the role of HBx and p53. *Risk*; 2: 6-12.
- Doitsh, G., Shaul, Y. (2004). Enhancer I predominance in hepatitis B virus gene expression. *Mol. Cell Biol*; 24:1799-1808.
- Doria, M., Klein, N., Lucito, R., and Schneider, R. J. (1995). Hepatitis B virus Hbx proteins actual specificity cytoplasmic activator of Ras and nuclear activator of transcription factors. *EMBO. J*; 14: 4747-4757.
- DR. (1984). Genetic regulation of the immune response to hepatitis B surface antigen (HBsAg). IV Distinct H-2 linked Ir genes control antibody response to different HBsAg determinants on the same molecule and map to the I-A and I-C subregions. *J Exp Med*; 159:41-56.
- Dufloy, A. R., Mehrotra, S., Yu, Z., Barraud, L., Trepo, C., and Cova, L. (1995). Spectrum of liver disease and duck hepatitis B virus infection in a large series of Chinese ducks with hepatocellular carcinoma. *Hepatology*; 21:1483–1491.
- Duplay, P. (1984). *J. Biol. Chem*; 259, 10606–10613.
- Edamoto, Y., Hara, A., Biernat, W., Terracciano, L., Cathomas, G., and Riehle, H.M. (2003). Alterations of RB1, p53 and Wnt pathways in hepatocellular carcinomas associated with hepatitis C, hepatitis B and alcoholic liver cirrhosis. *Int J Cancer*; 106(3): 334-341.
- Elizabeth, W., Hwang, M. D., Ramsey, C. M. D. (2011). Global Epidemiology of Hepatitis B Virus (HBV) Infection. *N A J Med Sci*; 4 (1):7-13.

References

- Elmore, L. W., Hancock, A. R., Chang, S. F., Wang, X. W., Chang, S., Callahan, C. P., Geller, D. A., Will, H., Harris, C. C. (1997). Hepatitis B virus X protein and P53 tumor suppressor interactions in the modulation of apoptosis. *Proc. Natl. acad. Sci. USA*; 95:14707-14712.
- Evans, M.D., Dizdaroglu, M., and Cooke, M.S. (2004). Oxidative DNA damage and disease: induction, repair and significance. *Mutat Res/Rev Mutat Res*; 567(1):1-61.
- Feitelson, M. A., and Miller, R. H. (1988). X gene-related sequences in the core gene of duck and heron hepatitis B viruses. *Proc. Natl. Acad. Sci. USA*; 85:6162–6166.
- Feitelson, M. A., Zhu, M., Duan, L. X., and London, W. T. (1993). Hepatitis B X antigen and p53 are associated in vitro and in liver tissues from patients with primary hepatocellular carcinoma. *Oncogene*; 8: 1109-1117.
- Ferber, M., Montoya, D., Yu, C., Aderca, I., McGee, A., and Thorland, E. (2003) Integrations of the hepatitis B virus (HBV) and human papillomavirus (HPV) into the human telomerase reverse transcriptase (hTERT) gene in liver and cervical cancers. *Oncogene*; 22(24): 3813-3820.
- Fields, S; and Jang, S. K. (1990). Presence of a potent transcription activating sequence in the p53 protein. *Science*; 249:1046–1049.
- Fischer, M., Runkel, L., and Schaller, H. (1995). HBx protein of hepatitis B virus interacts with the C-terminal portion of a novel human proteasome alpha-subunit. *Virus genes*; 10, 99-102.
- Fischer, N., Konevega, A. L., Wintermeyer, W., Rodnina, M. V., Stark, H. (2010). *Nature*; 466: 329.
- Forgues, M., Difilippantonio, M. J., Linke, S. P., Ried, T., Nagashima, K., Feden, J., Valerie, K., Fukasawa, K., and Wang, X. W. (2003). Involvement of Crm1 in hepatitis B virus X protein-induced aberrant centriole replication and abnormal mitotic spindles. *Mol. Cell Biol*; 23, 5282-5292.
- Frank, J., Penczek, P., Grassucci, R., Srivastava, S. (1991). Three-dimensional reconstruction of the 70S Escherichia coli ribosome in ice: the distribution of ribosomal RNA. *J. Cell Biol*; 115 (3): 597– 605.
- Franke, D. and Svergun, D.I. (2009). *DAMMIF, a program for rapid ab-initio shape determination in small-angle scattering*. *Journal of Applied Crystallography*: 42(2); p. 342-346.
- Franke, F., Jeffries, C.M., and Svergun, D.I. (2015). Supplementary Figure 5: Empirical and theoretical distributions of the Correlation Map test. *Nature Methods*: 12; 419–422.

References

- Friedman, P. N; Chen, X; Bargonetti, J; and Privest, C. (1993). The p53 protein is an unusually shaped tetramer that binds directly to DNA. *Proc. Natl. Acad. Sci. USA*; 90, pp. 3319-3323.
- Geng, X., Huang, C., Qin, Y., McCombs, J. E., Yuan, Q., Harry, B L., Palmer, A E., Xia, N S., and Xue, D. (2012). Hepatitis B virus X protein targets Bcl-2 proteins to increase intracellular calcium, required for virus replication and cell death induction, *Proc.Natl.Acad. Sci*; 109, p18471-18476.
- Glatter, O., and Kratky, O. (1982). *Small Angle X-ray Scattering*. Academic Press; ISBN 0-12, 286280-5.
- Gottlob, K., Pagano, S., Levrero, M., and Graessmann, A.(1998). Hepatitis B virus X protein transcription activation domains are neither required nor sufficient for cell transformation. *Cancer Res*; 58:3566-3570.
- Graewert, M.A., Franke1. D., Jeffries, C. M., Blanchet, C.E., Ruskule, D., Kuhle, K., Flieger, A., Schäfer,B., Tartsch,B., Meijers, R and Svergun, D.I. (2015). Automated Pipeline for Purification, Biophysical and X-Ray Analysis of Bio macromolecular Solutions. *Scientific Reports*; 5:10734
- Gressner, A.M., Lahme, B., and Mannherz, H.G. (1997). Polzar B. TGF- β -mediated hepatocellular apoptosis by rat and human hepatoma cells and primary rat hepatocytes. *J Hepatol*; 26(5): 1079-1092.
- Gressner, A.M., and Weiskirchen, R .(2006). Modern pathogenetic concepts of liver fibrosis suggest stellate cells and TGF- β as major players and therapeutic targets. *J Cell Mol Med*; 10(1):76-99.
- Grove, J., and Marsh, M. (2011).The cell biology of receptor-mediated virus entry. *J Cell Biol*; 26: 195 (7):1071-82.
- Guan, C. (1987). *Gene*; 67, 21–30.
- Halic, M., Becker, T., Pool, M. R., Spahn, C. M., Grassucci, R. A., Frank, J., and Beckmann, R. (2004). *Nature*; 427: 808.
- Halliwell, B. (1999). Oxygen and nitrogen are pro-carcinogens. Damage to DNA by reactive oxygen, chlorine and nitrogen species: measurement, mechanism and the effects of nutrition. *Mutation Research/Genetic Toxicology and Environmental Mutagenesis*; 443(1): 37-52.
- Hang, X., Dong, W., Guarino, L A. (1995). The Lef-3 gene of *Autographa californica* nuclear polyhedrosis virus endoes a single-stranded DNA-binding protein.*J. Virol*; 96, 3924-3928.

References

- Hanson, M.A., Cherezov, V., Griffith, M.T., Roth, C.B., Jaakola, V.P., Chien, E.Y., Velasquez, J., Kuhn, P., and R.C. Stevens. (2008). A Specific Cholesterol Binding Site is Established by the 2.8 Å Structure of the Human β 2-Adrenergic Receptor. *Structure*; 16: 897-905.
- Haviv, S., Shamy, M., Doitsh, G., and Shaul, Y. (1998). Hepatitis B virus X protein is detectable in nuclei of transfected cells and is active for transactivation. *Biochem. Biophys. Acta*; 1453: 330-340.
- Heymann, J. B., Cheng, N., Newcomb, W. W., Trus, B. L., Brown, J. C., Steven, A. C. (2003). *Nat. Struct. Biol*; 10; 334.
- Henkler, F., Hoare, J., Waseem, N., Goldin, R. D., McGarvey, M.J., Koshy, R., and King, I.A. (2001). Intracellular localization of the hepatitis B virus HBx protein. *J.Gen.Viroi*; 82:871-882.
- Hodgson, A. J., Hyser, J. M., Keasler, V. V., Cang, Y., and Slagle, B. (2012). Hepatitis B virus regulatory HBx protein binding to DDB1 is required but is not sufficient for maximal HBV replication. *Virology*; 426; 73-82.
- Holliday, R. E. (2006). A historical overview. *Epigenetics*; 1(2): 76-80.
- Hollinger, F.B. (1996). Hepatitis B virus. In: Fields, B.N., Knipe, D.M. and Howley, p.m (Eds), *Fields Virology*, 3rd ed., Raven Publishers, Philadelphia, PA; 2739-2807.
- Hollstein, M., Sidransky, D., Vogelstein, B., Harris. C. C. (1991). P53 mutations in human cancers. *Science*; 253: 49-53.
- Hoofnagle, J.H., Doo, E., Liang, T.J., Fleischer, R., Lok, A.S.(2007). Management of hepatitis B: summary of a clinical research workshop. *Hepatology*; 45:1056-75.
- Hou, J., Liu, Z., and Gu, F. (2005). Epidemiology and Prevention of Hepatitis B Virus Infection. *Int J Med Sci*; 2(1): 50–57.
- Howard, C.R. (1994). Classification and taxonomy of hepadnaviruses - current status. In: *Viral Hepatitis and Liver Disease*. Edited by: Nishioka, K., and Suzuki, H.
- Hsieh, Y.H., Su, I.J., Wang, H.C., Chang, W.W., Lei, H.Y., and Lai, M.D. (2004). Pre-S mutant surface antigens in chronic hepatitis B virus infection induce oxidative stress and DNA damage. *Carcinogenesis*; 25(10):2023-2032.
- Hu, J., McCall, C. M., Ohta, T., and Xiong, Y. (2004). Targeted ubiquitination of CDT1 by the DDB1- CUL4A-ROC1 ligase in response to DNA damage. *Nat Cell Biol*; 6, 1003-1009. 106.
- Hura, G.L. (2013). Comprehensive macromolecular conformations mapped by quantitative SAXS analyses. *Nat. Methods*; 6, 606–12

References

- Jacques, D. A., and Trewthella, J. (2012). Small-angle scattering for structural biology expanding the frontier while avoiding the pitfalls. *Protein Sci*; 19, 642–657.
- Jazayeri, M., Basuni, A.A., Sran, N., Gish, R., Cooksley, G. (2004). HBV core sequence: definition of genotype-specific variability and correlation with geographical origin. *J Viral Hepat*; 11: 488-501.
- Jeffries, C M., Graewert., M. A., Svergun, D. I., Blanchet C. E. (2015). Limiting radiation damage for high-brilliance biological solution scattering: practical experience at the EMBL P12 beamline PETRAIII. *J. Synchrotron Radiation*: 22; 273-279.
- Jensen, G. J., Ed. (2010). *Methods in Enzymology: Cryo-EM, Part A, Sample Preparation and Data Collection*; Academic Press, Elsevier: San Diego, CA; Vol. 481.
- Jilbert, A.R., Burrell, C.J., Triatni, M., and Kann, M. (2002). Hepatitis B virus replication. In: *Hepatitis B virus*. Edited by: Lai, C.L. and Locarnini, S. London, UK., International Medical Press; 43-53.
- Johnston, T. C. (1986). *J. Biol. Chem*; 261, 4805–4811.
- Jung, J.K., Arora, P., Pagano, J.S., and Jang, K.L. (2007). Expression of DNA methyltransferase 1 is activated by hepatitis B virus X protein via a regulatory circuit involving the p16INK4a-cyclin D1-CDK 4/6-pRb-E2F1 pathway. *Cancer Res*; 67(12):5771-5778.
- Jung, J.K., Park, S., and Jang, K.L. (2010). Hepatitis B virus X protein overcomes the growthinhibitory potential of retinoic acid by down regulating retinoic acid receptor- β 2 expression via DNA methylation. *J Gen Virol*; 91(2):493-500.
- Kann, M. (2002). Structural and molecular virology. In: *Hepatitis B virus*. Edited by: Lai, C.L. and Locarnini, S. London, U. K., International Medical Press; 9-21.
- Kastan, M. B., Zhan, Q., EL-Diery, W. S., Carrier, F., Jacks, T., Walsh, W. V., Plunkett, B. S., Vogelstein, B., Fornace Jr, A J. (1992). A mammalian cell cycle checkpoint pathway utilizing P53 and GADD45 is defective in ataxia-telangiectasia. *Cell*; 71:587-597.
- Keeffe, E.B., Dieterich, D.T., Han, S.H., Jacobson, I.M., Martin, P., Schiff, E.R., Tobias, H. (2008). A treatment algorithm for the management of chronic hepatitis B virus infection in the United States. *Clin Gastroenterol Hepatol*; 6:1315-41.
- Kellerman, O. K. (1982). *Methods in Enzymology*; 90, 459–463.

References

- Kew, M. C. (2011). Hepatitis B virus x protein in the pathogenesis of hepatitis B virus-induced hepatocellular carcinoma. *J Gastroenterol Hepatol* 26 Suppl; 1, 144-52.
- Kim, K. H., and Seong, B.L. (2003). Pro-apoptotic function of HBV X protein is mediated by interaction with c-FLIP and enhancement of death-inducing signal. *EMBO J*; 22: 2104 - 2116.
- Kim, S., Park, S. Y., Yong, H., Famulski, J. K., Chae, S., Lee, J. H., Kang, C. M., Saya, H., Chan, G. K., and Cho, H. (2008). HBV X protein targets hBubR1, which induces dysregulation of the mitotic checkpoint. *Oncogene*; 27, 3457-3464.
- Kim, Y., Jung, J.K., Lee, S.Y., and Jang, K.L. (2010). Hepatitis B virus X protein overcomes stress-induced premature senescence by repressing p16INK4a expression via DNA methylation. *Cancer Lett*; 288(2): 226-235.
- Kobiler, O., Drayman, N., Butin-Israeli, V., Oppenheim, A. (2012). Virus strategies for passing the nuclear envelope barrier; 3(6):526-39.
- Knoll, S., Fürst, K., Thomas, S., Baselga, S V., Stoll, A., Schaefer, S., and Pützer, B. (2011). Dissection of cell context-dependent interaction between HBx and p53 family members in regulation of apoptosis. *Cell Cycle*; 10:20, 3554-3565.
- Koike, K., Moriya, K., Iino, S., Yotsuyanagi, H., Endo, Y., Miyamura, T., and Kurokawa, K. (1994). High-level expression of hepatitis B virus HBx gene and hepatocarcinogenesis in transgenic mice. *Hepatology*; 19:810–819.
- Kuhlmann, I., Minihane, A.M., Huebbe, P., Nebel, A., and Gerald, R. (2010). Apolipoprotein E genotype and hepatitis C, HIV and herpes simplex disease risk: a literature review. *Lipids Health Dis*; 9(8): 1-14.
- Kusunoki, H., Tanaka, T., Kohno, T., Wakamatsu, K., and Hamaguchi, I. (2014). Structural characterization of the BH3-like motif of hepatitis B virus X protein. *Biochemical and Biophysical communications*; 450: 741-745.
- Kuzhanaivelu, N., Cong, Y S., Inouye, C., Yang, W M., and Seto, E. (1996). XAP2, a novel hepatitis B virus x-associated protein that inhibits X transactivation. *Nucl. Acids Res*; 24, 4741-4750.
- Kwong, J., Chow, L.S., Wong, A.Y., Hung, W.K., Chung, G.T., and To, K.F. (2007). Inactivation of the deleted in lung and esophageal cancer 1 gene in nasopharyngeal carcinoma. *Genes Chromosomes Cancer*; 46: 171–180.
- Lada, O., Benhamou, Y., Poynard, T. and Thibault, V. (2006). Coexistence of Hepatitis B surface antigen (HBs Ag) and anti-HBs antibodies in chronic hepatitis B virus carriers: influence of "a" determinant variants. *J Virol*; 80: 2968-75.

References

- Lane, D. P. (1992). Cancer. P53, Guardian of the genome. *Nature*; 358: 15-16.
- Lauritzen, C. (1991). *Protein Expression and Purification*; 2, 372–378.
- Lee, H., Lee, Y-H., Huh, Y-S., Moon, H., and Yun, Y. (1995). X-gene product antagonizes the p53-mediated inhibition of hepatitis B virus replication through regulation of the pregenomic/core promoter. *J. Biol. Chem*; 270: 31405-31412.
- Lee, S., Elenbase, B., Levine, A., Griffith, J. (1995). P53 and its 14kDa C-terminal domain recognize primary DNA damage in the form of insertion/deletion mismatches. *Cerll*; 81:10130-11020.
- Lee, W.M. (1997). Hepatitis B virus infection. *New Engl J Med*; 337:1733-1745.
- Lee, J. T., Davidow, L. S., and Warshawsky, D. (1999). Tsix, a gene antisense to Xist at the X inactivation centre. *Nat Genet*; 21(4): 400-404.
- Lee, D. K., Park, S. H., Yi, Y., Choi, S. G., Lee, C., and Parks, W. T. (2001). The hepatitis B virus encoded oncoprotein pX amplifies TGF- β family signaling through direct interaction with Smad4: potential mechanism of hepatitis B virus-induced liver fibrosis. *Sci Signal*; 15(4): 455-466.
- Lee, Y. I., Hwang, J. M., Im, J. H., Lee, Y. I., Kim, N. S., Kim, D. G., Yu, D. Y., Moon, H. B., and Park, S. K. (2004). Human hepatitis B virus-X protein alters mitochondrial function and physiology in human liver cells. *J. Biol. Chem*; 279:15460-15471.
- Lee, J. O., Kwun, H. J., Jung, J. K., Choi, K. H., Min, D. S., and Jang, K. L. (2005). Hepatitis B virus x protein represses E-cadherin expression via activation of DNA methyltransferase 1. *Oncogene*; 24; 6617-6625.
- Lee, S. H., Cha, E. J., Lim, J. E., Kwan, S. H., Kim, D. H., Cho, H., and Han, K. H. (2012) Structural characterization of an intrinsically unfolded Mini-HBx protein from Hepatitis B virus. *Molecules and Cells*; 34, 2, 165-169.
- Leopold, P.L., and Pfister, K.K. (2006). Viral strategies for intracellular trafficking: motors and microtubules. *Traffic*; 7(5):516-23.
- Leupin, O., Bontron, S., Schaeffer, C., and Strubin, M. (2005) Hepatitis B virus X protein stimulates viral genome replication via a DDB1-dependent pathway distinct from that leading to cell death. *J. Virol*; 79, 4238-4245.
- Li, S.K., Ho, S.F., Tsui, K.W., Fung, K.P., Waye, M.Y. (2008). Identification of functionally important amino acid residues in the mitochondria targeting sequence of hepatitis B virus X protein. *Virology*. 10; 381(1):81-8

References

- Liang, T. J., (2009). Hepatitis B: the virus and disease. *Hepatology* 49(5 Suppl); S13-21.
- Liaw, Y.F., Lau, G. K. K., Kao, J. H., and Gane, E. (2010). Hepatitis B e antigen seroconversion: a critical event in chronic hepatitis B virus infection. *Dig Dis Sci*; 55(10), 2727-34.
- Lim, S.G., Mohammed, R., Yuen, M.F., and Kao, J.H. (2009). Prevention of hepatocellular carcinoma in hepatitis B virus infection. *J Gastroenterol Hepatol*; 24(8), 1352-7.
- Lin, M.H., and Lo, S.C. (1989). Dimerization of hepatitis B viral X protein synthesized in a cell-free system. *Biochem.Biophys.Res.Commun*; 1989, 164:14-21.
- Lin, Y., Nomura, T., Yamashita, T., Dorjsuren, D., Tang, H., and Murakam, S. (1997). The Transactivation and p53-interacting Functions of Hepatitis B Virus X Protein Are Mutually Interfering but Distinct. *Cancer Research*; 57. 5137-5142.
- Liu, J., Lian, Z., Han, S., Waye, M. M. Y., Wang, H. M. C. (2006). Downregulation of E-Cadherin by hepatitis B virus X antigen in hepatocellular carcinoma. *Oncogene*; 25: 1008-1017.
- Liu, D., Zou, L., Li, W., Wang, L., and Wu, Y.(2009). High level expression and large- scale preparation of soluble HBx antigen from *Escherichia coli*. *Biotechnol. Appl. Biochem*; 54, 141-147.
- Lizzano, R. A., Yang, B., Clippinger, A. J., and Bouchard, M. J. (2011). The C-terminal region of the hepatitis B virus protein is essential for its stability and function. *Virus research*; 155:231-239.
- Lok, A. S., and McMahon, B. J. (2007). Chronic hepatitis B. *Hepatology*; 45:507-39.
- Lok, A.S., McMahon, B.J. (2009). Chronic hepatitis B –*Hepatology*; 50:661-2.
- Maguire H. F, Hoeffler J. P, and Siddiqui. A. (1991). HBV X protein alters the DNA binding specificity of CREB and ATF-2 by protein-protein interactions. *Science*; 252:842–844.
- Maina, C. V. (1988). *Gene*; 74, 365–373.
- Mandart, E., Kay, A., Galibert, F. (1984). Nucleotide sequence of a cloned duck hepatitis B virus genome: Comparison with woodchuck and human hepatitis B virus sequences. *J Virol*; 49(3):782–792.

References

- Martin-Lluesma, S., Schaeffer, C., Robert, E I., van Breugel, P.C., Leupin, O., Hantz, O., and Strubin, M. (2008). Hepatitis B virus X protein affects S phase progression leading to chromosome segregation defects by binding to damaged DNA binding protein 1. *Hepatology*; 48, 1467-1476.
- Mastroianni, C.M., Lichtner, M., Citton, R. (2011). Current trends in management of hepatitis B virus reactivation in the biologic therapy era. *World J Gastroenterol*; 17:3881-7.
- Mathew, E., Mirza, A., and Menhart, N. (2004). Liquid-chromatography-coupled SAXS for accurate sizing of aggregating proteins. *J. Synchr. Rad*; 11, 314–318.
- McClain, S.L., Clippinger, A.J., Lizzano, R., Bouchard, M.J. (2007). Hepatitis B virus replication is associated with an HBx-dependent mitochondrion-regulated increase in cytosolic calcium levels. *J Virol*; 81(21):12061–5.
- McMahon, B.J., Holck, P., Bulkow, L., Snowball, M. (2001). Serologic and clinical outcomes of 1536 Alaska Natives chronically infected with hepatitis B virus. *Ann Intern Med*; 135:759-68.
- McMahon, B.J. (2010). Natural history of chronic hepatitis B. *Clin Liver Dis*; 14:381-96.
- Melegari, M., Scaglioni, P. P., and Wands, J. R. (1998). Cloning and characterization of a novel hepatitis B virus bonding protein that inhibits viral replication. *J. Virol*; 72, 1737-1743.
- Milich, D., and Liang, T. J. (2003). Exploring the biological basis of hepatitis B e antigen in hepatitis B virus infection. *Hepatology*; 38(5), 1075-86.
- Mishiro, S., and Oda, T., Tokyo, Japan, Springer-Verlag: 54-56. Kim K. H, and Sevnig B. L, (2003). *EMBO. J*; 22: 2104-2116.
- Murata, M., Matsuzaki, K., Yoshida, K., Sekimoto, G., Tahashi, Y., and Mori, S. (2009). Hepatitis B virus X protein shifts human hepatic transforming growth factor (TGF)- β . signaling from tumor suppression to oncogenesis in early chronic hepatitis B. *Hepatology*; 49(4): 1203-1217.
- Murata, M., Thanan, R., Ma, N., and Kawanishi, S. (2012). Role of nitrate and oxidative DNA damage in inflammation-related carcinogenesis. *J Biomed Biotechnol*; 2012, 1-11.
- Negro, F. (2010). Adverse effects of drugs in the treatment of viral hepatitis. *Best Practice & Research Clinical Gastroenterology*; 24(2), 183-92.

References

- Netter, H. J., Chassot, S., Chang, S. F., Cova, L., and Will, H. (1997). Sequence heterogeneity of heron hepatitis B virus genomes determined by full-length DNA amplification and direct sequencing reveals novel and unique features. *J. Gen. Virol*; 78:1707–1718.
- Ng, K., Pullirsch, D., Leeb, M., Wutz, A. (2007). Xist and the order of silencing. *EMBO Rep*; 8(1): 34-39.
- Niederau, C., Heintges, T., Lange, S., Goldmann, G., Niederau, C. M., Mohr, L., and Häussinger, D. (1996). Long-term follow-up of HBeAg-positive patients treated with interferon alfa for chronic hepatitis B. *N Engl J Med*; 334(22), 1422-7.
- Niu, D., Feng, H., and Chen, WN. (2010). DLEC1 Expression Is Modulated by Epigenetic Modifications in Hepatocellular Carcinoma Cells: Role of HBx Genotypes. *Cancers*; 2(3): 1689-1704.
- Nomura, T., Lin, Y., Dorjsuren, D., Ohno, S., Yamashita, T., and Murakami, S.(1999). Human hepatitis B virus X protein is detectable in nuclei of transfected cells, and is active for transactivation. *Biochim.Biophys.Acta*; 1453:330-340.
- O'Connell, B.C., Harper, J.W. (2007). Ubiquitin proteasome system (UPS): what can chromatin do for you? *Curr. Opin. Cell Biol*; 19, 206-214.
- Ohi, M., Li, Y., Cheng, Y., and Walz, T. (2004). Negative Staining and Image Classification - Powerful Tools in Modern Electron Microscopy. *Biol.Proced. Online*; 6, 23-34.
- Orlova, E. V., Saibil, H. R. (2010). *Methods Enzymol*; 482: 321.
- Ott, J. J., Stevens, G. A., Groeger, J., and Wiersma, S. T. (2012). Global epidemiology of hepatitis B virus infection: New estimates of age-specific HBsAg seroprevalence and endemicity. *Vaccine*; 30 2212– 2219.
- Ou, H.D; Löhr, F; Vogel, V; Mänteles, W and Dötsch, V. (2007). Structural evolution of C-terminal domains in the p53 family. *The EMBO Journal*; 26, 3463–3473.
- Pan, J., Clayton, M., and Feitelson, M A. (2004). Hepatitis B virus X antigen promotes transforming growth factor- β 1 (TGF- β 1) activity by up-regulation of *TGF- β 1* and down-regulation of α 2-macroglobulin. *J Gen Virol*; 85(2): 275-282.
- Park, I. Y., Sohn, B. H., Yu, E., Suh, D. J., Chung, Y. H., and Lee, J. H. (2007). Aberrant epigenetic modifications in hepatocarcinogenesis induced by hepatitis B virus X protein. *Gastroenterology*; 132(4):1476-1494.
- Payer, B., and Lee, J. T. (2008). X chromosome dosage compensation: how mammals keep the balance. *Annu Rev Genet*; 42: 733-772.

References

- Perrillo, R. P. (2001) Acute flares in chronic hepatitis B: the natural and unnatural history of an immunologically mediated liver disease. *Gastroenterology*; 120:1009-22.
- Petoukhov, M. V., Franke, D., Shkumatov, A. V., Tria, G., Kikhney, A. G., Gajda, M., Gorba, C., Mertens, H. D. T., Konarev P. V., and Svergun, D. I. (2012). New developments in the ATSAS program package for small-angle scattering data analysis. *J. Appl. Cryst*: 45; 342-350.
- Qadri, I., Maguire, H. F., and Siddiqui, A. (1995). Hepatitis B virus transactivator protein X interacts with the TATA-binding protein. *Proc. Natl. Acad. Sci. USA*; 92:1003–1007.
- Qadri, I., Conaway, J.W., Conaway, R.C., Schaack, J., and Siddiqui, A. (1996). Hepatitis B virus transactivator protein, HBx, associates with components of TFIIH and stimulates the DNA helicase activity of TFIIH. *Proc Natl Acad Sci USA*; 93:10578- 10583.
- Qiu, G.H., Salto-Tellez, M., Ross, J.A., Yeo, W., Cui, Y., and Wheelhouse, N. (2008). The tumor suppressor gene DLEC1 is frequently silenced by DNA methylation in hepatocellular carcinoma and induces G1 arrest in cell cycle. *J Hepatol*; 48(3): 433-441.
- Rabl, J. (2008). Mechanism of gate opening in the 20S proteasome by the proteasomal ATPases. *Mol. Cell*; 30(3), 360-368.
- Radermacher. M., Wagenknecht, T., Verschoor, A., and Frank, J. (1987). Three-dimensional reconstruction from a single-exposure, random conical tilt series applied to the 50S ribosomal subunit of *Escherichia coli*. *J. Microsc*; 146 (Pt 2), 113-136.
- Rakotomalala, L., Studach, L., Wang, W. H., Gregori, G., Hullinger, R. L., and Andrisani, O. (2008). Hepatitis B virus X protein increases the Cdt1-to-gemini ratio inducing DNA re-replication and polyploidy. *J. Biol. Chem*; 283, 28729-28740.
- Reherrmann, B., Nascimbeni, M. (2005). Immunology of hepatitis B virus and hepatitis C virus infection. *Nat Rev Immunol*; 5:215-29.
- Rui, E., de Moura, P. R., and Kobarg, J. (2001). Expression of deletion mutants of the hepatitis B virus protein HBx in *E.coli* and characterization of their RNA binding activities. *Virus Res*; 74, 50-73.
- Rui, E., de Moura, P. R., Goncalves, K. D. E. A., and Kobarg, J. (2005). Expression and spectroscopic analysis of a mutant Hepatitis B virus onco-protein HBx without cysteine residues *J. Viral. Methods*; 126, 65-74.

References

- Rui, E., Moura, P. R., Goncalves, K. A., Rooney, R. J., and Kobarg, J. (2006). Interaction of the hepatitis B virus protein HBx with the human transcription regulatory p120E4F in vitro. *Virus Research*; 115:31-42.
- Russo, A. L., Thiagalingam, A., Pan, H., Califano, J., Cheng, K. H., and Ponte, J. F. (2005). Differential DNA hypermethylation of critical genes mediates the stage-specific tobacco smoke-induced neoplastic progression of lung cancer. *Clin Cancer Res*; 11(7): 2466-2470.
- Sanderson, N., Factor, V., Nagy, P., Kopp, J., Kondaiiah, P., and Wakefield, L. (1995). Hepatic expression of mature transforming growth factor beta 1 in transgenic mice results in multiple tissue lesions. *Proc Natl Acad Sci*; 92(7): 2572-2576.
- Seeger, C., Zoulim, F., and Mason, W. S. (2007). Hepadnavirus P-2977-3029. In: D.M. Knipe, P.M. Howley, D. E. Griffing, R.A. Lamb, M.A. Martin, B. Roizman, and S.E. Straus. (ed), *Fields virology*, 5th ed. Lippincott Williams and Wilkins, Philadelphia, pA.
- Scaglioni, P.P., Melegari, M. and Wands, J.R. (1996). Recent advances in the molecular biology of hepatitis B virus. *Baillieres Clin Gastroenterol*; 10: 207-25.
- Schoehn, G., Quate-Randall, E., Jimenez, J.L., Joachimiak, A., and Saibil, H.R. (2000). Three conformations of an archaeal chaperonin, TF55 from *Sulfolobus shibatae*. *J. Mol. Biol*; 296 (3): 813–819.
- Schek, N., Bartenschlager, R., Kuhn, C., Schaller, H. (1991). Phosphorylation and rapid turnover of hepatitis B virus X protein expressed in HepG2 cells from recombinant vaccinia virus. *Oncogene*; 6:1735–1744.
- Schuster, R., Gerlich, W. H., and Schaefer, S. (2000). Induction of apoptosis by the transactivating domains of the hepatitis B virus X gene leads to suppression of oncogenic transformation of primary rat embryo fibroblasts. *Oncogene*; 19:1173-1180.
- Schuster, R., Hildt, E., Chang, S. F., Terradillos, O., Pollicino, T., Lanford, R., Gerlich, W. H., Will, H., and Schaefer, S. (2002). Conserved transactivating and pro-apoptotic functions of hepadnaviral X protein in ortho- and avihepadnaviruses. *Oncogene*; 21:6606-6613.
- Scott, R. M., Snitbhan, R., Bancroft, W. H., Alter, H. J., Tingpalapong, M. (1980). Experimental transmission of hepatitis B virus by semen and saliva. *J Infect Dis*; 142:67-71.
- Seng, T. J., Currey, N., Cooper, W.A., Lee, C.S., Chan, C., Horvath, L. (2008). DLEC1 and MLH1 promoter methylation are associated with poor prognosis in non-small cell lung carcinoma. *Br J Cancer*; 99(2): 375-382.

References

- Shaw, P., Bovey, R., Tardy, S., Sali, R., Sordat, B., Costa, J. (1992). Induction of apoptosis by wild-type P53 in a human colon tumor-derived cell line. *Proc. Natl. Acad. Sci. USA*; 89:4495-4499.
- Shirakata, Y., Koike, K. (2003). Hepatitis B virus X protein induces cell death by causing loss of mitochondrial membrane potential. *J.Biol.Chem*; 278:22071-22078.
- Sidhu, K., Kumar, S., Reddy, V. S., and Kumar, V. (2014). Mass Spectrometric Determination of Disulfide Bonds in the Biologically Active Recombinant HBx Protein of Hepatitis B Virus. *Biochemistry*: 53, 4685–4695.
- Smith ML, Chen IT, Zhan Q, O'Connor PM, and Fornace AJ J. (1995). Involvement of p53 tumour suppression in repair of UV-type DNA damage. *Oncogene*; 10: 1053-1059.
- Song, B. C., Chung, Y. H., Kim, J. A., Choi, W. B., Suh, D. D., and Pyo, S. I.(2001). Transforming Growth factor- β 1 as a useful serologic marker of small hepatocellular carcinoma. *Cancer*; 94(1): 175-180.
- Song, C. Z., Bai, Y. L., Song, C. C., and Wang, Q. W. (2003). Aggregate formation of hepatitis B virus X protein affects cell cycle and apoptosis. *World J Gastroenterology*; 9 (7):1521-1524.
- Spandau, D. F., and Lee, C. H. (1988). *Trans-activation* of viral enhancers by the hepatitis B virus X protein. *J. Virol*; 62:427-434.
- Sprengel, R., Kuhn, C., Will, H., Schaller, H. (1985). Comparative sequence analysis of duck and human hepatitis B virus genomes. *J Med Virol*; 15(4):323–333.
- Studach, L. L., Rakotomalala, L., Wang, W. H., Hullinger, R. L., Cairo, S., Buendia, M. A., and Andrisani, O. M.(2009). Polo-like kinase 1 inhibition suppresses hepatitis B virus X protein-induced transformation in an in vitro model of liver cancer progression. *Hepatology*.
- Su, F., and Schneider, R. J. (1996). Hepatitis B virus HBx protein activates transcription factor NF-kappaB by acting on multiple cytoplasmic inhibitors of rel-related proteins. *J Virol*; 70 (7):4558-66.
- Svergun, D. (1992). *Determination of the regularization parameter in indirect-transform methods using perceptual criteria*. *Journal of Applied Crystallography*: 25(4); p.495-503.
- Svergun, D. I., Koch, M. H. J., Timmins, P. A., and May, R. P. (2013). *Small angle x-ray and neutron scattering from solutions of biological macromolecules*. (Oxford University Press).

References

- Takada, S., Kido, H., Fukutomi, A., Mori, T., and Koike, K. (1994). Interaction of hepatitis B virus X protein with a serine protease, trypsin TL2, as an inhibitor. *Oncogene*; 9:341–348.
- Takai, D., Yagi, Y., Habib, N., Sugimura, T., and Ushijima, T. (2000). Hypomethylation of LINE1 retrotransposon in human hepatocellular carcinomas, but not in surrounding liver cirrhosis. *Jpn J Clin Oncol*; 30(7): 306-309.
- Takagi, H. (1988). *Bio/technology* 6, 948–950.
- Tan, T. L., Fang, N., Neo, T. L., Singh, P., Zhang, J., Zhou, R., Koh, C. G., Chan, V., Lim, S. G., and Chen, W. N. (2008). Rac1 GTPase is activated by Hepatitis B virus replication-involvement of HBX. *Biochimica et Biophysica Acta*; 1783:360-374.
- Tang, H., Delgermaa, L., Huang, F., Oishi, N., Liu, L., He, F., Zhao, L., and Murakami, S. (2005). The Transcriptional Transactivation Function of HBx Protein Is Important for Its Augmentation Role in Hepatitis B Virus Replication. *Journal of virology*; p. 5548–5556.
- Tang, K. F., Xie, J., Chen, M., Liu, Q., Zhou, X. Y., Zeng, W., Huang, A L., Zuo, G. Q., Wang, Y., Xiang, R., and Ren, H, (2008). Knock of damage-specific DNA binding protein1 (DDB1) enhances the HBx-s: RNA- mediated inhibition of HBV replication. *Biologicals*; 36: 177- 183.
- Thiagalingam, S. A. M., Cheng, K. H., Lee, H. J., Mineva, N., Thiagalingam, A., and Ponte, J. F. (2006). Histone deacetylases: unique players in shaping the epigenetic histone code. *Ann N Y Acad Sci*; 983(1): 84-100.
- Tilley, S. J., Orlova, E. V., Gilbert, R. J., Andrew, P. W., Saibil, H. R. (2005). *Cell*; 121: 247.
- Truant, R., Antunovic, J., Greenblatt, J., Prives, C., and Cromlish, J. A. (1995). Direct interaction of the hepatitis B virus HBx protein with p53 leads to inhibition by HBx of p53 response element-directed transactivation. *J. Virol*; 69: 1851-1859.
- Tse, E.Y., Ko, F.C., Tung, E.K., Chan, L.K., Lee, T.K., Ngan, E.S., Man, K., Wong A.S., Ng, I.O., and Yam, J.W. (2012). Caveolin-1 overexpression is associated with hepatocellular carcinoma tumorigenesis and metastasis. *J Pathol*; 226(4):645-53.
- Twu, J. S., Lai, M. Y., Chen, D. S., and Robinson, W. S. (1993). Activation of protooncogene *c-jun* by the X protein of hepatitis B virus. *Virology*; 192, 346-350.

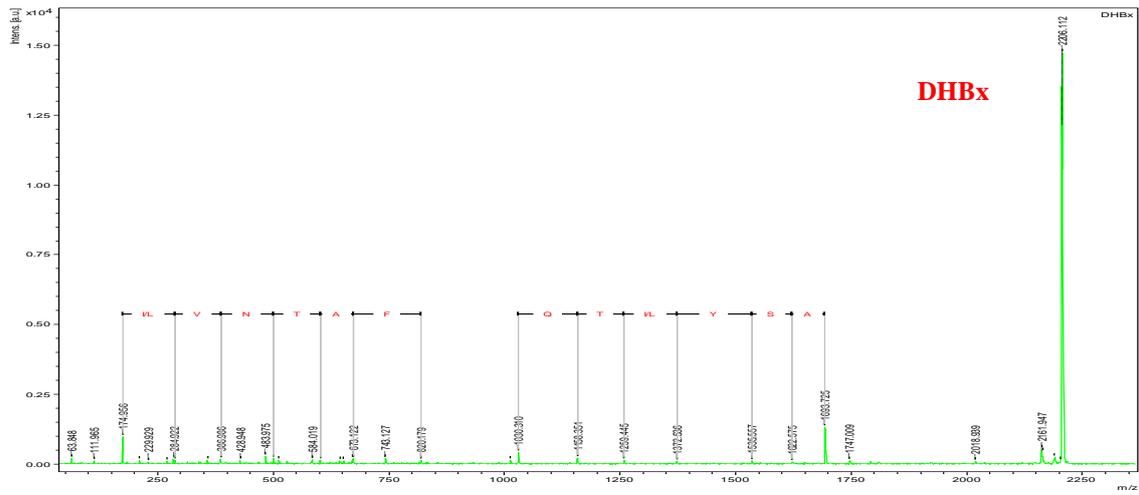
References

- Urban, S., Hildt, E., Eckerskorn, C., Sirma, H., Kekule, A., Hofschneider, P.H. (1997). Isolation and molecular characterization of hepatitis B virus X-protein from a baculovirus expression system. *Hepatology*; 26: 1045-1053.
- van Hemert, F. J., van de Kkundert, M. A., Lukashov, V. V., Kootstra, N. A., Berkhout, B., and Zaaijer, H. (2011). Protein X of hepatitis B Virus: Origin and structure Similarity with the central domain of DNA glycosylase. *PLoSone*; 6:8.
- Walker, A., Skamel, C., Vorreiter, J., and Nassel, M. (2008). Internal core protein cleavage leaves the hepatitis B virus capsid intact and enhances its capacity for surface display of heterologous whole chain proteins. *J. Biol. Chem*; 283:33508-33515.
- Wang, X. W., Forrester, K., Yeh, H., Feitelson, M. A., GU, J. R., Harris, C. C. (1994). Hepatitis B virus X protein inhibits P53 sequence specific DNA binding, transcriptional activity, and association with transcription factor ERCC3. *Proc. Natl. Acad. Sci USA*; 91: 2230-2234.
- Wang, H. D., Trivedi, A., and Jonson, D. L. (1998). Regulation of RNA polymerase I-dependent promoters by the hepatitis B virus X protein via activated Ras and TATA-binding protein. *Mol.cell. Bio*; 18, 7086-7094.
- Wang, F. Z., Sha, L., Zhang, W. Y., Wu, L.Y., Qiao, L., Li, N., Zhang, X D., and Ye, L. H. (2007). Involvement of hepatitis B X-interacting protein (HBXIP) in proliferation regulation of cells. *Acta Pharmacologica Sinica*; 28, 431-438.
- Warren, K. S., Heeney, J. L., Swan, R. A., Herlyanta, and Verschoor, E. J.(1999). A new group of Hepadnavirus naturally infecting over orangutans (*Pongo pygmaeus*) *J. Viro*; 37: 7860-7865.
- Wen, Y., Golubkov, V. S., Strongin, A.Y., and Jiang, W., Reed, J.C. (2008). Interaction of hepatitis B viral oncoprotein with cellular target HBXIP dysregulates centrosome dynamics and mitotic spindle formation. *J. Biol. Chem*; 283, 2793-2803.
- Wentz, M. J., Becke,r S. A., and Slagle, B. L. (2000). Dissociation of DDB1-binding and transactivation properties of the hepatitis B virus X protein. *Virus Research*; 68, 87-92.
- White, H. E., Orlova, E. V., Chen, S., Wang, L., Ignatiou, A., Gowen, B., Stromer, T., Franzmann, T. M., Haslbeck, M., Buchner, J., Saibil, H. R. (2006). *Structure*; 14: 1197.
- Whittaker, G. R., Kann, M., Helenius, A. (2000). Viral entry into the nucleus. *Annu Rev Cell Dev Biol*; 16:627-51.

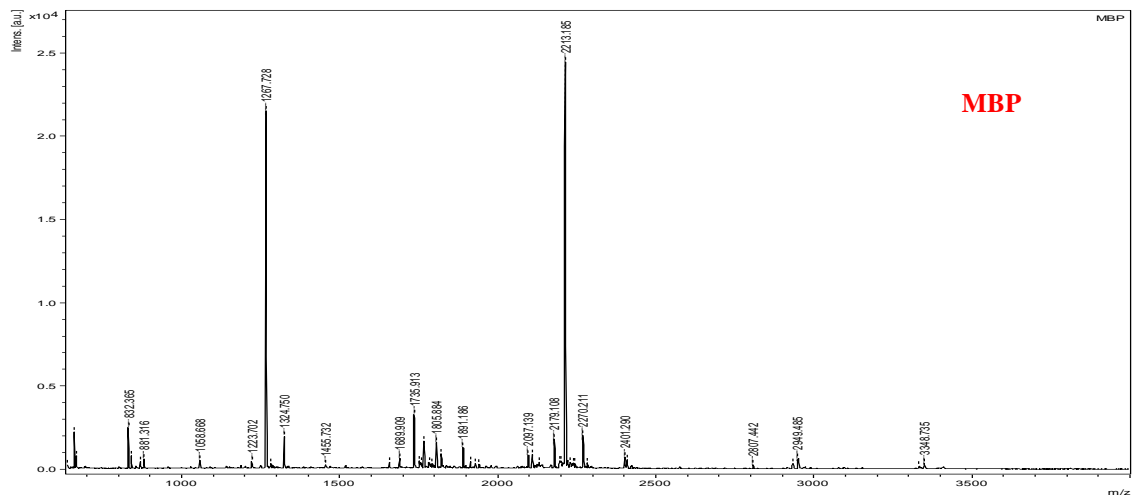
References

- Wiseman, H., Halliwell, B. (1996). Damage to DNA by reactive oxygen and nitrogen species: role in inflammatory disease and progression to cancer. *Biochem J*; 313(Pt 1): 17-19.
- Xie, K. L., Zhang, Y. G., Liu, J., Zeng, Y., and Wu, H. (2014). MicroRNAs Associated With HBV Infection And HBV-related HCC. *Theranostics*; 4(12):1176-1192.
- Yanisch-Perron, C., Vieira, J., and Messing, J. (1985). *Gene*; 33, 103–119.
- Yen, B. T. S. (1996). Hepadnaviral X protein: review of recent progress. *J. Biomed. Sci*; 3: 20-30.
- Yokosuka, O., and Arai, M. (2006). Molecular biology of hepatitis B virus: effect of nucleotide substitutions on the clinical features of chronic hepatitis B. *Med Mol Morphol*; 39: 113-20.
- Zhao, G. (2010). Two-dimensional crystallization conditions of human leukotriene C4 synthase requiring adjustment of a particularly large combination of specific parameters. *J. Struct. Biol*; 169(3), 450-454.
- Zhao, J., Wu, G., Bu, F., Lu, B., Liang, A., and Cao, L. (2010). Epigenetic silence of ankyrinrepeat- containing and proline-rich region-containing protein 1 (ASPP1) and ASPP2 genes promote tumour growth in hepatitis B virus-positive hepatocellular carcinoma. *Hepatology*; 51: 142-153.
- Zheng, D.L., Zhang, L., Cheng, N., Xu, X., Deng, Q., and Teng, X. M. (2009). Epigenetic modification induced by hepatitis B virus X protein via interaction with de novo DNA methyltransferase DNMT3A. *J Hepatol*; 50(2): 377-387.
- Zhu, Y. Z., Zhu, R., Fan, J., Pan, Q., Li, H., and Chen, Q. (2010). Hepatitis B x protein induces hypermethylation of p16^{ink4a} promoter via DNA methyltransferases in the early stage of HBV-associated hepatocarcinogenesis. *J Viral Hepatol* 2010; 17: 98-107.
- Zoulim, F. (2011). Hepatitis B virus resistance to antiviral drugs: where are we going? *Liver Int* 31 Suppl; 1, 111-6.

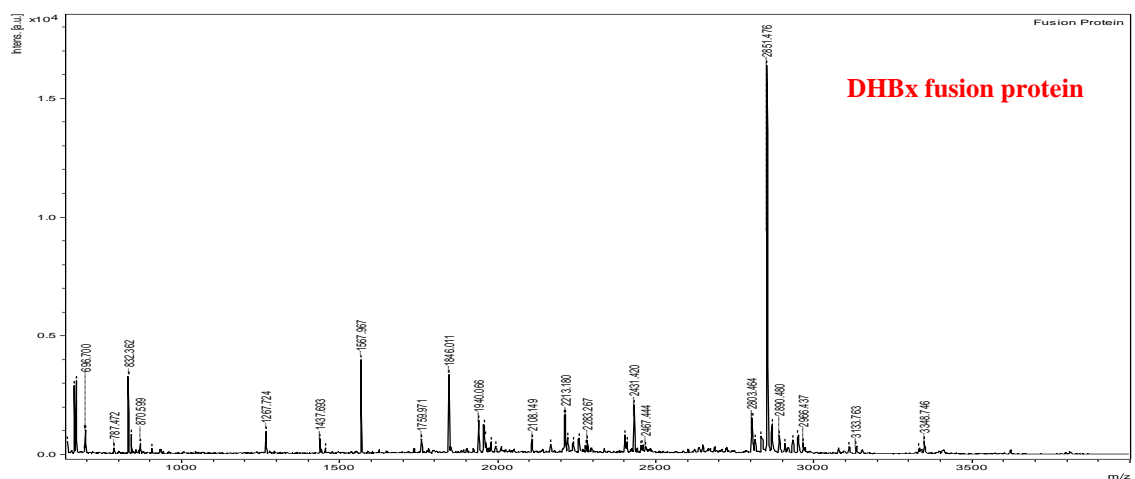
8. Appendix



A



B



C

Figure 55: Peptide identification of MS results for DHBx after incomplete cleavage. (A) Represents the partially cleaved DHBx, (B) Represents the Free MBP, and (C) Represents the DHBx fusion protein.

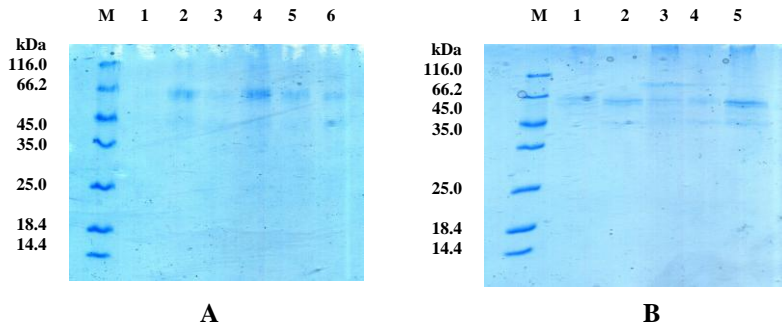


Figure 56: Observation of positive DHBx fusion protein crystals after screening. The crystals were applied to SDS-PAGE gel for molecular weight observation. The crystals were confirmed to be protein crystals. (A) Represents small protein crystals observed in Morpheus suite conditions, (B) Represent small protein crystals observed in Pact suite conditions.

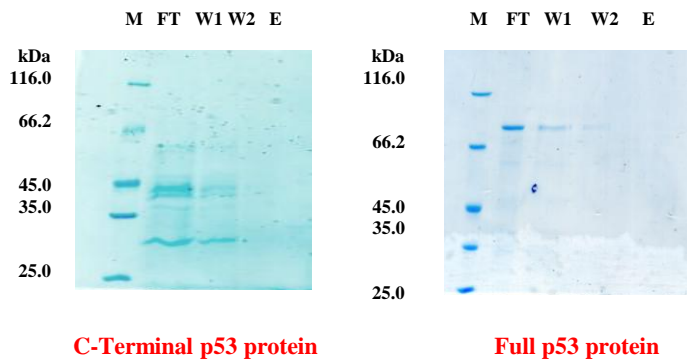


Figure 57: Negative binding of both full and C-terminal p53 proteins on amylose matrix with the absence of HBx fusion proteins. Both fusion proteins were applied on the amylose matrix as a control.

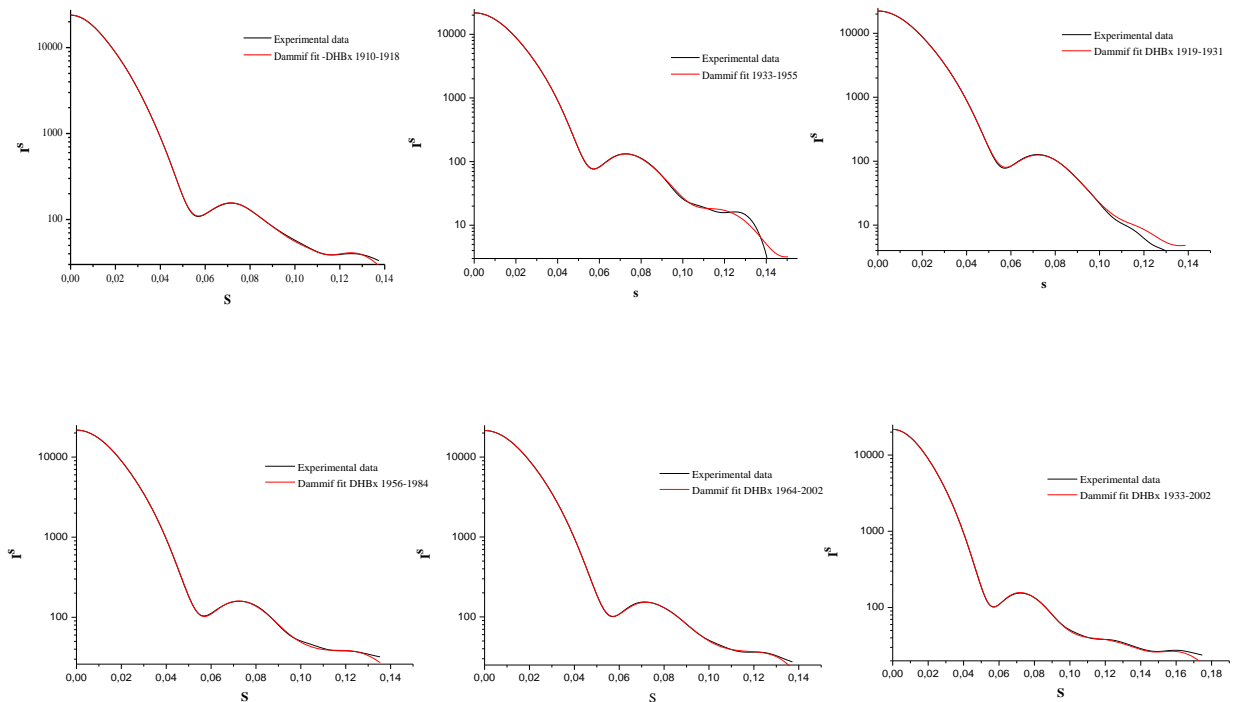


Figure 58: The fit graphs of the collected fractions for the DHBx fusion protein after SEC-SAXS preparation after using the DAMMIF program.

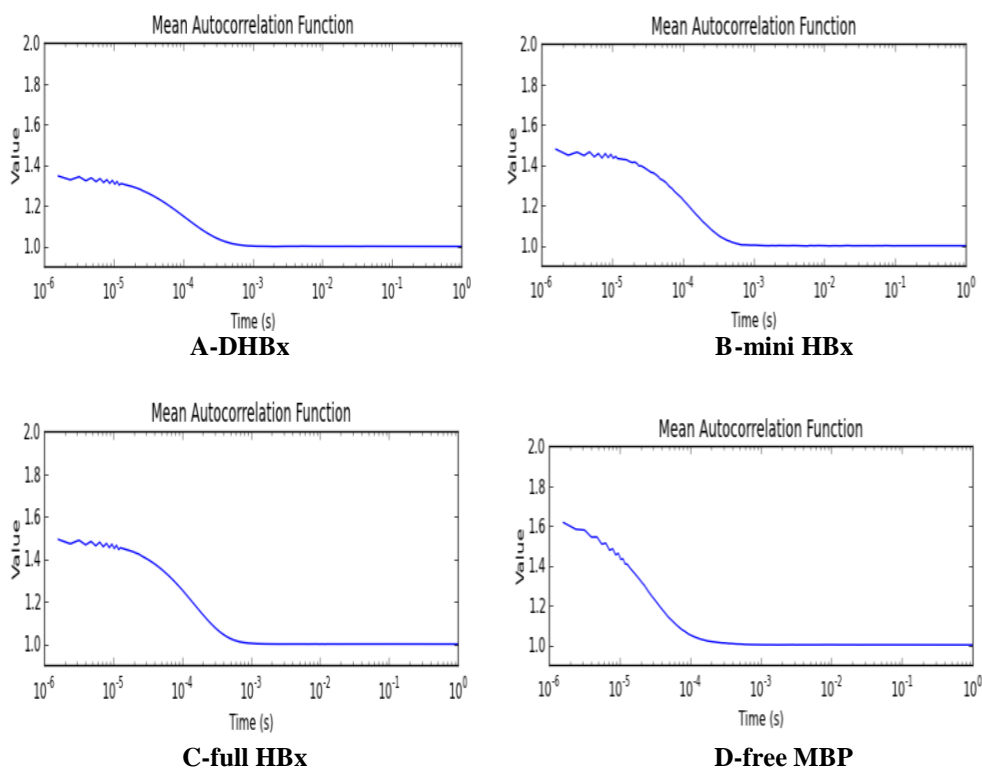


Figure 61: DLS histograms of the mean autocorrelation functions of the HBx fusion proteins. (A) Sample of the DHBx fusion protein, (B) Sample of the mini HBx fusion protein, (C) Sample of the full HBx fusion protein, (D) sample for the free MBP.

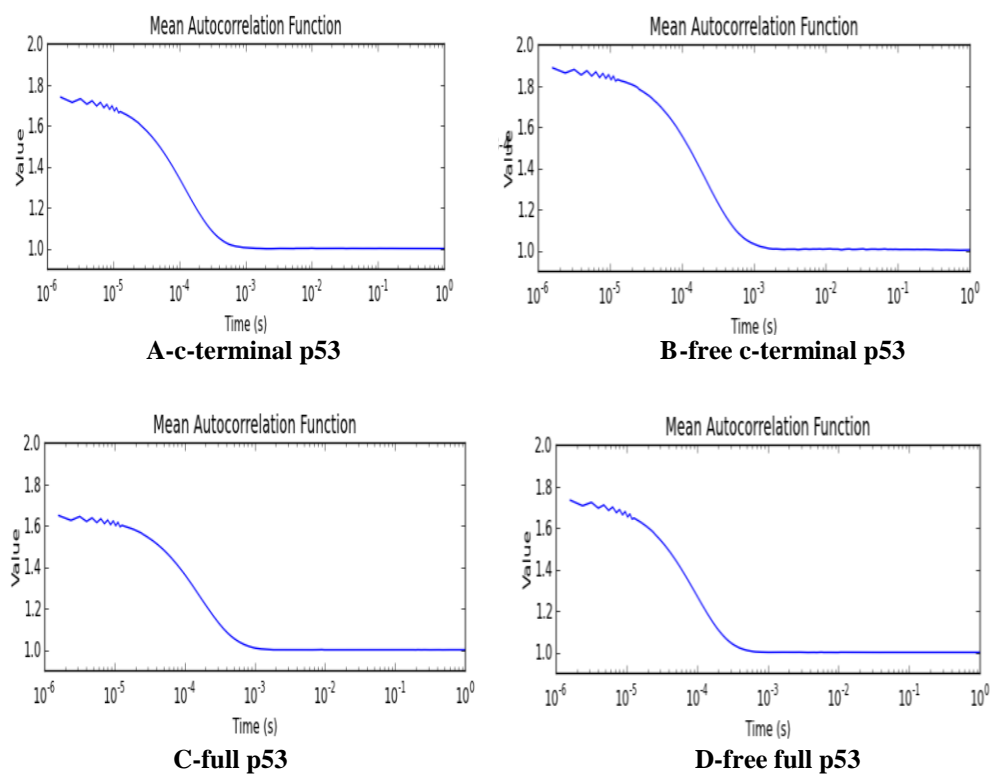


Figure 62: DLS histograms of the mean autocorrelation functions of the free p53 and the p53 proteins. (A) Sample of the c-terminal p53 protein, (B) Sample of the free c-terminal protein, (C) Sample of the full p53 protein, (D) sample for the free full p53 protein.

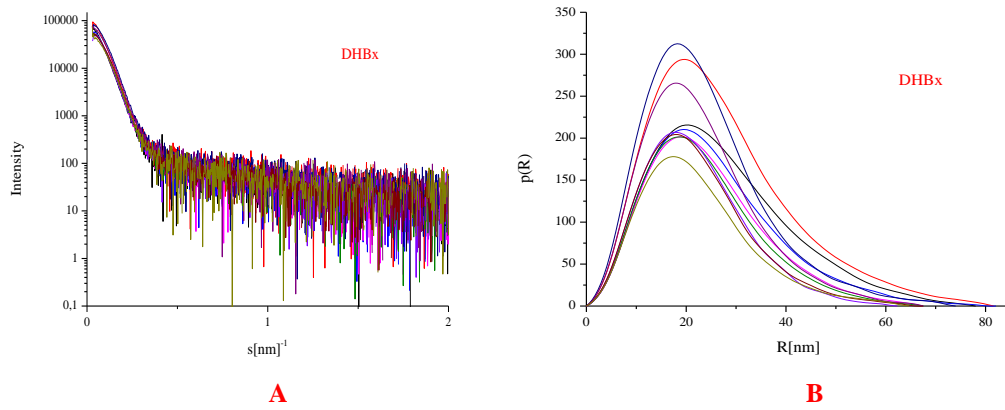


Figure 63: Processed solution SEC-SAXS scattering data for the DHBx fusion protein for the first peak (A-left panel), and the fit graph (B-right panel).

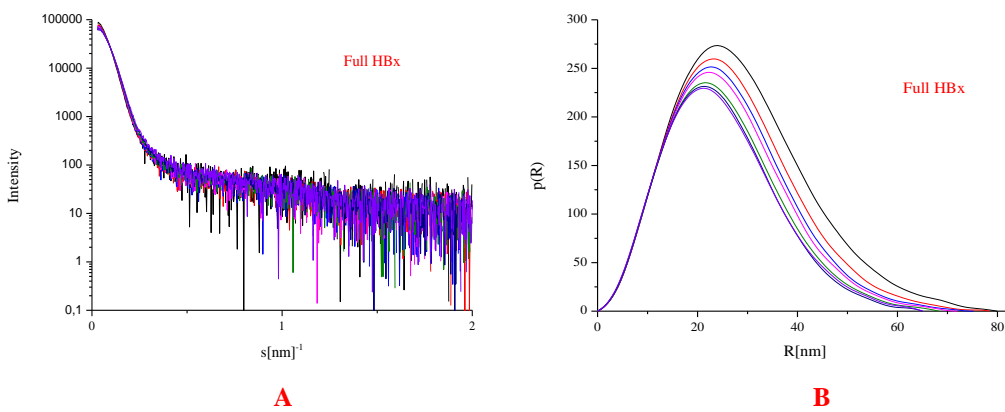


Figure 64: Processed solution SEC-SAXS scattering data for the full HBx fusion protein for the first peak (A-left panel), and the fit graph (B-right panel).

9. Risk and safety statements
9.1. Chemicals (GHS classification)

Table 17: Chemicals (GHS classification)

Compound	CAS-No.	Supplier	GHS hazard	Hazard statements	Precautionary statements
Acetic acid	64-19-7	Chem-solute	GHS02 GHS05	H226, H314	P280, P305+351+338, P310
Acrylamide 30%	79-06-1	Carl Roth	GHS06 GHS08	H301, H312, H316, H317, H319, H332, H340, H350, H361f, H372	P201, P280, P301+310, P305+351+338, P308+313
ATP	34369-07-8	Sigma	-	-	-
Agarose	9012-36-6	Serva	-	-	-
Aammonium acetate	631-61-8	Sigma	-	-	-
(NH4)2SO4	7283-20-2	Carl Roth	-	-	-
Ampicillin	69-52-3	Carl Roth	GHS08	H334, H317	P280, P261, P302+P352, P342+P311
APS	7727-54-0	Carl Roth	GHS03 GHS07 GHS08	H272, H302, H315, H317, H319, H334; H335	P280, P305+351+338, P302+352, P304+341, P342+311
bis-Tris	6976-37-0	Sigma	GHS07	H315, H319, H335	P261, P305 + P351 + P338
Bromophenol blue	115-39-9	Applichem	-	-	-
Boric acid	10043-35-3	Carl Roth	-	H360	P201, P202, P281, P303+313, P405, P501
CaCl₂	10043-52-4	Merck	GHS07	H319	P305+351+338
Citric acid	77-92-9	Sigma	GHS05	H318	P305+351+338, P311
Coomassie brilliant blue R250	6104-59-2	Serva	-	-	-
EGCG	989-51-5	Sigma	-	-	-
DMSO	67-68-5	Sigma	GHS08	H315, H319	P280, P302+352, P305 +351+338, P332+313,P362

Risk and Safety Statements

Compound	CAS-No.	Supplier	GHS hazard	Hazard statements	Precautionary statements
DTT	578517	Applichem	GHS07	H302, H315, H319, H335	P302+352, P305+351+338
EDC	25952-53-8	Applichem	GHS05, GHS07	H315, H318, H335	P261, P280, P305 + P351 + P338
EDTA	60-00-4	Sigma	GHS07	H319	P305+351+338
Ethanol	64-17-5	Carl Roth	GHS02	H225	P210
Ethidiumbromide	1239-45-8	Sigma	GHS06, GHS08	H302, H330, H341	P260, P281, P284, P310
Glutaraldehyde	111-30-8	Applichem	GHS05, GHS07, GHS08, GHS09	H302 + H332, H314, H317, H334, H335, H400	P261, P273, P280, P305 + P351 + P338, P310
Glycerol	56-81-5	Sigma	-	-	-
GSH	70-18-8	Carl Roth	-	-	-
Guanidin hydrochlorid	50-01-1	Applichem	GHS07	H302, H315, H319	P305+P351+P388, P302+P352
HEPES	7365-45-9	Sigma	-	-	-
Hydrochloric acid >25%	7647-01-0	Merck	GHS05, GHS07	H314, H335	P261, P280, P310, P305+351+338
Imidazole	288-32-4	Carl Roth	GHS05, GHS06, GHS08	H301; H314; H361	P260, P281, P303+P361+P353, P301+P330+P331, P305+P351+P338, P308+P313
IPTG	367-93-1	Carl Roth	-	-	-
Isopropanol	67-63-0	Carl Roth	GHS02, GHS07	H225, H319, H336	P210, P233, P305+351+338
KCl	7447-40-7	Carl Roth	-	-	-
K₂HPO₄	7758-11-4	Carl Roth	-	-	-
KH₂PO₄	7778-77-0	Merck	-	-	-
Li₂SO₄	10102-25-7	Merck	GHS07	H302	-

Risk and Safety Statements

Compound	CAS-No.	Supplier	GHS hazard	Hazard statements	Precautionary statements
MgCl ₂	7786-30-3	Carl Roth	-	-	-
MgSO ₄	7487-88-9	Merck	-	-	-
MPD	107-41-5	Carl Roth	GHS07	H315, H319	-
2-mercaptoethanol	60-24-2	Fisher Scientific	GHS06, GHS09	H302, H411, H315, H335, H311, H319	P280, P312, P302+P350, P261, P273, P301+P312, P305+351+338
NaOAc	127-09-3	Applichem	-	-	-
Na ₂ HPO ₄	7558-79-4	Carl Roth	-	-	-
NaH ₂ PO ₄	10049-21-5	Applichem	-	-	-
NaF	7681-49-4	Merck	-	H301, H315, H319	P301 + P310, P305 +P351 + P338
NaCl	7647-14-5	Carl Roth	-	-	-
NaH ₂ PO ₄	10049-21-5		-	-	-
NaOH	1310-73-2	Merck	GHS05	H314	P280, P310, P305+351+338
Na ₃ -citrate	6132-04-3	Sigma	-	-	-
NiSO ₄	10101-97-0	Applichem	GHS08, GHS09, GHS07	H332, H315, H334, H317, H341, H350i, H360D, H372 H410	P280, P273, P201, P342+P311, P308+P313, P302+P352
Paraffin	8002-74-2	Applichem	-	-	-
PEG 400	25322-68-3	Sigma	-	-	-
PEG 6000	25322-68-3	Merck	-	-	-
PEG 8000	25322-68-3	Sigma	-	-	-
PMSF	329-98-6	Applichem	GHS06, GHS05	H301, H314	P280, P305+P351+P338, P310
SDS	151-21-3	Sigma	GHS02 GHS06	H228, H302, H311, H315, H319, H335	P210, P261, P280, P312, P305+351+338

Risk and Safety Statements

Compound	CAS-No.	Supplier	GHS hazard	Hazard statements	Precautionary statements
Silver nitrate	7761-88-8	Carl Roth	GHS09	H272, H314, H410	P273, P280, P301+310+331, P305+351+338, P309+310
Tannic acid	1401-55-4	Sigma	-	-	-
TCA	76-03-9	Sigma	GHS05 GHS09	H314, H410	P273, P280, P301+330+331, P305+351+338, P309+P310
TEMED	110-18-9	Merck	GHS02 GHS05 GHS07	H225, H302, H314, H332	P261, P280, P305+351+338
Tris	1185-53-1	Fluka	GHS07	H315, H319, H335	P261, P305+351+338
Yeast extract	8013-01-2	Serva	-	-	-
ZnCl₂	7646-85-7	Sigma	GHS05, GHS07, GHS09	H302-H314-H410	P273, P280, P305 + P351 + P338, P310, P501
β-OG	29836-26-8	Carl Roth	-	-	-

9.2. Commercial crystallization solutions

Table 18: Commercial crystallization solutions and kits

Name	Supplier	Risk label	Risk phrases	Safety phrases
Floppy Choppy	Jena Bio Science	C, Xn, Xi	R35, R41, R42, R36/37/38	S22, S26, S45, S24/25, S36/37/39:
PCT	Hampton	-	-	-
Classic Suite	Qiagen	T, N	R10, R45, R46, R60, R61, R23/25, R36/37/38, R48/20/22, R51/53	S20, S26, S45, S53, S36/37/39
PACT premier	Molecular Dimensions	T	R23/25, R52/53	S20, S36, S45, S61
Morpheus	Molecular Dimensions	T, N	R10, R45, R46, R60, R61, R63, R23/25, R36/37/38, R48/20/22, R51/53	S20, S26, S45, S53, S61, S36/37/39
ComPAS Suite	Qiagen	T	R10, R45, R23/24/25, R36/38, R39/23/24/25, R51/53	S13, S26, S45, S53, S61, S36/37/39.
Stura/Footprint	Molecular Dimensions	T, N	R10, R45, R46, R60, R61, R25, R36/37/38, R48/20/22, R51/53	S20, S26, S45, S53, S61, S36/37/39
JCSG+ Suite	Qiagen	T, N	R10, R21, R41, R45, R23/25, R37/38, R51/53	S13, S20, S26, S45, S53, S36/37/39
Ammonium sulfate Suite	Qiagen	T+, N	R10, R25, R26, R45, R46, R60, R61, R48/23/25, R51/53	S45, S53, S61, S36/37.
Cryos Suite	Qiagen	T, N	R10, R45, R46, R60, R61, R23/25, R36/37/38, R48/20/22, R51/53	S20, S26, S45, S53, S61, S36/37/39.
peqGOLD Plasmid Mini Kit	Peqlab	-	-	-
NucleoSpin® Gel and PCR Clean-up	Macherey & Nagel	Xn	R 20/21/22, R32, 52/53	S13, S61

9.3. GHS and risk symbols and information about hazard-, risk-, safety and precaution-statements:

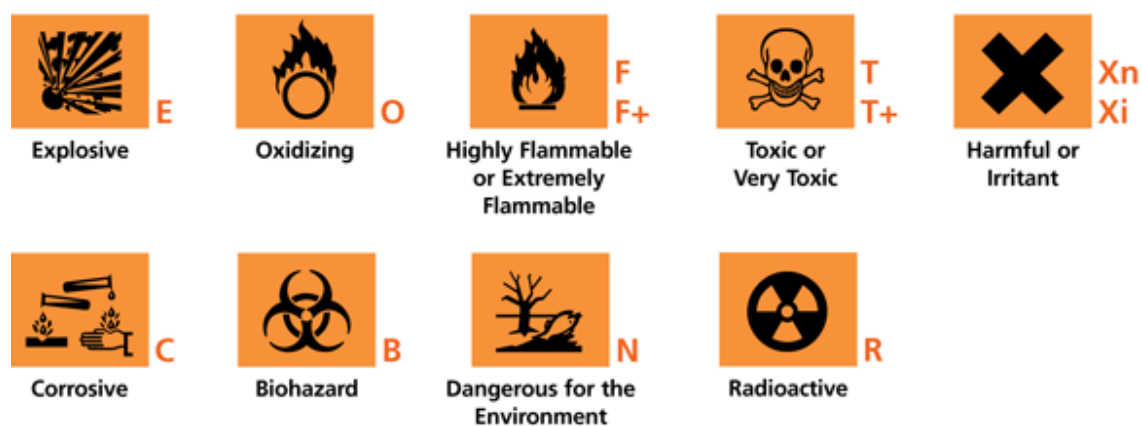


Figure 65: Hazard symbols according to (<http://www.sigmaaldrich.com>) for formulations and respective risk labels.



Figure 66: GHS pictograms according to (<http://www.evansvanodine.com>)- Evans Vanodine International plc/ global Hygiene Solutions/UK).

Table 19: GHS hazard statements

GHS hazard statements	
H 225	Highly flammable liquid and vapor
H 226	Flammable liquid and vapor
H 228	Flammable solid
H 272	May intensify fire; oxidizer
H 301	Toxic if swallowed
H 302	Harmful if swallowed
H 311	Toxic in contact with skin
H 312	Harmful in contact with skin
H 314	Causes severe skin burns and eye damage
H 315	Causes skin irritation
H 316	Causes mild skin irritation
H 317	May cause an allergic skin reaction
H 318	Causes serious eye damage
H 319	Causes serious eye irritation
H 330	Fatal if inhaled
H 331	Toxic if inhaled
H 332	Harmful if inhaled
H 334	May cause allergy or asthma symptoms or breathing difficulties if inhaled
H 335	May cause respiratory irritation
H 336	May cause drowsiness or dizziness
H 340	May cause genetic defects
H 341	Suspected of causing genetic defects
H 350	May cause cancer
H 350i	May cause cancer by inhalation
H 360	May damage fertility or the unborn child
H 360D	May damage the unborn child
H 361	Suspected of damaging fertility or the unborn child
H361f	Suspected of damaging fertility
H 370	Causes damage to organs
H 372	Causes damage to organs through prolonged or repeated exposure
H 410	Very toxic to aquatic life with long lasting effects
H 411	Toxic to aquatic life with long lasting effects

Table 20: GHS precautionary statements

GHS precautionary statements	
P201	Obtain special instructions before use
P210	Keep away from heat/sparks/open flames/hot surfaces – No smoking
P233	Keep container tightly closed
P260	Do not breathe dust/fume/gas/mist/vapors/spray
P261	Avoid breathing dust/fume/gas/mist/vapors/spray
P264	Wash thoroughly after handling
P273	Avoid release to the environment
P281	Use personal protective equipment as required
P280	Wear protective gloves/protective clothing/eye protection/face protection
P284	Wear respiratory protection
P309	IF exposed or you feel unwell
P310	Immediately call a POISON CENTER or doctor/physician
P311	Call a POISON CENTER or doctor/physician
P312	Call a POISON CENTER or doctor/physician if you feel unwell
P321	Specific treatment (see respective MSDS)
P362	Take off contaminated clothing and wash before reuse
P501	Dispose of contents/container to
P301+310	If swallowed: Immediately call a poison center or doctor/physician
P301+P312	If swallowed: call a poison center or doctor/physician if you feel unwell
P301+P330+P331	If swallowed: Rinse mouth. Do not induce vomiting
P302+P352	If on skin: Wash with soap and water
P303+P361+P353	If on skin (or hair): Remove/Take off immediately all contaminated clothing. Rinse skin with water/shower
P304+341	If inhaled: If breathing is difficult, remove victim to fresh air and keep at rest in a position comfortable for breathing
P305+351+338	If in eyes: Rinse cautiously with water for several minutes. Remove contact lenses if present and easy to do – continue rinsing
P308+313	If exposed or concerned: Get medical advice/attention
P332+313	If skin irritation occurs: Get medical advice/attention
P342+311	Call a poison center or doctor/physician
P403+233	Store in a well-ventilated place. Keep container tightly closed

Table 21: Risk statements

Risk statements	
R8	Contact with combustible material
R10	May cause fire
R20	Flammable
R21	Harmful by inhalation
R22	Harmful in contact with skin
R25	Harmful if swallowed
R35	Toxic if swallowed
R36	Causes severe burns
R38	Irritating to eyes Irritating to skin
R41	Risk of serious damage to eyes
R42	May cause sensitization by inhalation
R43	May cause sensitization by skin contact
R45	May cause cancer
R46	May cause heritable genetic damage
R60	May impair fertility
R61	May cause harm to the unborn child
R39/23/24/25	Toxic: danger of very serious irreversible effects through inhalation, in contact with skin and if swallowed
R36/37/38	Irritating to eyes, respiratory system and skin
R23/24/25	Toxic by inhalation, in contact with skin and if swallowed
R20/21/22	Harmful by inhalation, in contact with skin and if swallowed
R48/20/22	Harmful: danger of serious damage to health by prolonged exposure through inhalation and if swallowed
R23/25	Toxic by inhalation and if swallowed
R36/38	Irritating to eyes and skin
R51/53	Toxic to aquatic organisms, may cause long-term adverse effects in the aquatic environment
R37/38	Irritating to respiratory system and skin

Table 22: Safety statements

Safety statements	
S20	When using, do not eat or drink. Do not breathe dust
S22	In case of contact with eyes, rinse immediately with plenty of water and seek medical advice
S26	In case of accident or if you feel unwell, seek medical advice immediately (show the label where possible).
S28	After contact with skin, wash immediately with plenty of (<i>to be specified by the manufacturer</i>)
S45	If swallowed, seek medical advice immediately and show this container or label
S46	Avoid exposure - obtain special instructions before use
S53	Avoid release to the environment
S61	Refer to special instructions/safety data sheet
S24/25	Avoid contact with skin and eyes
S36/37	Wear suitable protective clothing and gloves
S36/37/39	Wear suitable protective clothing, gloves and eye/face protection

10. Acknowledgement:

- First of all I kneel to Allah, truly thankful for supporting me to continue my research and complete this thesis.
- Secondly, I send all my respect and gratitude to the Iraqi Ministry of High Education and Scientific Research along with the DAAD for providing me with this scholarship and financially supporting my Ph.D. study.
- I would like to dedicate my work to my family, especially my husband Ali, who has supported me throughout the years of study, and to my son Yousif, for cheering me up when necessary, also to my daughter, yet to be born.
- I would like to express my deepest appreciation and gratitude to Prof. Christian Betzel. It would have been very difficult to continue and complete my study without his support. More importantly, his kindness and scientific guidance were major factors that helped me to continue my work and complete my thesis. I also thank him for introducing me into the field of "crystallography" and providing me with an opportunity to study in this field and in his group.
- I also would like to thank Prof. Reinhard Bredehorst for being the second reviewer of the thesis.
- I would like to thank Dr, Lars Redecke, for providing me with this project and also for his guidance throughout my years of study, wishing him success in his career.
- I also would like to thank Dr. Nasser Yousef for helping and guiding me especially in my first year of study, wishing all the best for him and his family.
- Also thanks to Dr. Sven Falke for his guidance in learning how to analyze SAXS data among other guidance when ever needed, wishing him all the best and successes in his career.
- Deeply thankful to Dr. Maria Riedner, at the Organic Chemistry, Hamburg University for her helps in MS and also her guidance, wishing her all the best.
- I would also like to send my regards and gratitude to Dr. Cy Jeffries from EMBL for his help and support through SEC-SAXS, wishing him all the best and success.
- I would like to thank Dr. Thorsten Mielke and Mr. Jörg Bürger at the Max Planck Institute for Molecular Genetics, Berlin for their help in EM.

Acknowledgment

- I would like to thank Dr. Holger Nickel and Mr. Hendrik at the Pall Life Science / Pall Corp. Germany, for providing the Octet HTX device, which was used for protein-protein interaction measurements, also thanks to Miss Katharina Berg, Biochemistry and Molecular Biology department, Hamburg University, for helping in data analysis.
- I would like to thank all of the people in the Laboratory for Structural Biology of Infection and Inflammation at DESY, also in the Laboratory of Biochemistry and Molecular Biology.
- Finally, I would like to thank all my colleagues who have been in the labs throughout my years of study for providing me with help and support and for being good companions during difficult working times. Wish them all the best.

Rana Abdullah Hussein

11. Curriculum Vitae

Personal Data:

Family Name: Hussein

First Name: Rana

Date of Birth: 17th of September 1979

Birthplace: Baghdad, Iraq

Nationality: Iraqi

Graduation:

1997: High Secondary School, Baghdad, Iraq

1997-2001: B. Sc. In Biotechnology, Faculty of Food Science and Biotechnology, Baghdad University, Iraq

2001-2004: M. Sc. in Biotechnology, Faculty of Food Science and Biotechnology, Bagdad University, Iraq

Since 2011: Studying Ph. D. at the University of Hamburg, Germany

Work experience:

2006 – till now: Assistant Lecturer in the Faculty of food Science and Biotechnology, Baghdad University, Iraq.

2011 – 2016: Scholarship to obtain a Ph.D. degree at the University of Hamburg funded by The Iraqi Ministry of Higher Education and Scientific Research along with the DAAD (Deutscher Akademischer Austausch Dienst/German academic Exchange Service).

Publications:

Meyer, A., Dierks, K., Hussein, R., Brillet, K., Brognaro, H and Betzel, C. (2015). Systematic analysis of protein–detergent complexes applying dynamic light scattering to optimize solutions for crystallization trials. *Acta Cryst; F71: 75–81.*

Selbstständigkeitserklärung

Hiermit erkläre ich an Eides statt, dass ich die an der Universität Hamburg zur Promotion eingereichte Dissertation mit dem Titel "Strukturuntersuchungen von Hepatitis-B-Virus X Proteine" im Institut für Biochemie des Fachbereichs Chemie der Universität Hamburg ohne sonstige nicht angeführte Hilfe durchgeführt und bei der Abfassung der Dissertation keine anderen als die dort aufgeführten Hilfsmittel benutzt habe.

Ferner versichere ich, dass ich bisher an keiner in- oder ausländischen Universität ein Gesuch um Zulassung zur Promotion eingereicht und daher weder diese noch eine andere Arbeit als Dissertation vorgelegt habe.

Rana Abdullah Hussein